

NCC1-123

11-09-87

P-87

**Low-Speed Wind Tunnel Investigation of the Static Stability
and Control Characteristics of an Advanced Turboprop
Configuration with the Propellers Placed Over The Tail**

by

GRAHAM SCOTT RHODES

A thesis submitted to the Graduate Faculty of
North Carolina State University
in partial fulfillment of the
requirements for the Degree of
Master of Science

DEPARTMENT OF MECHANICAL AND AEROSPACE ENGINEERING

Raleigh

1990

APPROVED BY:



Chairman of Advisory Committee

(NASA-CR-186900) LOW-SPEED WIND TUNNEL
INVESTIGATION OF THE STATIC STABILITY AND
CONTROL CHARACTERISTICS OF AN ADVANCED
TURBOPROP CONFIGURATION WITH THE PROPELLERS
PLACED OVER THE TAIL M.S. Thesis (North

N90-26017

Unclassified
63/08 0296994

Abstract

RHODES, GRAHAM SCOTT. Low-speed Wind Tunnel Investigation of the Static Stability and Control Characteristics of an Advanced Turboprop Configuration with the Propellers Placed Over The Tail. (Under the direction of Dr. John N. Perkins)

As part of a cooperative agreement between NASA Langley Research Center and North Carolina State University, an exploratory wind-tunnel investigation was performed in the 30x60 Foot Wind Tunnel to determine the low-speed static stability and control characteristics into the deep-stall regime of an advanced turboprop aircraft with the propellers located over the horizontal tail. By this arrangement, the horizontal tail could potentially provide acoustic shielding to reduce the high community noise caused by the propeller blades. The current configuration was a generic turboprop model equipped with 1 foot diameter single-rotating eight-bladed propellers that were designed for efficient cruise operation at a Mach Number of 0.8. The data presented **here** is static force data.

The effects of power on the configuration characteristics were generally favorable. An arrangement with the propellers rotating with the outboard blades moving down was found to have significantly higher installed thrust than an arrangement with the propellers rotating with the inboard blades moving down. The primary unfavorable effect was a large pitch trim change which occurred with power, but the trim change could be minimized with a proper configuration design.

Acknowledgements

I would like to thank my graduate advisor, Dr. John N. Perkins, for his support throughout this quest. In addition, I would like to thank Joseph L. Johnson, Jr., and Paul L. Coe, Jr., both of the NASA Langley Research Center, for their support, interest, and insight into the project. My appreciation goes to the tunnel technicians, who endured five weeks of night shift, computer problems, and engineers. To the remaining people at the Flight Dynamics Branch, I appreciate the opportunity to spend a year working with you. The experience and information I acquired will prove to be a great asset during my future as an Aerospace Engineer.

To my parents, thanks for the support and encouragement. Without your help through the years, I would never have made it this far.

Table of Contents

Acknowledgements.....	ii
Table of Contents.....	iii
List of Tables.....	v
List of Figures.....	vi
Symbols.....	viii
Abbreviations.....	x
Introduction.....	1
Model and Test Technique.....	6
Results and Discussion.....	16
Characteristics of Wing Body.....	19
Basic Longitudinal Characteristics.....	19
Effect of Trailing Edge Flaps.....	22
Effect of Droop on Lateral and Directional Characteristics.....	22
Effect of Flaps on Lateral/Directional Characteristics.....	26
Longitudinal Characteristics of the Unpowered Configuration.....	26
Effect of Elevator.....	26
Effect of Flaps.....	30
Lateral/Directional Characteristics of Unpowered Configuration.....	30
Effect of Rudder.....	30
Effect of Ailerons.....	33
Effect of Power and the Direction of Propeller Rotation.....	33
Effect on Body/Pylon/Nacelle.....	33
Effect on Longitudinal Characteristics of Full Configuration.....	40
Effect on Lateral/Directional Characteristics of Full Configuration..	43
Effect of Fillet Fairings on Propellers Rotating in Both Directions..	46
Characteristics of Final Configuration.....	46
Effect of Fillets on Full Configuration Without Power.....	46
Effect of Power on Longitudinal Characteristics.....	50
Effect of Power on Lateral/Directional Characteristics.....	50
Effect of Flaps	54
Effect of Flaps on Lateral/Directional Characteristics.....	54
Effect of Rudder on Directional Characteristics.....	54
Effect of Elevator on Longitudinal Characteristics.....	57
Effect of Power on Trim Capability.....	60

Table of Contents - continued

Effect of Ailerons on Lateral Characteristics.....	61
Engine-Out Characteristics.....	61
Comparison To Theoretical Results.....	65
Comparing the Results.....	65
Concluding Remarks.....	73
References.....	75

List of Tables

Table 1 - Model reference geometry.....	7
Table 2 - Coordinate For NLF(1)-0416 Airfoil Section.....	9
Table 3 - Strain-Gage Balance Characteristics.....	17

List of Figures

Figure 1 - Photograph of Over-The-Tail Advanced Turboprop Model.....	10
Figure 2 - Three-view drawing of model.....	11
Figure 3 - Model Mounted In 30x60 Foot Wind Tunnel.....	14
Figure 4 - Propeller Configurations Tested.....	15
Figure 5 - Axis System For Forces and Moments.....	18
Figure 6 - Effect of Droop on Lift of Wing/Body.....	20
Figure 7 - Effect of Droop on Pitching Moment of Wing/Body.....	20
Figure 8 - Wing Stall Pattern.....	21
Figure 9 - Effect of Droops on Wing/Body Drag.....	23
Figure 10 - Effect of Flaps on Lift of Wing/Body.....	24
Figure 11 - Effect of Flaps on Pitching Moment of Wing/Body.....	24
Figure 12 - Effect of Droops on Wing/Body Rolling Moment.....	25
Figure 13 - Effect of Droops on Wing/Body Yawing Moment.....	25
Figure 14 - Effect of Droops on Lateral Stability.....	27
Figure 15 - Effect of Flaps on Wing/Body Yawing Moment.....	28
Figure 16 - Effect of Flaps on Wing/Body Rolling Moment.....	28
Figure 17 - Effect of Flaps on Wing/Body Directional Stability.....	29
Figure 18 - Effect of Flaps on Wing/Body Lateral Stability.....	29
Figure 19 - Effect of Elevator on Configuration Pitching Moment.....	31
Figure 20 - Inboard and Full Elevator Effectiveness.....	31
Figure 21 - Effect of Flaps on Configuration Lift.....	32
Figure 22 - Effect of Flaps on Configuration Pitching Moment.....	32
Figure 23 - Effect of Full Rudder on Configuration Yawing Moment.....	34
Figure 24 - Lower and Full Rudder Effectiveness.....	34
Figure 25 - Effect of Ailerons on Configuration Rolling Moment.....	35
Figure 26 - Aileron Effectiveness.....	35
Figure 27 - Effect of Power on Drag of Body/Pylons/Nacelles.....	37
Figure 28 - Illustration of a propeller at angle of attack (exaggerated).....	38
Figure 29 - Illustration of crossflow effect.....	39
Figure 30 - Effect of Power on Lift of Body/Pylons/Nacelles.....	41
Figure 31 - Effect of Power on Pitching Moment of Body/Pylons/Nacelles.....	41
Figure 32 - Effect of Power on Configuration Lift.....	42
Figure 33 - Effect of Power on Configuration Pitching Moment.....	42
Figure 34 - Effect of Power on Configuration Drag.....	44

List of Figures - continued

Figure 35 - Effect of Power on Directional Stability.....	45
Figure 36 - Effect of Power on Lateral Stability.....	45
Figure 37 - Effect of Fillets on Drag and Installed Thrust.....	47
Figure 38 - Effect of Fillets on Full Configuration Lift.....	48
Figure 39 - Effect of Fillets on Configuration Pitching Moment.....	48
Figure 40 - Effect of Fillets on Configuration Drag.....	49
Figure 41 - Effect of Power on Final Configuration Lift.....	51
Figure 42 - Effect of Power on Final Configuration Pitching Moment.....	51
Figure 43 - Effect of Power on Final Configuration Drag.....	52
Figure 44 - Effect of Power on Yawing Moment.....	53
Figure 45 - Effect of Power on Directional Stability.....	53
Figure 46 - Effect of Flaps on Final Configuration Lift.....	55
Figure 47 - Effect of Flaps on Final Configuration Pitching Moment.....	55
Figure 48 - Effect of Flaps on Directional Stability.....	56
Figure 49 - Effect of Flaps on Lateral Stability.....	56
Figure 50 - Final Configuration Full Rudder Authority.....	58
Figure 51 - Effect of Power on Rudder Effectiveness.....	58
Figure 52 - Effect of Elevator on Pitching Moment.....	59
Figure 53 - Effect of Power on Elevator Effectiveness.....	59
Figure 54 - Effect of Power on Trim Capability.....	62
Figure 55 - Effect of Ailerons on Rolling Moment.....	63
Figure 56 - Effect of Ailerons on Yawing Moment.....	63
Figure 57 - Effect of Power on Aileron Effectiveness.....	64
Figure 58 - Engine-out Yawing Moment.....	66
Figure 59 - Engine-out Rolling Moment.....	66
Figure 60 - Orthographic View of QUADPAN Panel Model.....	67
Figure 61 - Comparison to Potential Lift.....	68
Figure 62 - Comparison to Potential Pitching Moment.....	68
Figure 63 - Comparison to Potential Directional Stability.....	70
Figure 64 - Comparison to Potential Lateral Stability.....	70
Figure 65 - Predicted Power Effects on Lift.....	71
Figure 66 - Predicted Power Effects on Pitching Moment.....	71
Figure 67 - Predicted Power Effects on Directional Stability.....	72
Figure 68 - Predicted Power Effects on Lateral Stability.....	72

Symbols

b	Wing span, inches
c	Local chord, inches
\bar{c}	Geometric average wing chord based on trapezoidal reference area, inches
C_D	Drag coefficient, Drag/ qS
C_l	Rolling moment coefficient, Rolling Moment/ qSb
$C_{l\beta}$	Lateral stability, $dC_l/d\beta$, per degree
$C_{l\delta_a}$	Aileron control effectiveness, $dC_l/d\delta_a$, per degree
C_L	Lift coefficient, Lift/ qS
C_{Lmax}	Maximum lift coefficient
$C_{L\alpha}$	Slope of the lift curve, $dC_L/d\alpha$, per degree
C_m	Pitching moment coefficient, Pitching Moment/ qSc
$C_{m\alpha}$	Slope of pitching moment curve, $dC_m/d\alpha$, per degree
$C_{m\delta_e}$	Elevator control effectiveness, $dC_m/d\delta_e$, per degree
C_n	Yawing moment coefficient, Yawing Moment/ qSb
C_{Np}	Propeller normal force coefficient, Prop Normal Force/ qS
$C_{n\beta}$	Directional stability, $dC_n/d\beta$, per degree
$C_{n\delta_r}$	Rudder control effectiveness, $dC_n/d\delta_r$, per degree
d	Propeller diameter, feet
J	Propeller Advance Ratio, $J=V/Nd$
l_t	Distance from CG to MAC_t
L/D	Lift to Drag Ratio, C_L/C_D
N	Propeller Speed, revolutions per second
q	Wind tunnel free stream dynamic pressure, pounds per square foot
r	Radial station on propeller blade, feet
Re	Reynold's Number based on MAC, $(\rho * V * MAC) / \mu$

S	Wing reference area, $S=\bar{c}b$
S_t	Area of horizontal stabilizer, square feet
T'_c	Thrust Coefficient, Thrust/ qS
V	Wing tunnel free stream velocity, feet per second
V_H	Horizontal Stabilizer Volume Coefficient, $S_t l_t / S * MAC$
V_r	Resultant air velocity due to free stream and propeller rotation, fps
$\left(\frac{x_p}{c}\right)$	Non-dimensional chordwise location of propeller disk
$\left(\frac{z}{c}\right)$	Non-dimensional vertical location of thrust axis
α	Angle of attack, degrees
α_b	Propeller blade angle of attack at radial station r , degrees
β	Sideslip angle, degrees
β_b	Propeller blade angle at radial station r , degrees
δ_a	Aileron deflection angle, degrees, positive right wing TED
δ_e	Elevator deflection angle, degrees, positive TED
δ_f	Flap deflection angle, degrees, positive TED
δ_r	Rudder deflection angle, degrees, positive TEL
ρ	Air density, slugs per cubic foot
μ	Coefficient of viscosity for air, pound-second per square foot

Abbreviations

AC	Aerodynamic Center
ATP	Advanced TurboProp
CG	Center of Gravity
IBD	Propellers spinning with InBoard blades moving Down
LE	Leading Edge
MAC	Mean Aerodynamic Chord, inches
MAC _t	Mean Aerodynamic Chord of Horizontal Stabilizer
OBD	Propellers spinning with OutBoard blades moving Down
OTT	Over-The-Tail propeller
psf	Pounds per Square Foot
RPM	Rotational speed of the propellers, Revolutions Per Minute
SM	Static Margin, $100\% * dC_m/dC_L $
TED	Trailing Edge Down
TEL	Trailing Edge Left

Introduction

The NASA/Industry Advanced Turboprop Project (ATP) was begun in 1978 to investigate the possibilities of using fuel efficient advanced turboprop aircraft in the place of current turbojet and turbofan transport aircraft. The driving force for the project was a need to overcome the rapidly increasing fuel costs which occurred since the 1973 Middle East oil embargo. Existing turbojet and turbofan aircraft have the advantage of relatively high cruise speeds compared to turboprop aircraft. Current turboprop propeller blades are fuel efficient at Mach Numbers below approximately 0.6 but lose this efficiency rapidly at higher Mach Numbers largely due to compressibility effects. A major aspect of the ATP since 1978 was the design of new propeller blades which operate efficiently at the higher cruise Mach Numbers of turbojet and turbofan aircraft. The emerging propeller designs included highly swept blade planforms, large blade angles, and a large number of blades per engine for both single-rotating and counter-rotating configurations. The new propellers operate with an installed propulsive efficiency that is increased by approximately 10 to 20% from turbofans at cruise Mach Numbers around 0.8. Flight tests have shown this increased propulsive efficiency from the new propellers alone could provide a fuel savings as large as 30%. When considering additional improvements in the areas of mechanical engine components and efficient engine design, the potential fuel savings for an advanced turboprop aircraft is at or above 50% compared to existing turbojets and turbofans.¹⁻³

One of the major problems surrounding aircraft powered by advanced turboprops is the large level of noise produced by the propeller blades. The noise from the new blades is primarily aerodynamic pressure field noise from the blades themselves and from structural vibrations induced by the acoustic effects of the blades on the wing and fuselage. Thin, swept propeller blades have reduced noise compared to straight propeller blades at low operating speeds, but at high cruise speeds, the supersonic helical tip speed blades

maintain a high overall noise level. For a conventional wing-mounted-engine configuration, the propellers would be located close to the fuselage and beside the cabin area resulting in a high degree of cabin noise. In addition, the level of noise on the ground, the community noise level, could be quite high during takeoff and enroute. It was desirable to reduce both the cabin and community noise levels without the need for additional aircraft structure or weight which would reduce the benefits of the advanced turboprop concept.¹⁻⁵

Previous theoretical and experimental work has shown that the wing could provide a significant degree of acoustic shielding to reduce the cabin noise level to a more acceptable level when properly arranged with the turboprop blades. This shielding is due to the wing both blocking and reflecting sound pressure waves away from the cabin area of the fuselage.^{4,5} The propellers and wing would be arranged to reflect the noise above the wing for a high-mounted wing and below the wing for a low-mounted wing. For conventional wing-mounted engines, with the propeller disk roughly centered above and below the wing, the direction of propeller rotation is important. A low wing aircraft would require the outboard blades to be moving down to reduce cabin noise and a high wing aircraft would require the inboard blades to be moving down to reduce cabin noise. In either case, the wing sweep and chordwise location of the propeller disk are important because the chordwise position where shielding begins varies with Mach Number. For a high wing with the inboard propeller blades moving down, it is reasonable to expect a reduction in community noise as well since the sound waves would be reflected above the wing and away from the community.

From another point of view, an aft-fuselage-mounted-engine configuration would place the propeller blades far behind the cabin to reduce the cabin noise level somewhat, though flight tests indicate acoustic treatment would still be required to achieve acceptable cabin noise levels. A tail-mounted engine configuration would require significant supporting structure. Past research indicates the amount of additional acoustic treatment

required may be reduced by carefully positioning the fuselage/tail mounting structure and turning the propellers with the outboard blades moving down^{5,6}.

Because of the highly loaded blades of advanced turboprop propellers, the effects of the propulsion system can be more severe than conventional turboprops. The present investigation represents a cooperative agreement between NASA and North Carolina State University to determine the propulsion system installation effects on the static stability and control characteristics of a generic advanced turboprop commuter/transport configuration at low subsonic speeds.

The present investigation combines the concept of acoustic shielding and aft-fuselage-mounted-engines by their application on an advanced turboprop configuration which places the propeller blades over the horizontal stabilizer. This configuration is called the Over-The-Tail (OTT) advanced turboprop. For this case, the horizontal stabilizer would, potentially, provide the aforementioned acoustic shielding to reduce ground and community noise levels. Since the entire propeller would be located above the horizontal stabilizer, the direction of propeller rotation should not greatly effect the degree of community noise shielding, though the sweep of the horizontal tail and position of the propeller disk would remain important. The cabin noise level would be reduced as well because the propellers are located near the rear of the fuselage, far behind the cabin.

Several previous wind-tunnel investigations have been performed on aft-fuselage-mounted-engine advanced turboprop aircraft. All of these showed generally favorable effects of power on the static stability and control of the aircraft. In particular, the aft-mounted propellers increased longitudinal and directional stability with no major detrimental effects on control effectiveness. The configurations generally had enough rudder authority to overcome and trim the large yawing moment with an engine-out condition⁷⁻⁹.

An OTT design has several complicated aspects which must be considered. Since the propellers would be located above the horizontal tail, it is possible the thrust line would

be located above the center of gravity. For power on cases, this would result in a large decrement in pitching moment which must be balanced in order to trim the aircraft.

A major aerodynamic concern is caused by the propellers being located close to the horizontal and vertical surfaces. Past research has shown a jet blowing over one side of a lifting wing increases the circulation about the wing resulting in an increased lift¹⁰. A propeller located close to a wing should have a similar effect. For example, the propellers blowing over the upper surface of the horizontal stabilizer would potentially increase the lift of the horizontal stabilizer. This increased stabilizer lift would have a corresponding decrement in pitching moment, an additional trim change with power. The increased stabilizer lift and decrement in pitching moment vary inversely with the gap between the propeller blade tip and the surface of the stabilizer.

The trim changes which appear inherent to the OTT configuration would place a burden on the elevator and may significantly reduce the available pitch control for high power settings. Most large transport aircraft have all-moving horizontal stabilizers, and an OTT design may require one in order to trim at cruise while maintaining sufficient elevator pitch control¹¹. In addition, there would be a high degree of trim drag for all flight regimes other than landing, where there is no appreciable thrust. The problems of pitch control and trim drag can be remedied to a large degree by a proper configuration design. Ideally, the OTT configuration would have a low-mounted horizontal stabilizer with anhedral to move the thrust line close to the center of gravity. In addition, the propeller should be angled downward slightly to direct the thrust line through the center of gravity to completely eliminate a pitching moment change due to thrust. The pitch change due to increased stabilizer lift with power could be minimized with a large gap between the propeller and the stabilizer.

The OTT arrangement has at least one potential performance advantage. Past research has shown that a jet blowing over the upper surface of a lifting wing reduces the pressure drag on the wing significantly. Research at NASA-Langley Research Center has

shown that a propeller blowing over a surface has a similar effect¹²⁻¹⁴. With the OTT configuration, this drag reduction would be seen at cruise as a reduction in trim drag. This drag reduction would at least serve to balance the trim drag increase discussed above. For the properly designed configuration, there is potential for lower trim drag than a conventional two-surface turboprop aircraft.

Model and Test Technique

The present investigation was performed in NASA-Langley's 30x60 Foot Wind Tunnel¹⁵ and utilized the approximately 1/9th scale generic turboprop model shown in figure 1. The model is a conventional two-surface wing/tail configuration with a unique engine/nacelle location that places the propellers above the horizontal tail. The horizontal stabilizer has no dihedral and no effort was made to place the thrust line close to the center of gravity. Figure 2 is a three-view drawing of the model and table 1 lists the geometric properties of the model. The model construction was conventional, utilizing fiberglass, balsa wood, and aluminum for most components. The model is approximately 10 feet long with a wing span of 9.91 feet. The wing's MAC is 14.0 inches. The wing airfoil is an NLF(1)-0416 section. The airfoil coordinates are listed in table 2. The wing was equipped with a 26 inch span leading edge droop. The 8-bladed propeller installation included the high speed Hamilton Standard SR-7 blades^{3,16} which were constructed from carbon-fiber composites to maintain physical integrity despite the low thickness of the sections. The propellers were located such that the blade tips were separated from the horizontal and vertical stabilizers by a distance of only 1/8th inch. The propellers have a d of 1 foot and the same scale as the configuration. The blades were set at a nominal blade angle of 43 degrees at the 75% radius station. The two propellers turned in opposite directions to effectively eliminate propwash "swirl" effects on the configuration lateral and directional trim characteristics.

Small air turbines were used to drive the propellers. The air was supplied by flexible tubing from external pressure domes. The maximum supplied pressure was 250 pounds per square inch. A copper tube "trombone" was placed inside the model between the air source and the air turbines to remove the effects of the high pressure air on the force data. Several checkout data runs were performed in the absence of the air turbines to verify that the trombone was effective.

Table 1 - Model Reference Geometry

Fuselage:	Length.....	8.82 feet
	Maximum diameter.....	11.2 inches
	Body Station of nose.....	0 inches
	Waterline of CG.....	20.488 inches
	Body Station of CG.....	52.12 inches
Wing:	Airfoil.....	NLF(1)-0416
	Thickness.....	16%
	Area.....	9.91 square feet
	MAC.....	14.0 inches
	Span.....	108.86 inches
	Aspect Ratio.....	8.3
	Taper Ratio.....	0.376
	Quarter-chord sweep.....	1.41 degrees
	Dihedral.....	4.0 degrees
	Root incidence.....	1.5 degrees
	Tip incidence.....	0.5 degrees
Body Station of AC.....	52.12 inches from nose	
Waterline of AC.....	18.77 inches	
LE break chord.....	15.57 inches	
Horizontal Tail:	Airfoil.....	NACA 64A010
	Thickness.....	10%
	Tail volume, V_H	0.825
	Area.....	3.25 square feet
	MAC _t	12.71 inches
	Span.....	40.0 inches
	Aspect Ratio.....	3.42
	Taper Ratio.....	0.326
	Quarter-chord sweep.....	33.0 degrees
	Dihedral.....	0 degrees
	Root incidence.....	0 degrees
	Tip incidence.....	0 degrees
	Body Station of AC.....	93.9 inches from nose
	Waterline of AC.....	23.61 inches
Area of inner elevator.....	66.2 square inches	
Area of full elevator.....	116.44 square inches	
Span Station of elev. break..	12.45 inches	
Vertical Tail:	Airfoil.....	NACA 64A010
	Thickness.....	10%
	Area.....	1.69 square feet
	Mean Aerodynamic Chord....	15.09 inches
	Span.....	16.9 inches
	Aspect Ratio.....	1.17
	Taper Ratio.....	0.454
	Quarter-chord sweep.....	33.3 degrees
	Body Station of AC.....	93.17 inches
	Waterline of AC.....	34.5 inches
Inner rudder area.....	36.34 square inches	

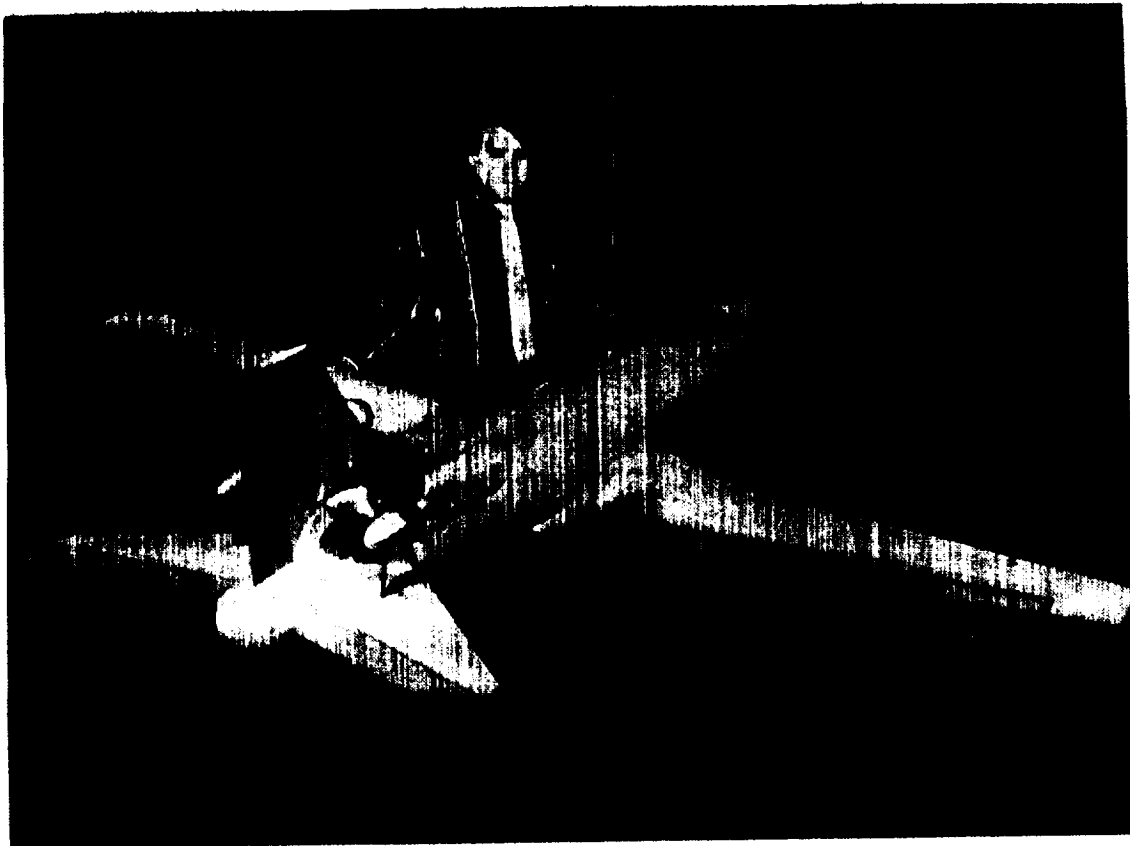
Table 1 - continued

Vertical Tail: (continued)	Full rudder area.....	61.52 square inches
	Waterline of rudder break...	36.33 inches
Pylons:	Airfoil.....	NACA 64A010
	Thickness.....	10%
Propellers:	Diameter.....	12.0 inches
	Number of blades.....	8
	Blade type.....	SR-7 Hamilton Standard
	Arrangement.....	Single Rotating
	Blade Sweep Angle.....	41 degrees
	75% Radius Blade Angle.....	43 degrees
	Body Station of prop disk.....	94.53 inches from nose

Table 2 Coordinates For NLF(1)-0416 Airfoil Section

Upper Surface x/c	Upper Surface y/c	Lower Surface x/c	Lower Surface y/c
0	0	0	0
0.00509	0.01446	0.00049	0.00403
0.01393	0.02573	0.00073	-0.00439
0.02687	0.03729	0.00709	-0.01154
0.04383	0.0487	0.01956	-0.01883
0.06471	0.05964	0.03708	-0.02594
0.08936	0.06984	0.05933	-0.03254
0.11761	0.07904	0.08609	-0.03847
0.14925	0.08707	0.11708	-0.04361
0.18404	0.09374	0.152	-0.04787
0.22169	0.09892	0.1905	-0.05121
0.26187	0.10247	0.23218	-0.05357
0.30422	0.10425	0.27659	-0.05494
0.34839	0.10405	0.32326	-0.05529
0.39438	0.10162	0.37167	-0.05462
0.44227	0.09729	0.42127	-0.05291
0.49172	0.09166	0.4715	-0.05009
0.54204	0.08515	0.52175	-0.04614
0.59256	0.07801	0.57122	-0.04063
0.64262	0.07047	0.62019	-0.0325
0.69155	0.06272	0.67014	-0.02231
0.73872	0.05493	0.72107	-0.01221
0.7835	0.04724	0.77156	-0.00364
0.8253	0.03977	0.82012	0.00278
0.86357	0.03265	0.86536	0.00667
0.89779	0.02594	0.90576	0.00792
0.92749	0.01974	0.93978	0.00696
0.95224	0.014	0.96638	0.00478
0.97197	0.00862	0.9852	0.00242
0.98686	0.00398	0.99633	0.00065
0.99656	0.00098	1	0
1	0		

ORIGINAL PAGE
BLACK AND WHITE PHOTOGRAPH



ORIGINAL PAGE IS
OF POOR QUALITY

Figure 1 - Photograph of Over-The-Tail Advanced Turboprop Model

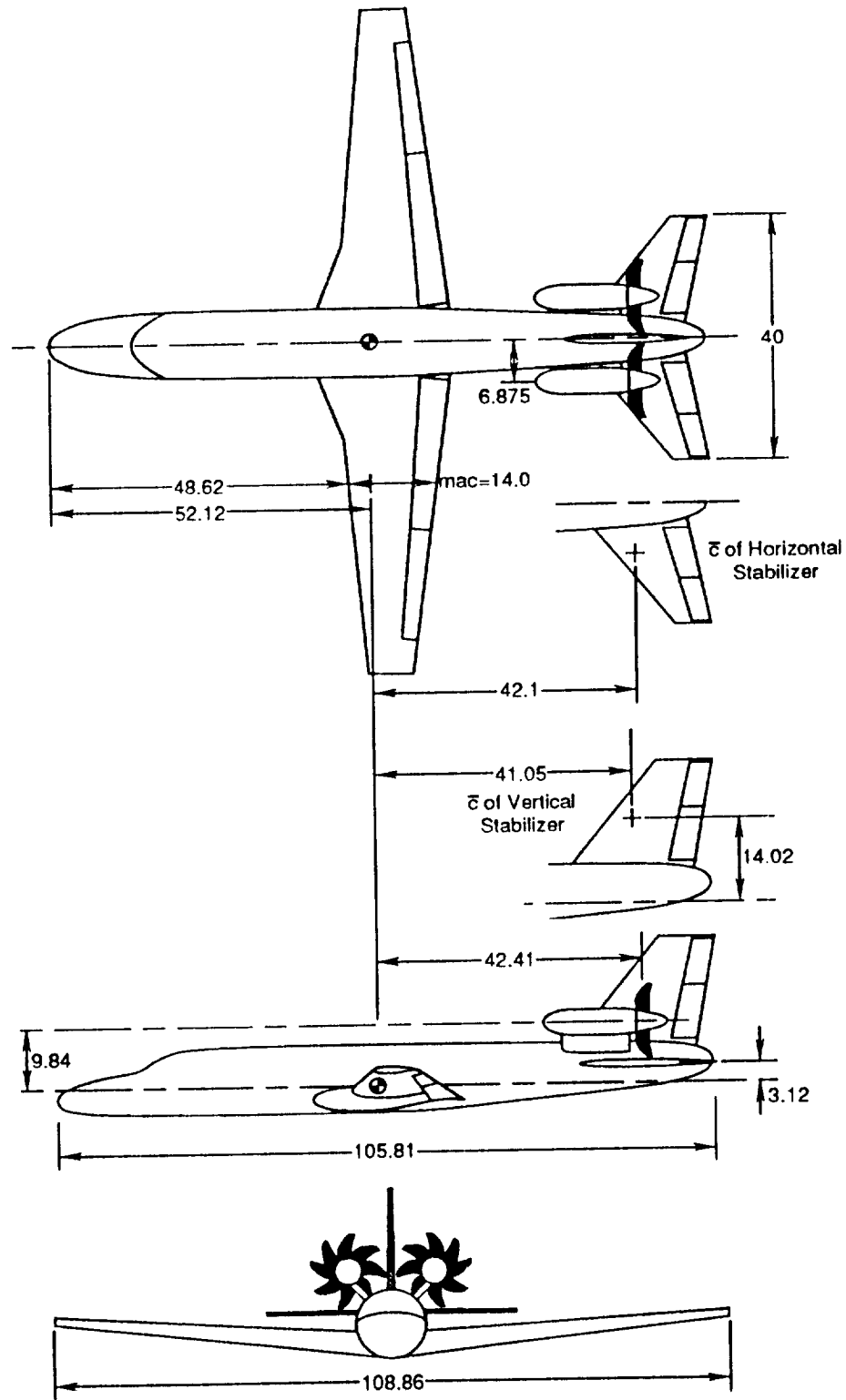


Figure 2 - Three-view drawing of model

Figure 3 shows the model mounted in the wind tunnel on a C-strut/sting assembly and equipped with an internal six-component strain-gage balance for measuring aerodynamic forces and moments. The model attitude was adjusted in angle of attack and sideslip to approximately account for flow angularity in the tunnel. Weight tare corrections were applied to all force data so that the representative data is purely aerodynamic. No other corrections were applied to the data¹⁷. In addition to force data, limited smoke flow visualization was performed to visualize the flow field surrounding the propeller assembly. Also, the wing and tail were tufted in order to determine their stall patterns. All data was gathered at a q of 4 psf for a Re of 430,490 based on the MAC.

Angular brackets were used to set control surface deflections to measure control effectiveness and authority. The wing trailing edge flaps were tested at $\delta_f=0$ and 35 degrees, and additionally at $\delta_f=20$ degrees during the power off model build-up runs. The ailerons were tested at $\delta_a=0, +10, \text{ and } +20$ degrees. The rudder was split into an upper rudder and lower rudder of approximately equal areas. The full rudder was tested at $\delta_r=-30, -20, -10, \text{ and } 0$ degrees. In addition, the lower rudder was tested independently at the same angles. Similarly, the elevator was split into an inboard elevator and an outboard elevator. The full elevator was tested at $\delta_e=-30, -20, 0, 20, \text{ and } 30$ degrees while the inboard elevator was tested independently at $-20, 0, \text{ and } 20$ degrees.

The propulsive effects were tested for propeller RPM's of 3500 rpm and 4500 rpm. For the complete configuration, the 3500 rpm case provided an installed thrust coefficient, T'_c , of approximately 0.2 for a J of 0.995. The 4500 rpm case provided a T'_c of approximately 0.36 for a J of 0.774. The $T'_c=0.2$ cases with $\delta_f=35$ degrees were representative of a 3 degree takeoff climb and the $T'_c=0.36$ cases with $\delta_f=35$ degrees were representative of a missed approach full power climb. Variations in T'_c due to configuration changes represent part of the importance of the investigation. The propellers were tested for cases with the propeller blades spinning IBD and OBD. In addition, fillet fairings were tested to close in the inboard area between the tail surfaces and propellers as an attempt to

duct the flow behind the propellers and produce more thrust. Figure 4 shows the different propeller configurations.

In addition to the wind-tunnel investigation, an analysis of the basic configuration was performed utilizing the subsonic potential panelling code, QUADPAN¹⁸. The QUADPAN code is a doublet surface panel method which has the capability to model propeller slipstream effects using a simple slipstream model. Such a panelling code is a quick, relatively simple, means to calculate aerodynamic characteristics of complete configurations for preliminary design and analysis^{19,20}.

ORIGINAL PAGE
BLACK AND WHITE PHOTOGRAPH



ORIGINAL PAGE IS
OF POOR QUALITY

Figure 3 - Model Mounted In 30x60 Foot Wind Tunnel

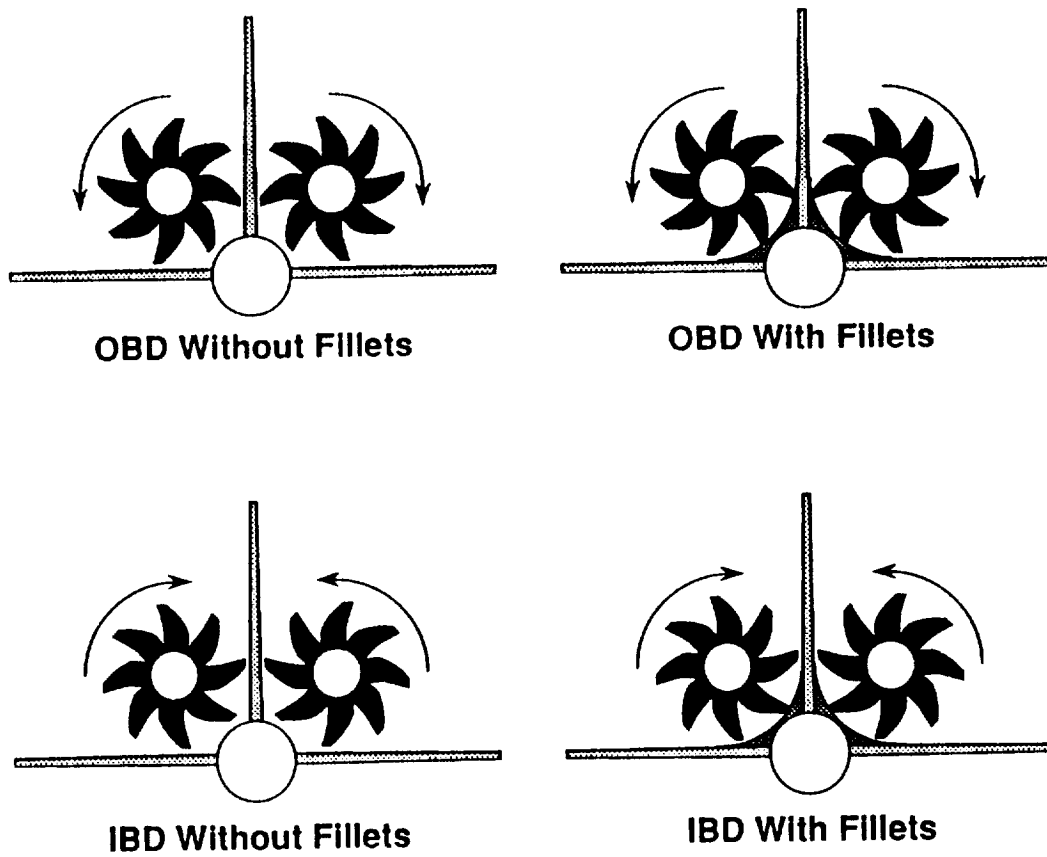


Figure 4 - Propeller Configurations Tested

Results and Discussion

All longitudinal forces and moments are referenced to the stability axes and all lateral/directional forces and moments are referenced to the body axes. Figure 5 shows the axis system graphically. The moment reference center was located 52.12 inches from the nose of the model which corresponded to the 25% chord station of the wing's mean aerodynamic chord.

Table 3 shows the characteristics and accuracy of the internal strain-gage balance used to measure the aerodynamic forces and moments. The accuracy shown was calculated for a steady static load, and is the minimum expected accuracy of the balance. In the wind tunnel, the data acquired with the wind on must be time averaged or filtered because the flow is somewhat unsteady due to free stream turbulence and vibrations which occur on the C-strut model support. The longitudinal forces and moments are quite large and do not vary much due to this unsteadiness; however, the lateral and directional forces and moments are relatively small when the model is at a small or zero sideslip. The effect of unsteadiness on these forces and moments is measurable. Due to limitations in the data acquisition system at the 30x60 Foot Wind Tunnel, this unsteadiness is not completely removed when the data is filtered. For this reason, the lateral and directional data presented here will appear scattered. This inaccuracy is most obvious in the static stability derivatives. For this reason, only large changes in these derivatives are considered important.

Power effects were measured for the propellers spinning at 3500 rpm and 4500 rpm. The effective installed thrust varied somewhat depending on the configuration. For this reason, all figures reference the speed of the propellers rather than the T_c . For cases where T_c is important, T_c is presented in the text.

Table 3 Strain-Gage Balance Characteristics

<i>Component</i>	<i>Minimum Load</i>	<i>Maximum Load</i>	<i>Accuracy</i>
Normal Force	-400 pounds	400 pounds	+/- 2 pounds
Axial Force	0 pounds	200 pounds	+/- 1 pound
Side Force	-200 pounds	200 pounds	+/- 1 pound
Pitching Moment	-2000 inch-pounds	2000 inch-pounds	+/- 10 inch-pounds
Yawing Moment	-2000 inch-pounds	2000 inch-pounds	+/- 10 inch-pounds
Rolling Moment	-1230 inch-pounds	1230 inch-pounds	+/- 6.15 inch-pound

*Forces and Moments in Coefficient Form
q=4 pounds per square foot*

<i>Coefficient</i>	<i>Minimum</i>	<i>Maximum</i>	<i>Accuracy</i>
C _L	-10.1	10.1	+/- 0.0505
C _D	0	5.05	+/- 0.0252
C _Y	-5.05	5.05	+/- 0.0252
C _m	-3.604	3.604	+/- 0.018
C _n	-0.4635	0.4635	+/- 0.00232
C _l	-0.285	0.285	+/- 0.00143

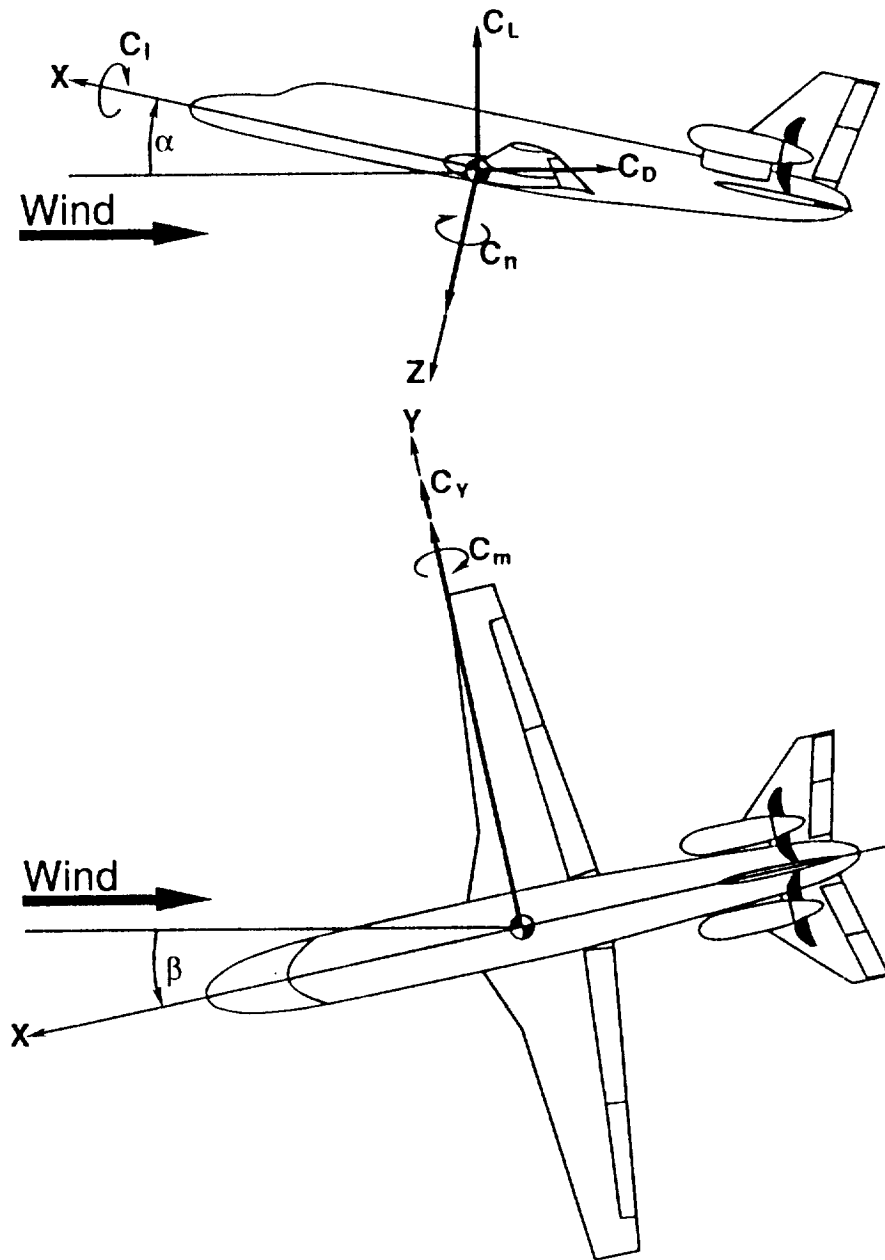


Figure 5 - Axis System For Forces and Moments

Characteristics of Wing Body

Basic Longitudinal Characteristics. Figures 6 and 7 represent the longitudinal characteristics of the wing/body with pylons and nacelles including the effect of a 26" outboard leading edge wing droop. The lift curve of the wing and body without the droop exhibits a slope, $C_{L\alpha}$ of 0.085 per degree with a C_{Lmax} of 1.44 at an α of 14 degrees. The stall point is quite sharp and the loss of lift after stall is significant. A sharp drop-off in lift at stall has been shown to be characteristic of aircraft with poor roll departure tendencies at stall. The roll departure problems are due to non-symmetric stall patterns on the two wings when the aircraft is in sideslip, which results in one wing producing more lift than the other causing the aircraft to roll into a spin or spiral. If the drop-off in lift at stall were small, the difference in lift between the wings would not be large enough to cause violent roll problems. However a large drop-off in lift indicates a possible large difference in lift between wings with a correspondingly large rolling moment. A stall pattern which begins at the wing tip would enhance this rolling moment due to a large lever arm for the differential lift. The leading edge "droop" modification is intended to reduce this problem by providing improved flow over the wing tips in two manners. First, the shape of the droop improves the two-dimensional stall characteristics of the airfoil near the tip, postponing the tip stall. Second, the sharp droop edge produces a strong vortex which sheds across the wing providing energy to the flow and acts as an aerodynamic fence which reduces spanwise flow, a contributor to tip stall and the roll departure problem²¹. With the droop installed, $C_{L\alpha}$ does not change, while C_{Lmax} decreases slightly to 1.42 at an α of 14 degrees. In fact, the lift curve is flatter at the stall point. There is still a large drop-off in lift after stall, but an increase in lift into the deep post-stall α range indicates the droop is effective in improving the flow over the wing showing potential for some reduction in rolling moment asymmetries at higher α 's. Figure 8 shows the wing planform and stall pattern with the leading edge droop mounted. It is seen that the flow at the wing tip remains un-stalled until higher alphas, indicative that the droop is effective. The droop

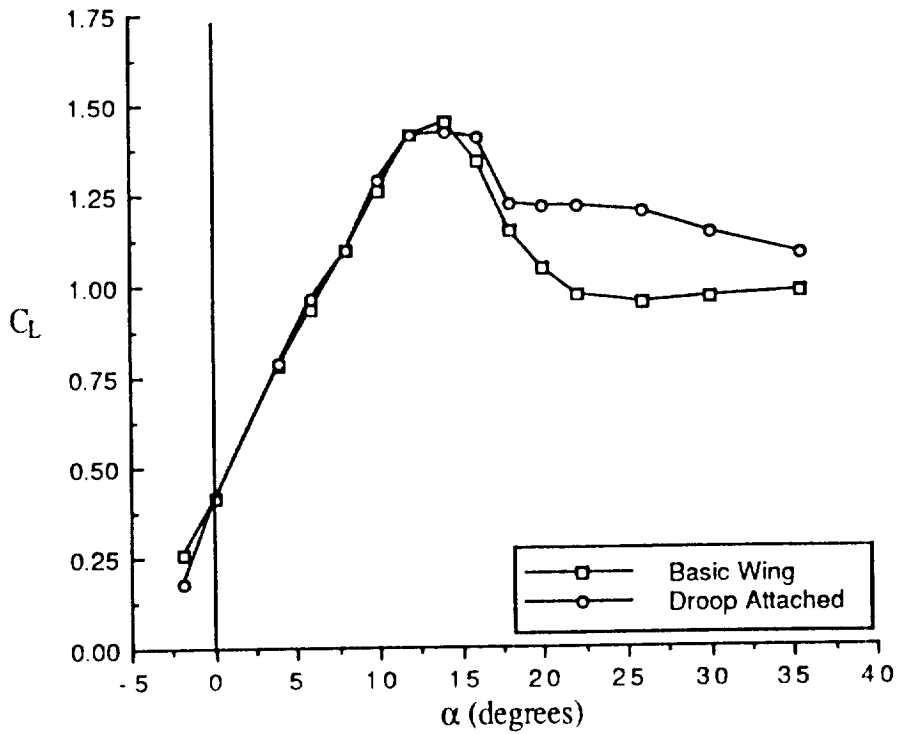


Figure 6 - Effect of Droop on Lift of Wing/Body, $\delta_f = 0^\circ$

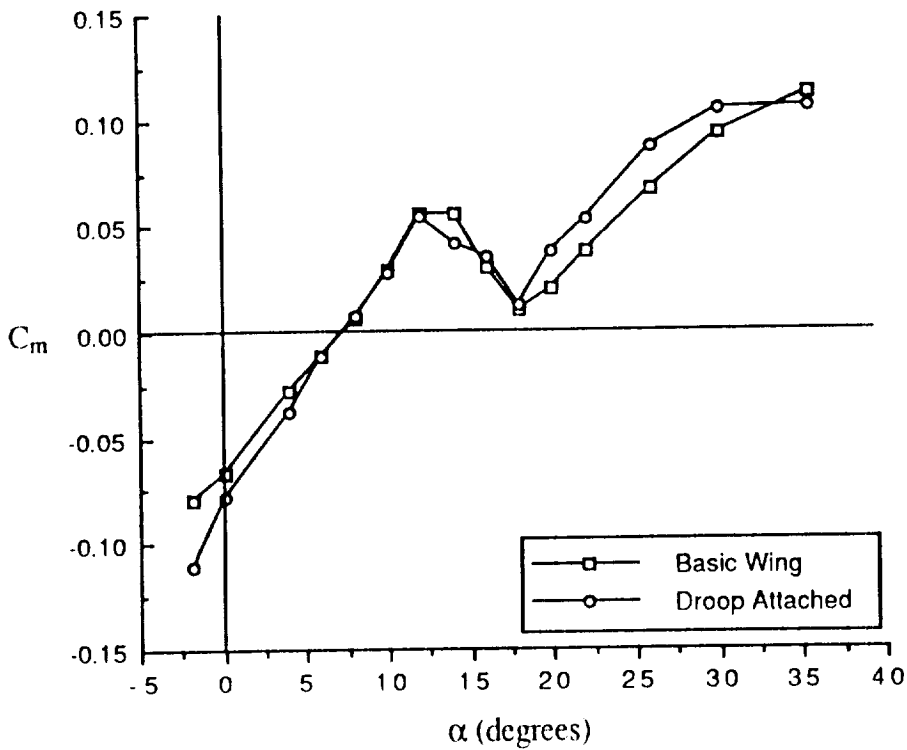


Figure 7 - Effect of Droop on Pitching Moment, $\delta_f = 0^\circ$

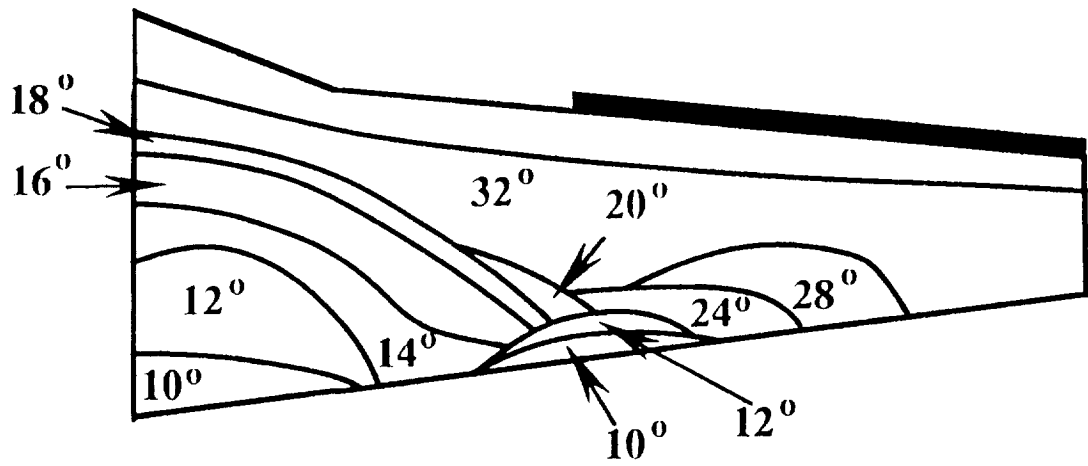


Figure 8 Wing Stall Pattern

is expected to improve roll tendencies at stall somewhat, but not to eliminate the problem entirely since the initial lift drop-off is still large. Without the droop, the pitching moment varies linearly with α until stall. At stall, there is a stable break in $C_{m\alpha}$ immediately followed by an unstable break. The leading edge droop has little effect on pre-stall pitching moment, but somewhat flattens out the breaks in $C_{m\alpha}$ at stall. The effect of the droop in the deep post-stall α range is simply a shift in the curve. There are no major improvements, but there are no detrimental effects either. Figure 9 shows is the drag curve for the configuration with and without the droop. There is no significant drag penalty with the droop attached. All remaining data will be presented with the leading edge droop installed.

Effect of Trailing Edge Flaps. Figures 10 and 11 represent the effect of the wing trailing edge flaps on the wing/body with pylon and nacelles. As expected, a flap deflection causes an increment in the lift curve due to increased circulation about the wing. The average increase in C_L prior to stall is 0.39 due to a 35 degree flap deflection. The maximum lift with 35 degrees of flaps increases to $C_{Lmax}=1.59$ at an α of 10 degrees. The stall pattern is more abrupt with flaps. The pitching moment curve shows a decrement in C_m due to a flap deflection. This result is expected and is caused by an increase in the aft loading on the wing when the flap is deflected, behind the center of gravity. The average change in C_m due to a flap deflection of 35 degrees is -0.038.

Effect of Droop on Lateral and Directional Characteristics. Figures 12 and 13 show the effect of the leading edge droop on C_l and C_n . At small angles of attack, both with and without the droop, C_l changes slightly with α . This tendency is to be expected to some extent with any configuration, due to characteristics of the configuration, irregular free-stream flow and misalignment of the model with the free-stream. At high angles, without the droop, there is a jump in C_l at an α of 20 degrees which indicates the possibility of roll departure. With the droop, a jump in C_l near stall still exists at higher alphas, but the jump is smaller, showing the effectiveness of the droop. There is a slight shift in C_n which is

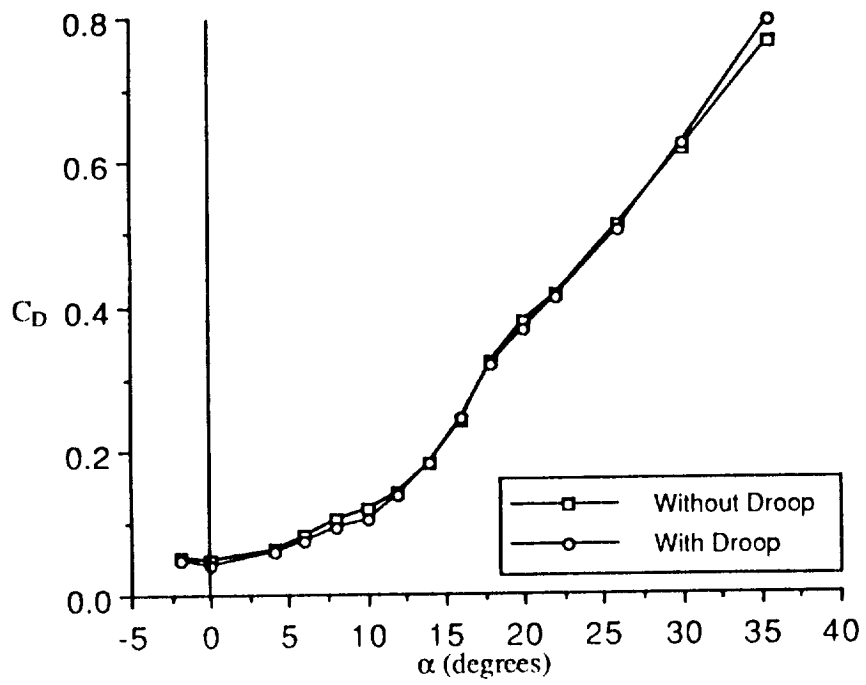


Figure 9 - Effect of Droops on Wing/Body Drag, $\delta_f = 0^\circ$

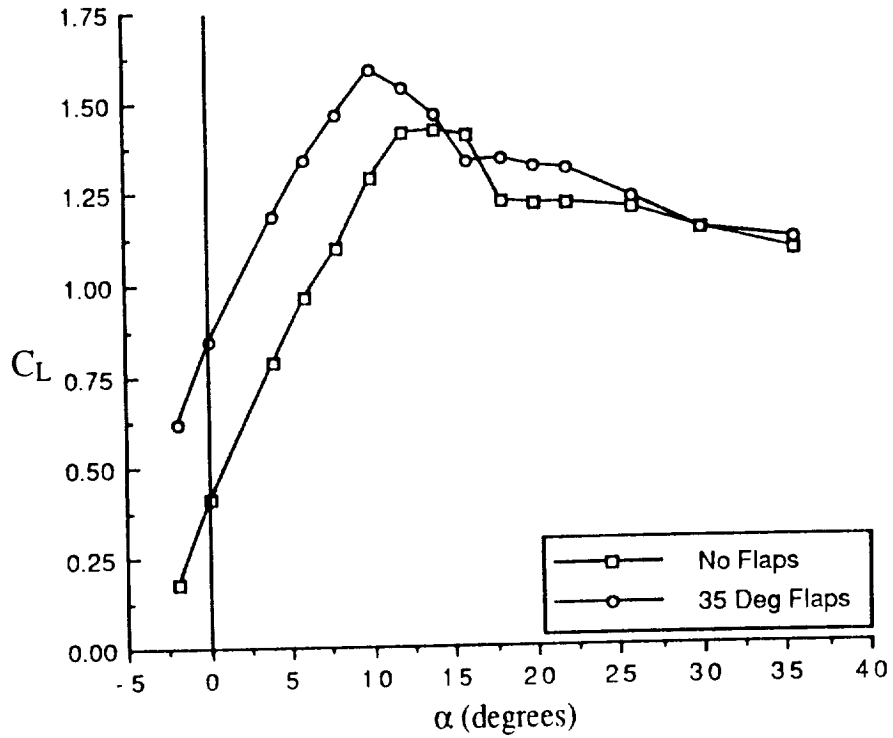


Figure 10 - Effect of Flaps on Lift of Wing/Body

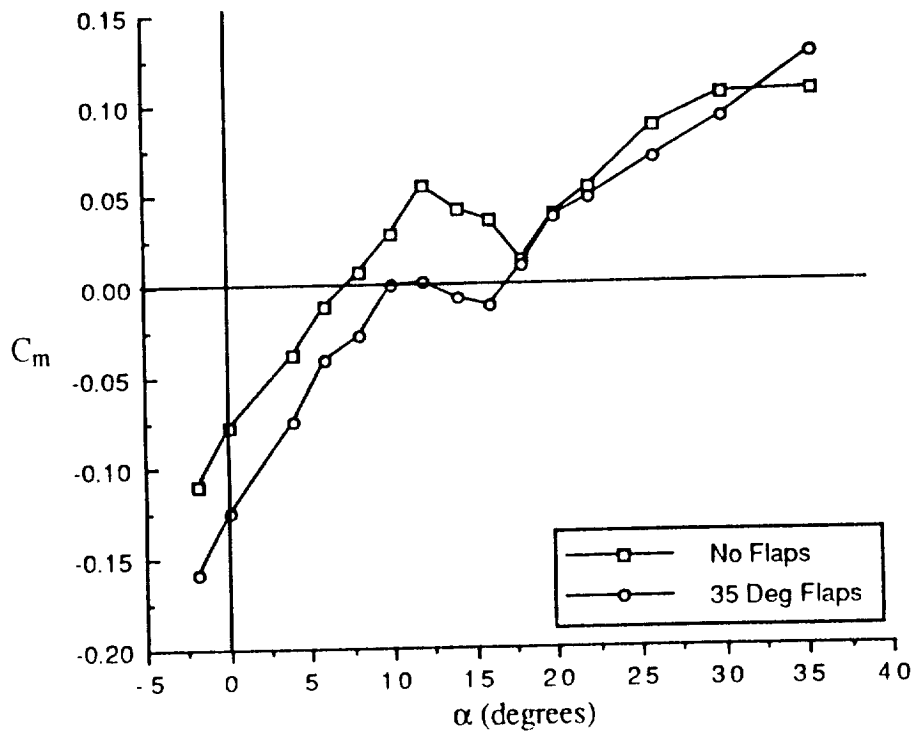


Figure 11 - Effect of Flaps on Pitching Moment of Wing/Body

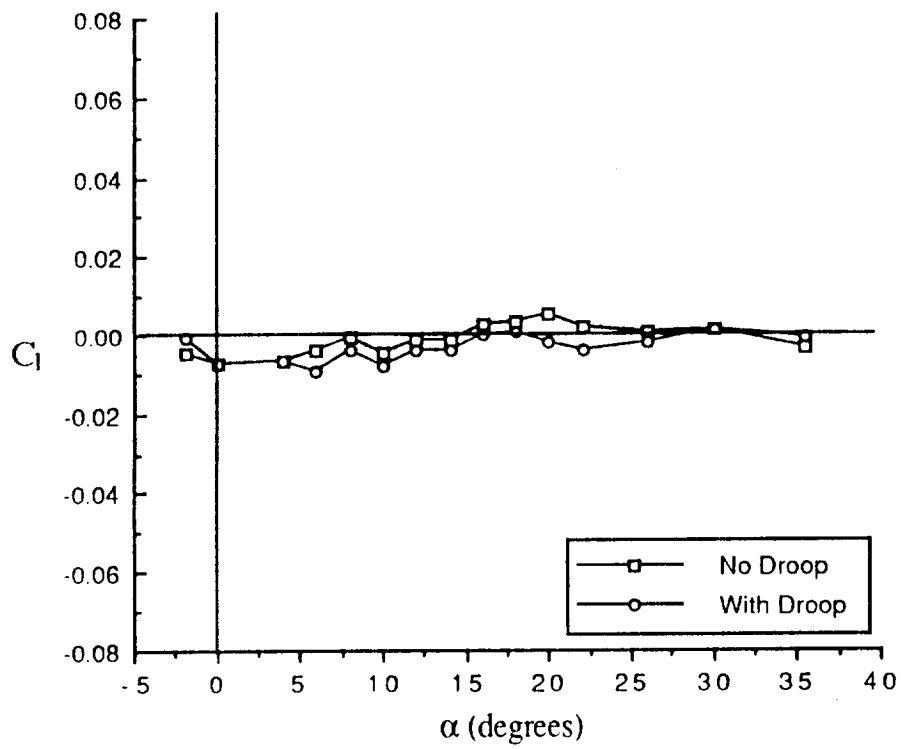


Figure 12 - Effect of Droops on Wing/Body Rolling Moment, $\delta_f = 0^\circ$

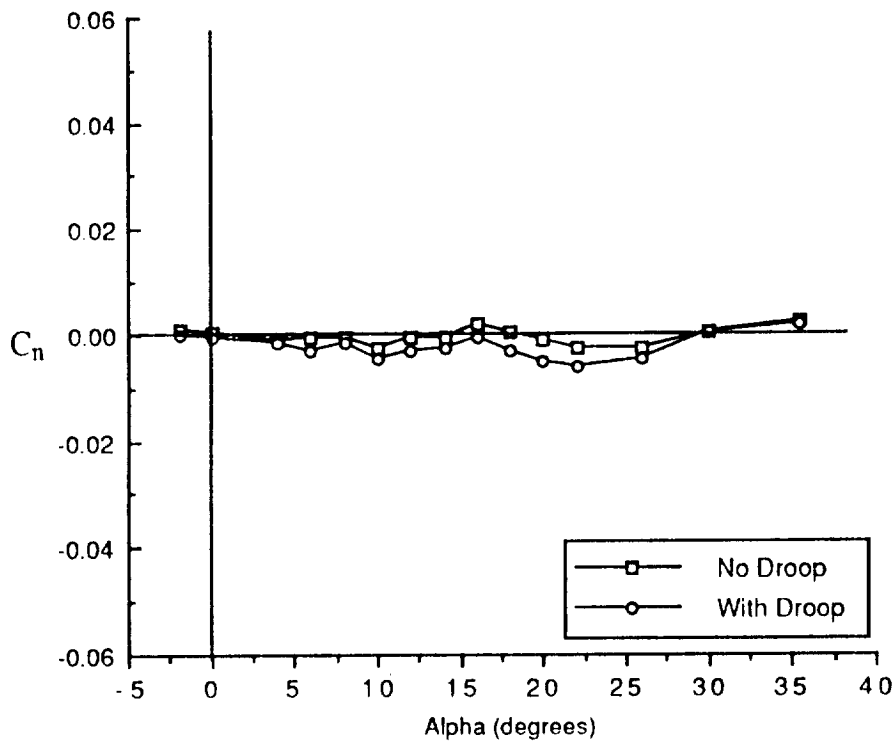


Figure 13 - Effect of Droops on Wing/Body Yawing Moment, $\delta_f = 0^\circ$

most likely due to the droops being slightly asymmetric. Another indication of the effectiveness of the droop is the increase in lateral stability ($-C_{l\beta}$) shown in figure 14 in the post-stall angle-of-attack region, α above 14 degrees.

Effect of Flaps on Lateral/Directional Characteristics. Figures 15 and 16 show the variation in C_n and C_l with and without flaps deflected. As expected, the flaps have little effect on C_n . The largest contribution to the yawing moment variation is the body, pylons, and nacelles, all of which have more vertical area ahead of and behind the CG. There is a noticeable affect on C_l . In the pre-stall region, the flaps provide an increment in C_l showing possible asymmetries in the model or free-stream flow. With flaps, the jump in C_l in the post-stall region is increased from the no flaps case. This shows possible asymmetric flap deflections and possibly a higher tendency to autorotate at stall with the flaps deflected. This result was anticipated to some extent by the increase in loss of lift at stall with the flaps deflected. Figures 17 and 18 show the effect of the flaps on directional and lateral stability. As expected, the basic wing/body is directionally unstable (negative $C_{n\beta}$) through most of the range of α . The flaps increase the directional stability slightly through most of the α range because there is a slight increase in the vertical area behind the CG when the flaps are deflected. The flaps are shown to increase the configuration's lateral stability.

Longitudinal Characteristics of the Unpowered Configuration

Effect of Elevator. The elevator for the configuration was split into two halves of nearly equal area to determine the effect of propeller blowing on the control surface effectiveness. The results presented in this section compare the full elevator to only the inboard elevator without power as a reference to later results with power. Figure 19 shows the configuration pitching moment curve with a variety of elevator settings. In the linear range of alphas for no elevator deflection, $C_{m\alpha}$ is -0.0921 which corresponds to a SM of 14.9%. For each case there is an increase in longitudinal static stability after stall because of the loss of positive C_m from to the wing. The graph shows the full elevator is capable of

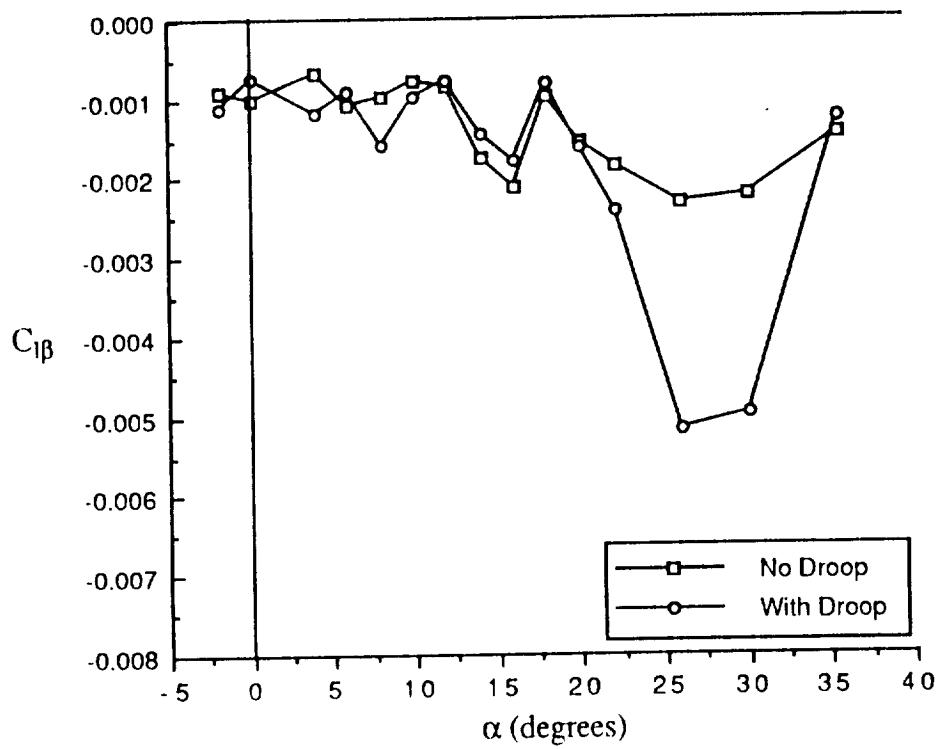


Figure 14 - Effect of Droops on Wing/Body Lateral Stability, $\delta_f = 0^\circ$

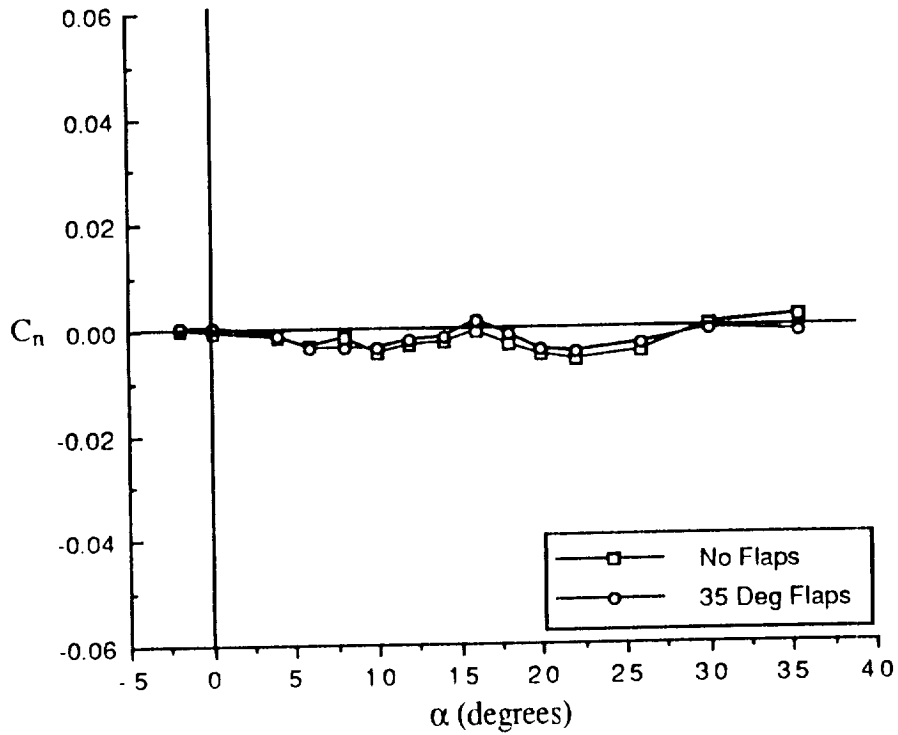


Figure 15 - Effect of Flaps on Wing/Body Yawing Moment, $\delta_f = 0^\circ$

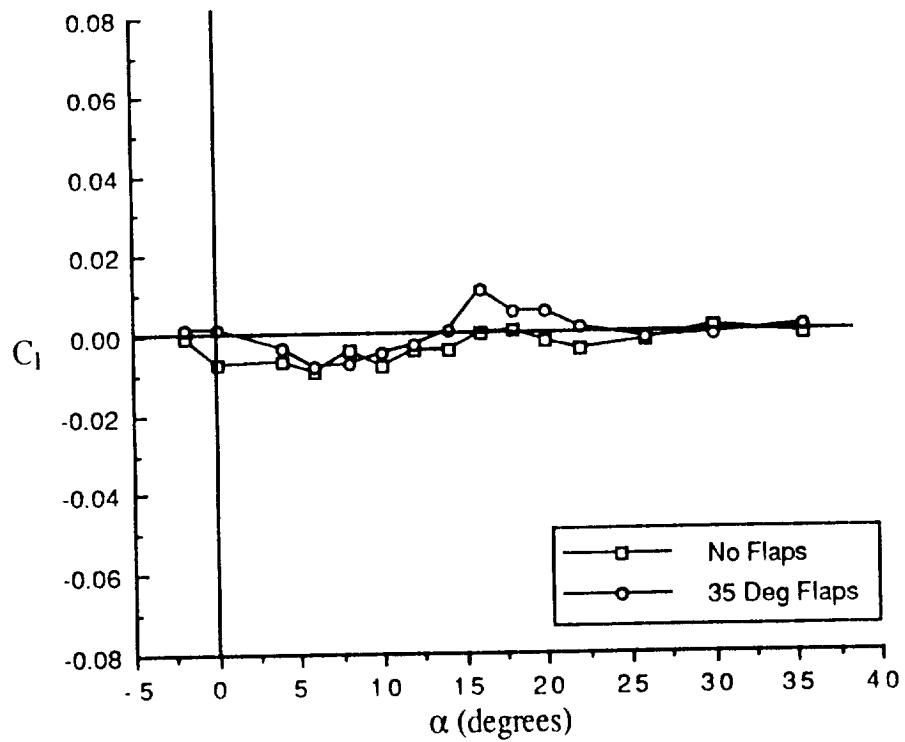


Figure 16 - Effect of Flaps on Wing/Body Rolling Moment, $\delta_f = 0^\circ$

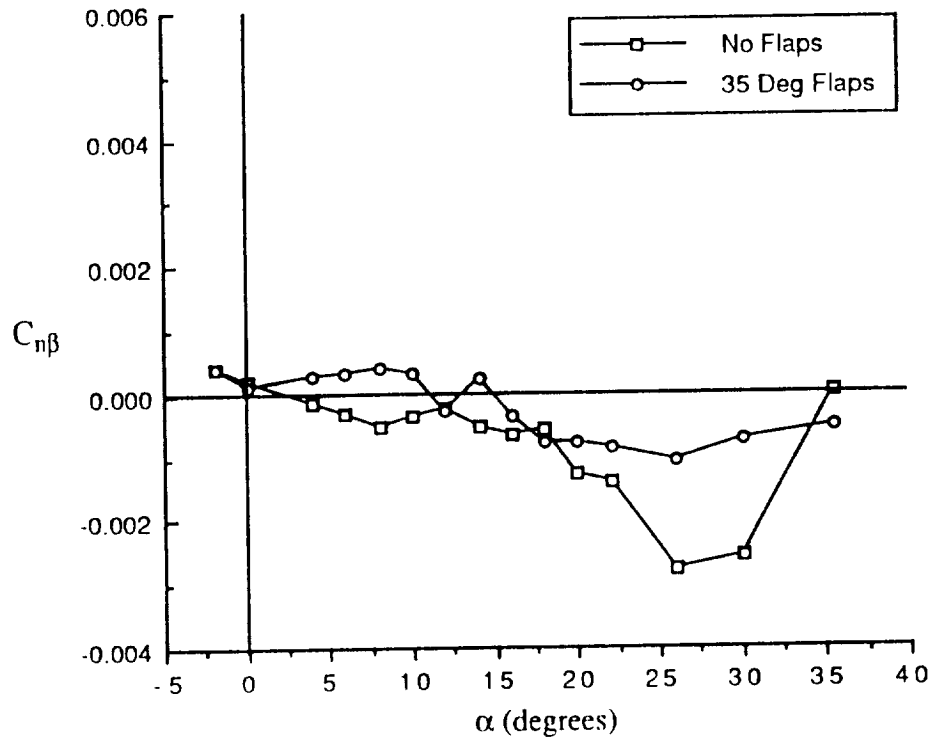


Figure 17 - Effect of Flaps on Wing/Body Directional Stability, $\delta_f = 0^\circ$

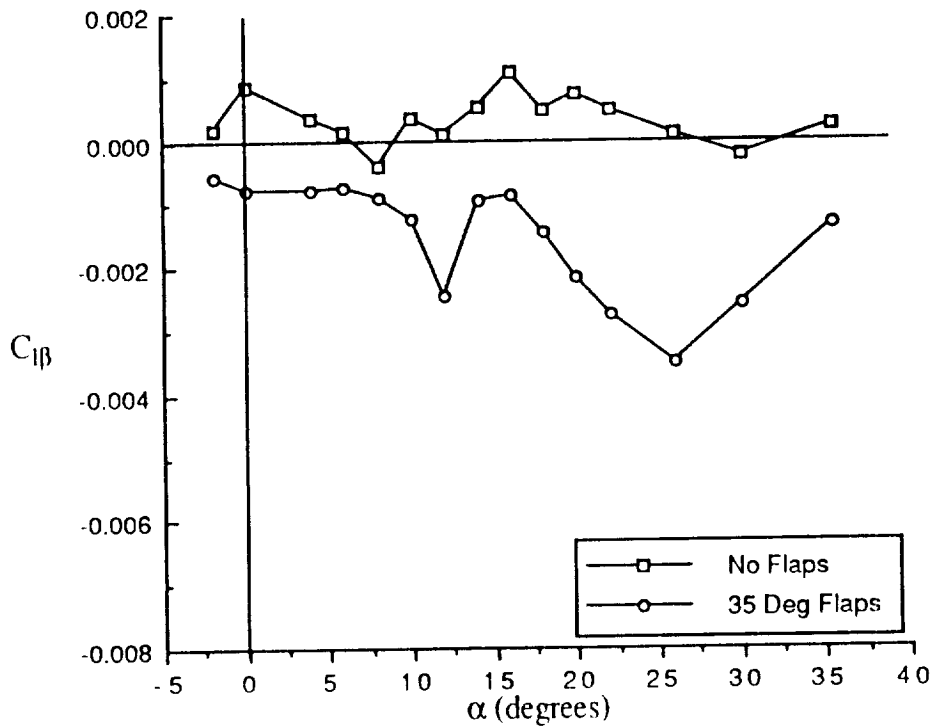


Figure 18 - Effect of Flaps on Wing/Body Lateral Stability, $\delta_f = 0^\circ$

trimming the aircraft to approximately 22 degrees α without power. The effect of elevator is basically a vertical shift in C_m , with some loss of effectiveness at higher angles. Figure 20 shows the elevator effectiveness for the full elevator as well as the inboard elevator. The effectiveness for both cases decreases smoothly through the α range with an anomaly at stall. The inboard elevator provides an average of 57% of the effectiveness of the full elevator. This percentage corresponds to the area ratio of the inboard elevator area to the full elevator area, which is 0.569.

Effect of Flaps. Figure 21 shows the effect of the wing trailing edge flaps on the configuration. As expected, the flaps cause an increment in lift through the linear range of α 's. There is no change in the $C_{L\alpha}$. The C_{Lmax} shifts from 1.52 at 14 degrees α without flaps to 1.62 at 10 degrees α with 35 degrees of flaps. The stall pattern with flaps is somewhat sharper than without flaps. This parallels the results found for the wing/body configuration. The flaps cause a nose-up pitching moment increment through most of the α range as indicated by figure 22. This effect is somewhat unexpected. Normally a nose-down change in pitching moment is expected because the flaps cause an increase in the aft-loading, behind the CG, on the wing. In fact, referring to figure 11, this is the result for the wing/body configuration of this model. The change in the effect of the flaps on pitching moment is due to the downwash effects on the horizontal tail. With the tail on, there is a positive shift in C_m due to the following: An increased downwash from the wing with flaps increases the down-loading on the horizontal tail. This increased down-loading is acting on a surface with a large V_H , with a corresponding large shift in C_m . For this configuration, the positive C_m change due to down-loading of the horizontal tail is larger than the negative C_m change due to the flaps, resulting in a net increment in C_m with flaps.

Lateral/Directional Characteristics of Unpowered Configuration

Effect of Rudder. The rudder for the configuration was split into two halves for the same reason the elevator was split. Here, the lower half of the rudder would have an increased effectiveness due to the propeller blowing. The results presented in this section

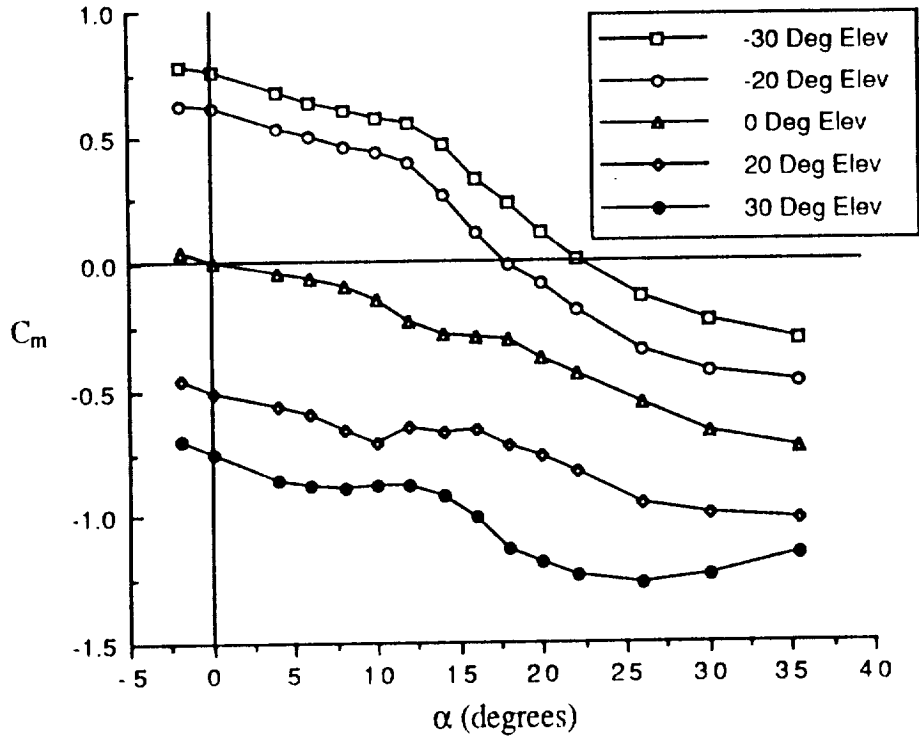


Figure 19 - Effect of Elevator on Configuration Pitching Moment, $\delta_f=35^\circ$

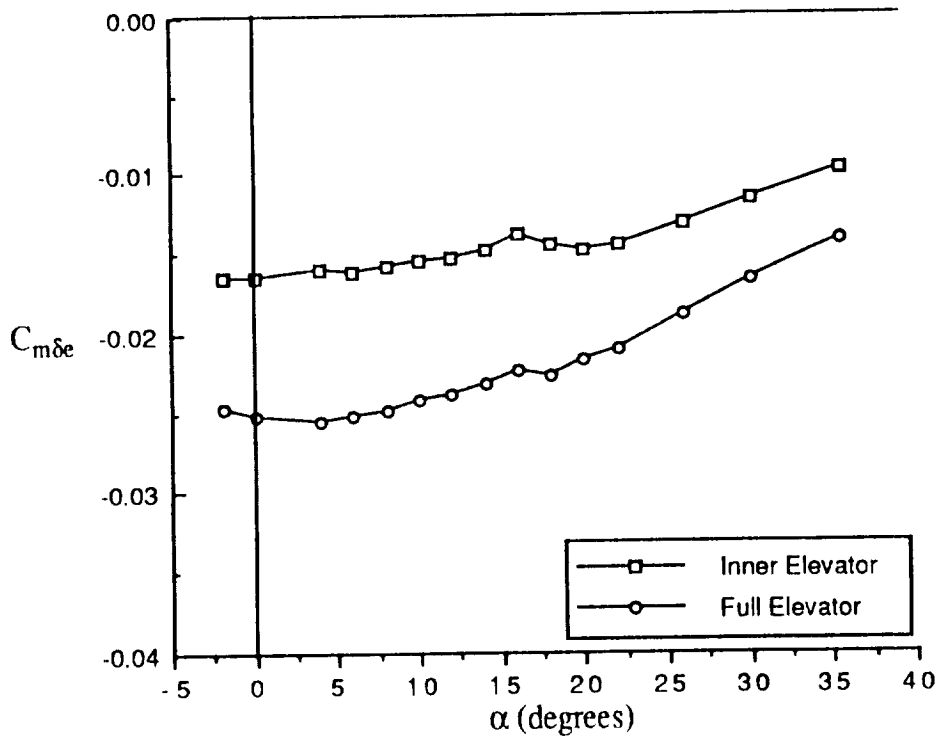


Figure 20 - Inboard and Full Elevator Effectiveness, $\delta_f=35^\circ$

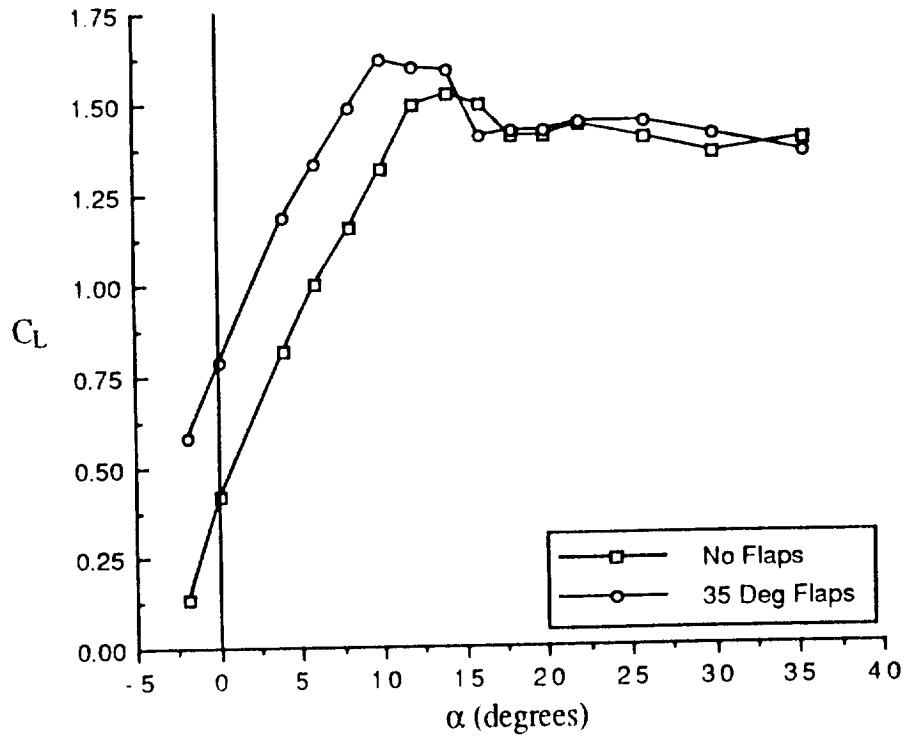


Figure 21 - Effect of Flaps on Configuration Lift

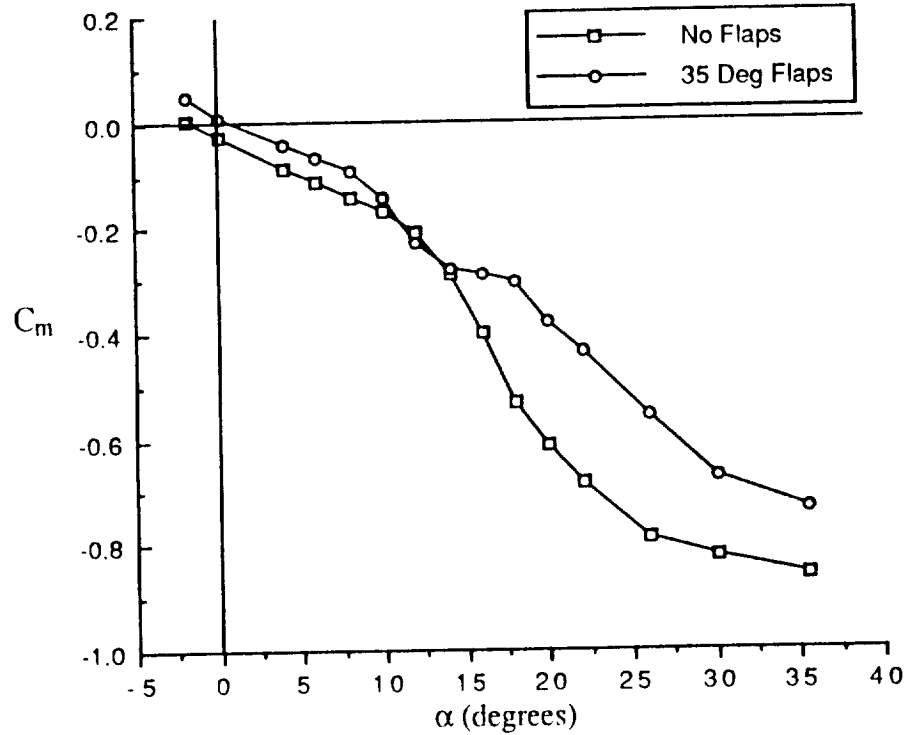


Figure 22 - Effect of Flaps on Configuration Pitching Moment

compare the full rudder to only the lower rudder without power as a reference to later results with power. Figure 23 shows the effect on C_n for a neutral rudder, full positive, and full negative rudder. It appears the rudder authority is constant through the useful range of α 's, and beyond stall to approximately 16 degrees α . Above 16 degrees, the authority drops off smoothly. Figure 24 shows a comparison between the full rudder effectiveness and the lower rudder effectiveness. The lower rudder provides an average of 62% of the effectiveness of the full rudder, and this ratio corresponds approximately to the ratio between the lower rudder area to the full rudder area which is 0.59. This plot as well shows the rudder effectiveness is constant to approximately 16 degrees α . The rudder loses effectiveness above the stall α because the vertical fin is embedded in the turbulent wake behind the wing and fuselage.

Effect of Ailerons. Figure 25 shows the rolling moment variation with neutral ailerons, 10 degrees ailerons, and 20 degrees ailerons. Figure 26 shows the aileron effectiveness through the angle-of-attack range. The ailerons are most effective at zero degrees angle-of-attack, and the effectiveness decreases approximately linearly with α . This reduction in aileron effectiveness with α is likely due to trailing edge separation. There is an anomaly at stall for both graphs which is probably due to model asymmetries. The slight increase in aileron effectiveness at 35 degrees α is another anomaly which was repeated by several different runs.

Effect of Power and the Direction of Propeller Rotation

Effect on Body/Pylon/Nacelle. Figure 27 shows the effect of power on the drag of the body alone with the pylons and nacelles. As expected, with power, the drag shifts to negative through most of the α range. This shows that there is enough thrust to induce acceleration. The thrust coefficient of the installed propellers at zero α , T'_c , is calculated as $T'_c = (C_D)_{\text{With Power}} - (C_D)_{\text{Props Off}}$. At any angle of attack, a negative value of $(C_D)_{\text{With Power}} - (C_D)_{\text{Props Off}}$ is an indication that the propellers are producing thrust. At a given alpha for two test cases, the lower value of $(C_D)_{\text{With Power}} - (C_D)_{\text{Props Off}}$ represents the case with the

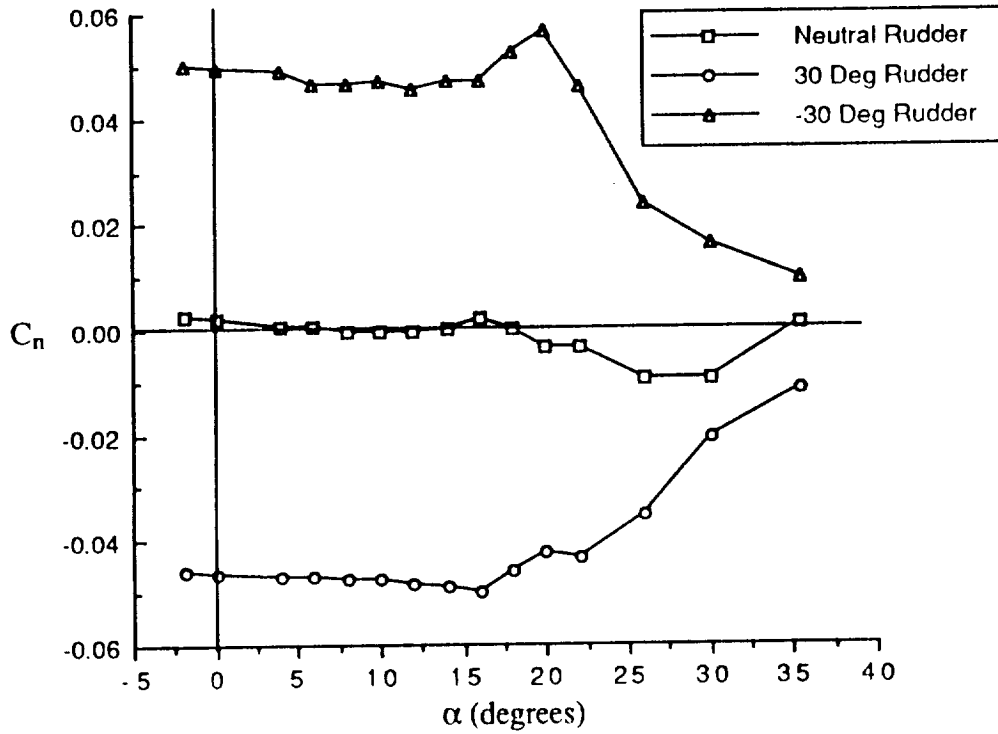


Figure 23 - Effect of Full Rudder on Configuration Yawing Moment, $\delta_f = 35^\circ$

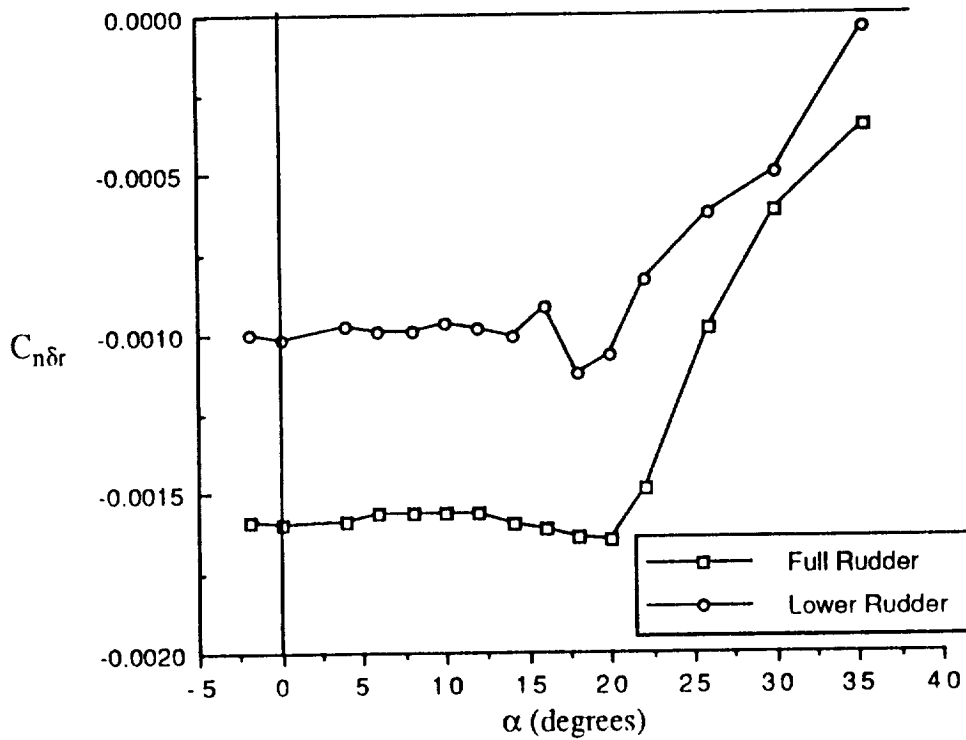


Figure 24 - Lower and Full Rudder Effectiveness, $\delta_f = 35^\circ$

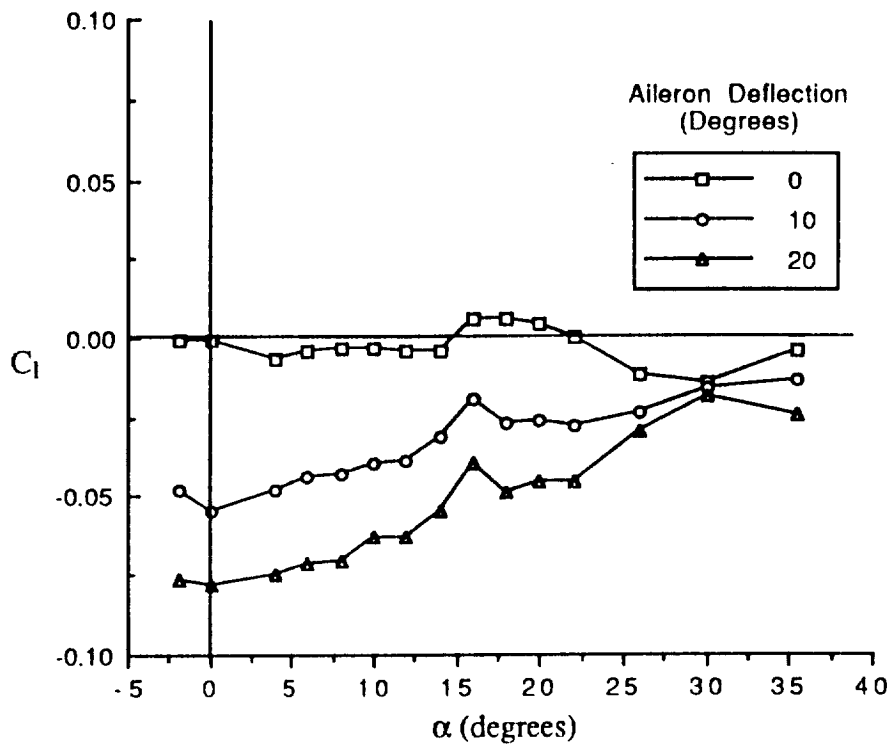


Figure 25 - Effect of Ailerons on Configuration Rolling Moment, $\delta_r=35^\circ$

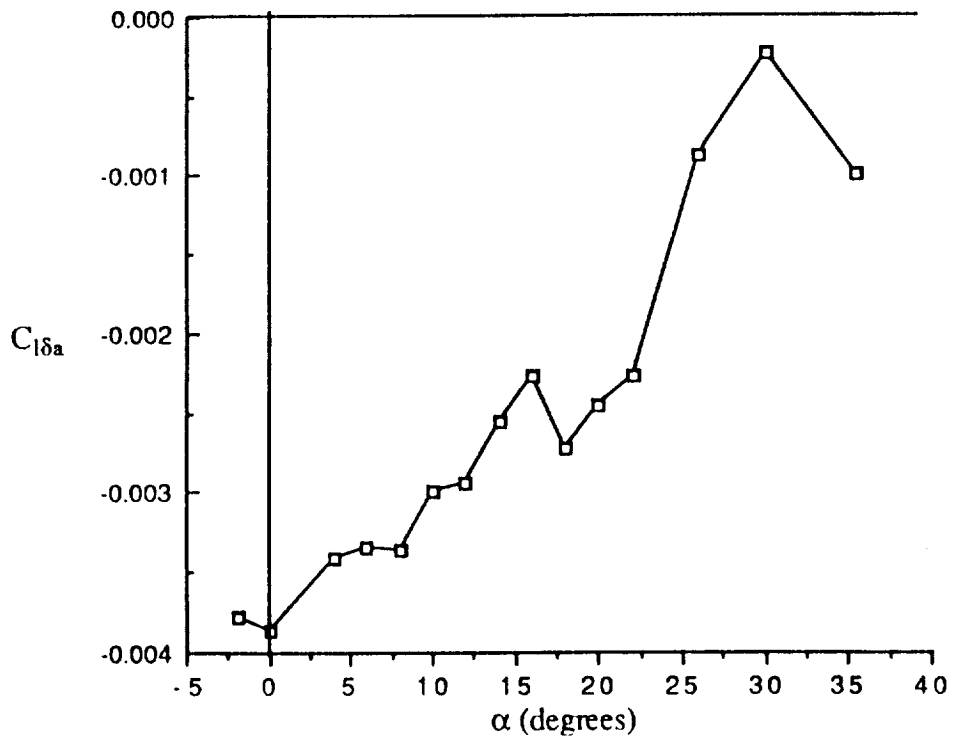


Figure 26 - Aileron Effectiveness, $\delta_r=35^\circ$

higher T'_c . From the graph, it is seen that at higher angles of attack, the case with the propellers rotating down outboard has much more installed thrust than the case with the propellers rotating down inboard. This is due to a "crossflow" effect which occurs with propellers at angle of attack. Figure 28 shows a propeller at a positive angle of attack. Due to the free stream flow and the rotation of the propeller, the down-going blade operates at a higher α than the up-going blade²². This means the down-going blade is more highly loaded than the up-going blades, and there is a higher pressure change across the down-going blades than across the up-going blades. This results in a "crossflow" behind the propeller disk from the down-going side (high pressure) to the up-going side (low pressure). Figure 29 shows that a diverging crossflow exists when the propellers rotate IBD, and a converging crossflow exists when the propellers rotate OBD. This results in a higher boat-tail drag for the IBD case compared to a lower boat-tail drag for the OBD case. Evidence of this crossflow is provided by the following. Previous investigations present results of a nacelle side force and yawing moment produced with a tractor propeller configuration^{16,23}. These forces and moments are caused by unequal pressure forces on either side of the nacelle, a characteristic of the crossflow phenomenon. Additionally, one report mentions a propeller tip free-vortex which moves away from the propeller centerline on the side of the up-going blades²⁴. For a two-propeller installation, vortices on opposite sides of the configuration would converge to the body with the propellers rotating OBD and would diverge with the propellers rotating IBD. Since a free vortex follows the local free stream velocity, this motion might well be evidence of the crossflow.

The difference in boat-tail drag between the two direction of rotation cases appears as a large difference in installed T'_c between the two cases. Theoretically, two free propellers at zero angle of attack rotating at the same speed would have the same thrust, regardless of direction of rotation. Looking back at figure 27, the T'_c for the IBD case at 4500 RPM is 0.41 and the T'_c for the OBD case is 0.45. The difference is due to slight angularity in the propeller inflow which causes the propellers to be at incidence relative to

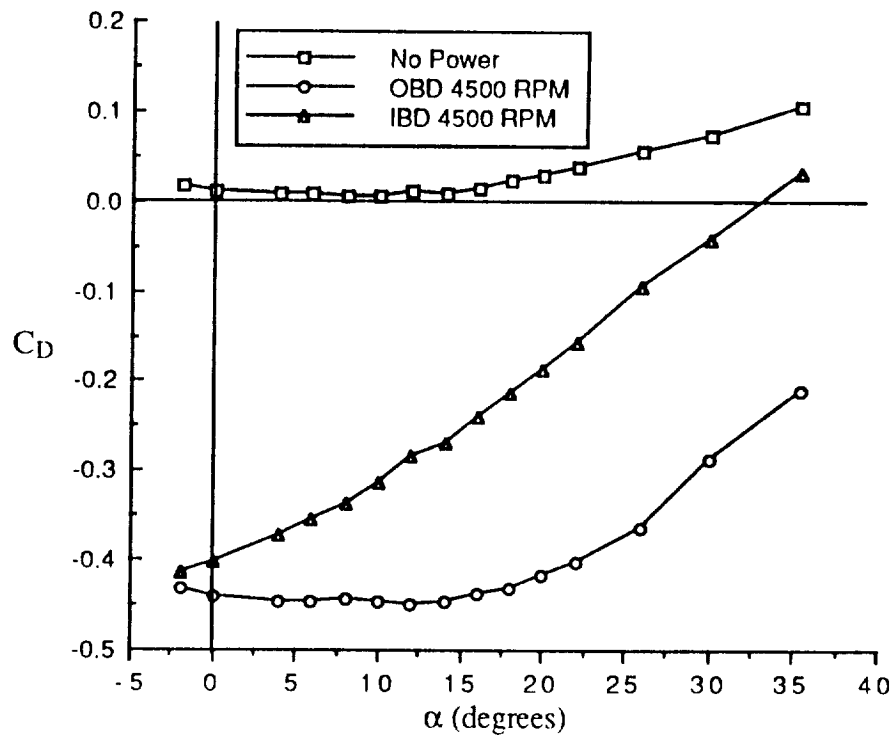
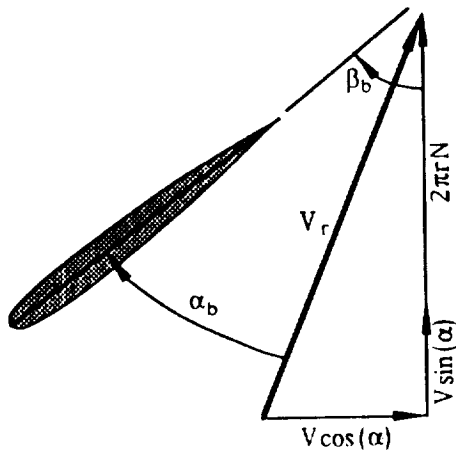
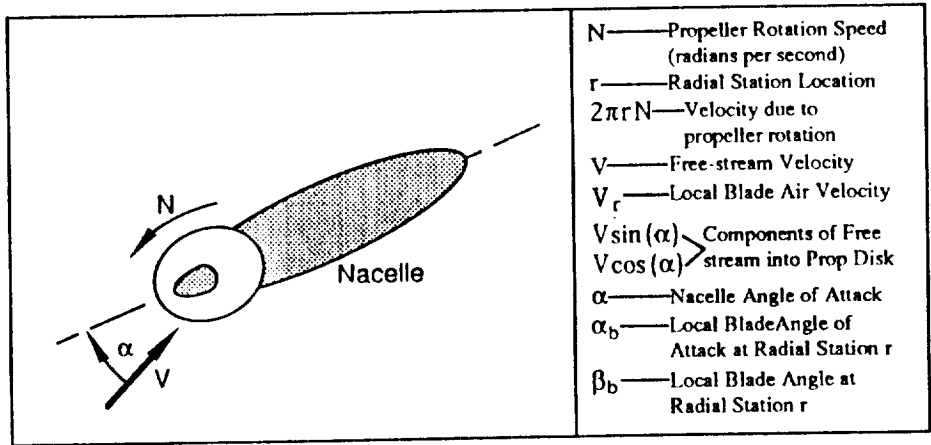
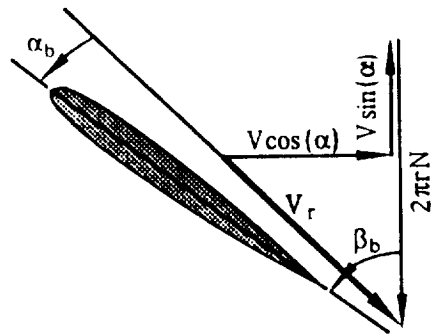


Figure 27 - Effect of Power on Drag of Body/Pylons/Nacelles



Down-Going Blade

$$\alpha_b = \beta_b - \tan^{-1} \left(\frac{V \cos(\alpha)}{2\pi r N + V \sin(\alpha)} \right)$$



Up-Going Blade

$$\alpha_b = \beta_b - \tan^{-1} \left(\frac{V \cos(\alpha)}{2\pi r N - V \sin(\alpha)} \right)$$

$$(\alpha_b)_{\text{Down-Going}} > (\alpha_b)_{\text{Up-Going}}$$

Figure 28- Illustration of a propeller at angle of attack (exaggerated)

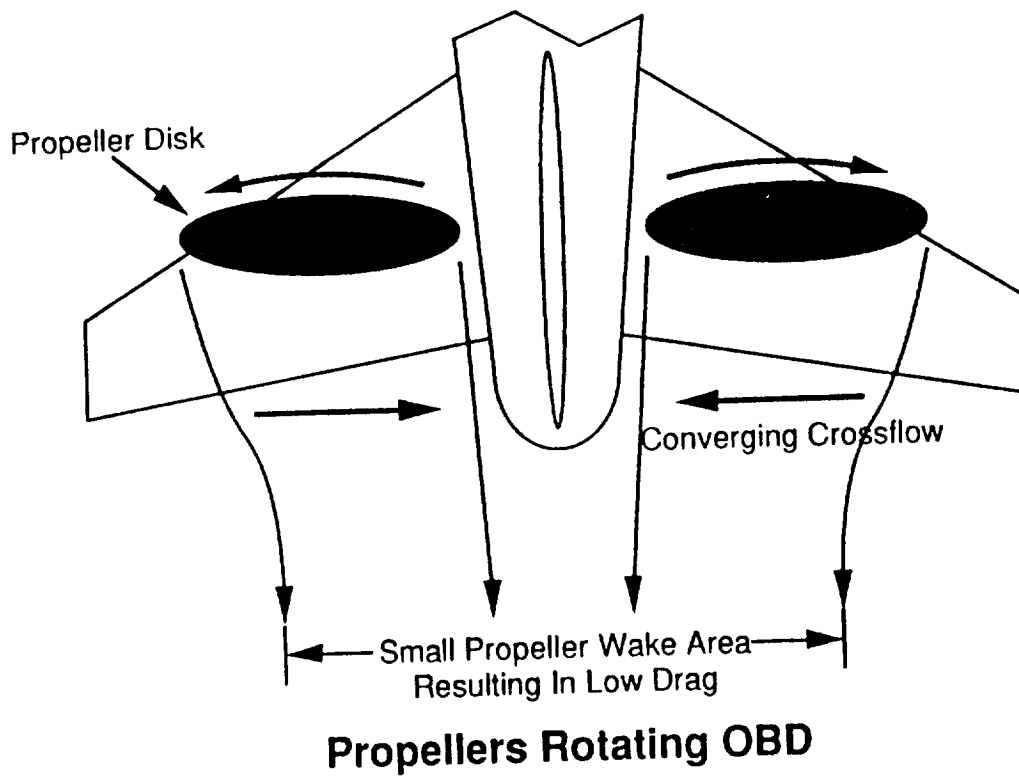
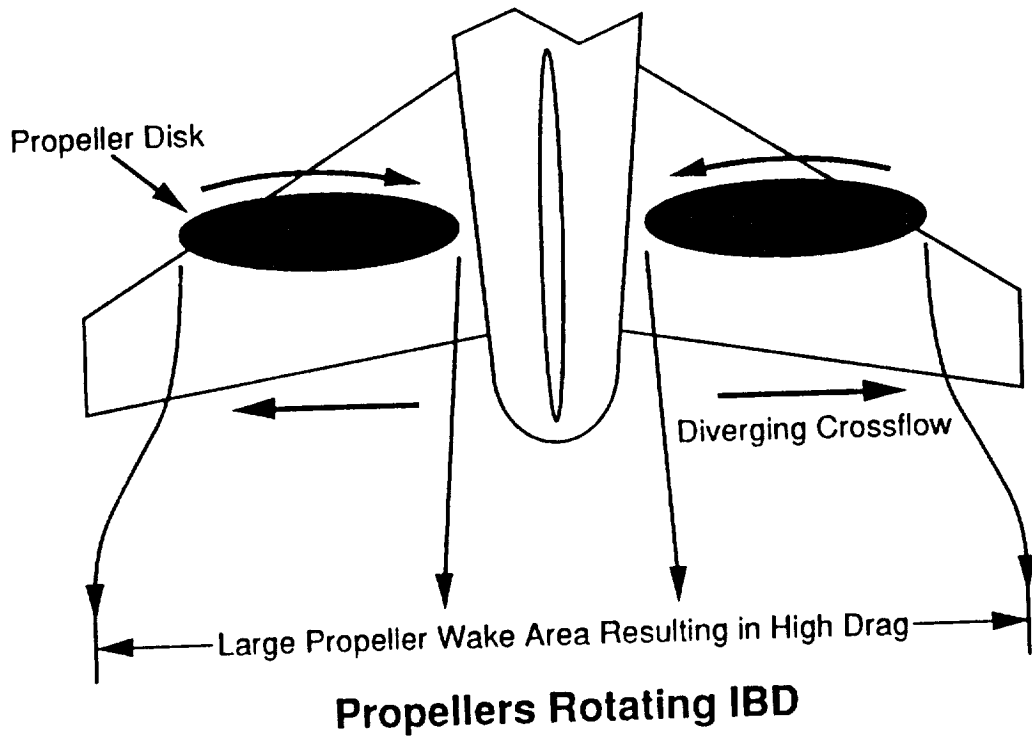


Figure 29 - Illustration of Crossflow Effect

the flow even when the configuration is at zero α . This angular inflow is an effect of the wake and downwash of the nacelles and pylons ahead of the propeller disk.

Figures 30 and 31 show the effect of power on C_L and C_m for the body alone with the pylons and nacelles. The body itself produces a small amount of lift which increases with α . The addition of power causes an increase in the slope of the lift curve. This increase in lift comes from the component of thrust acting in the direction of lift at α and from the propeller normal force which occurs at α . A small portion of the additional lift is due to an improved flowfield over the pylons with power. Plotted also on the C_L plot is the basic body lift added with the lift due to the thrust vector alone, with T'_c calculated from the drag data. The remaining lift above this line is due to the improved flow over the pylon and the propeller normal force. It is seen that these propellers are capable of producing a large amount of normal force, a characteristic of the wide, highly loaded blades. The shift in C_L at zero α is due to either the improved flow over the pylons or due to a slight angularity of the flow entering the propeller disk due to the pylon. A look at the C_m curve shows the props produce a negative shift in C_m . At zero degrees alpha, This is mostly due to the thrust vector being located above the CG. Also shown on the graph, by the dotted line, is the basic aircraft C_m plus the change due offset thrust, T'_c , and to the additional lift provided by the propeller normal force, C_{N_p} . The propeller normal force was assumed to be the total lift with power less the basic body lift and component of T'_c . This curve closely matches the shift in C_m and change in SM. The improved flow over the nacelles contributes to this stable change in $C_{m\alpha}$.

Effect on Longitudinal Characteristics of Full Configuration. Figures 32 and 33 show the effect of the direction of propeller rotation on the full configuration longitudinal characteristics. There is a slight change in $C_{L\alpha}$ from 0.098 to 0.105 per degree with full power. The direction of rotation does not affect the slope change. The lift at zero α is increased with power. This result is primarily due to the effect of the propellers blowing over the horizontal stabilizer since there can be no appreciable component of thrust or

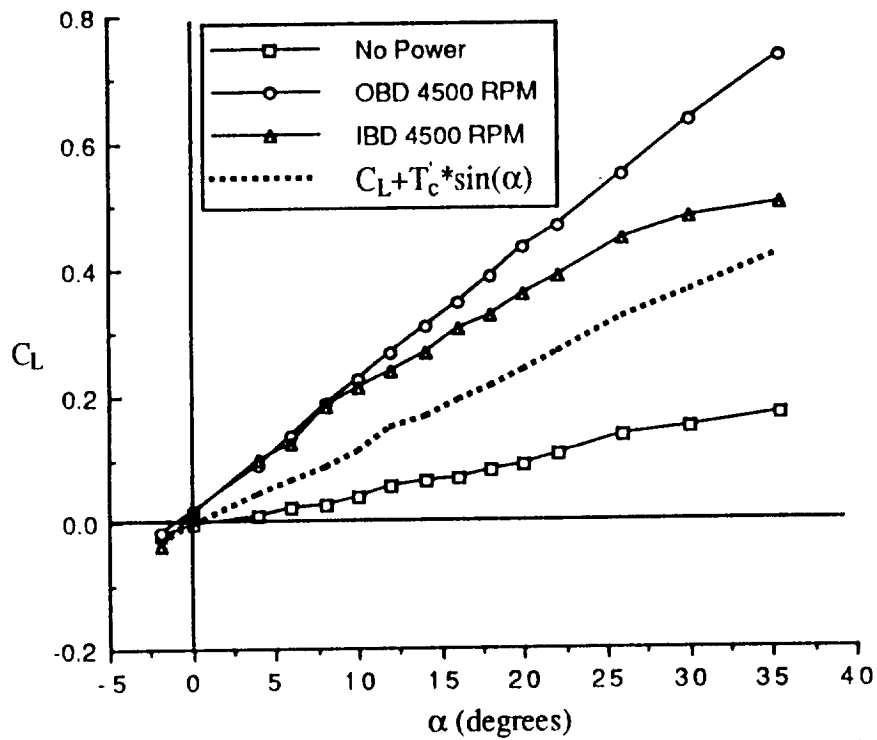


Figure 30 - Effect of Power on Lift of Body/Pylons/Nacelles

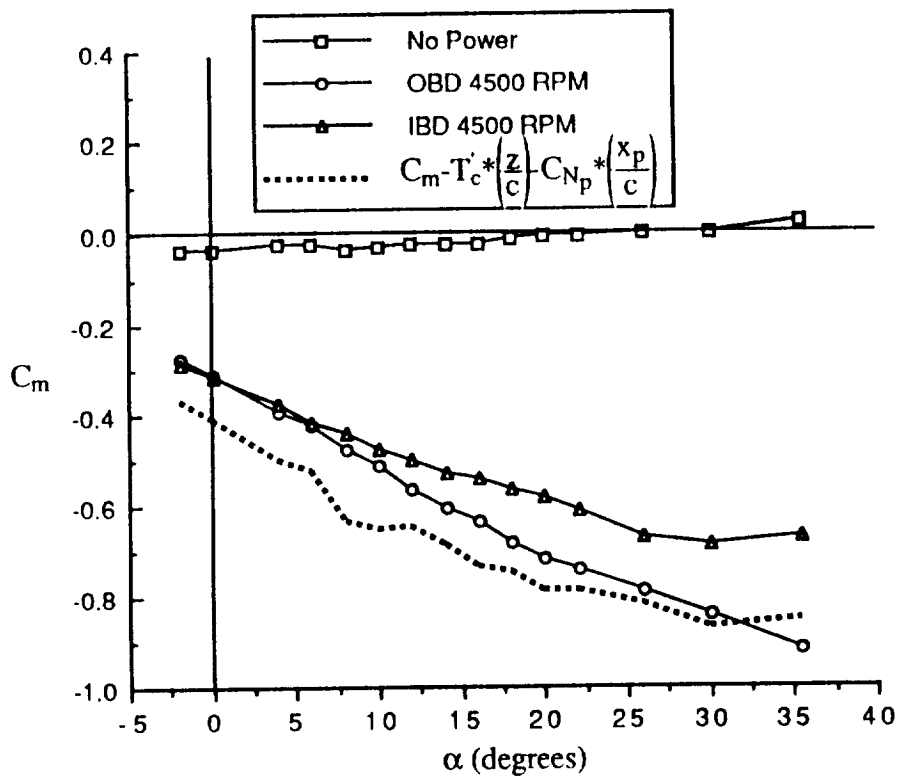


Figure 31 - Effect of Power on Pitching Moment of Body/Pylons/Nacelles

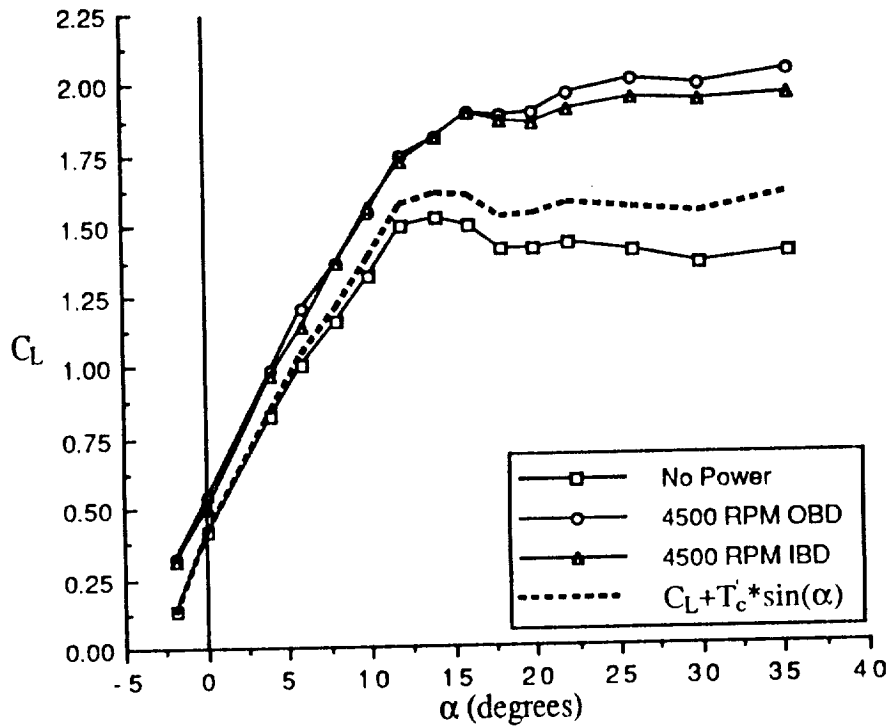


Figure 32 - Effect of Power on Configuration Lift, $\delta_f = 0^\circ$

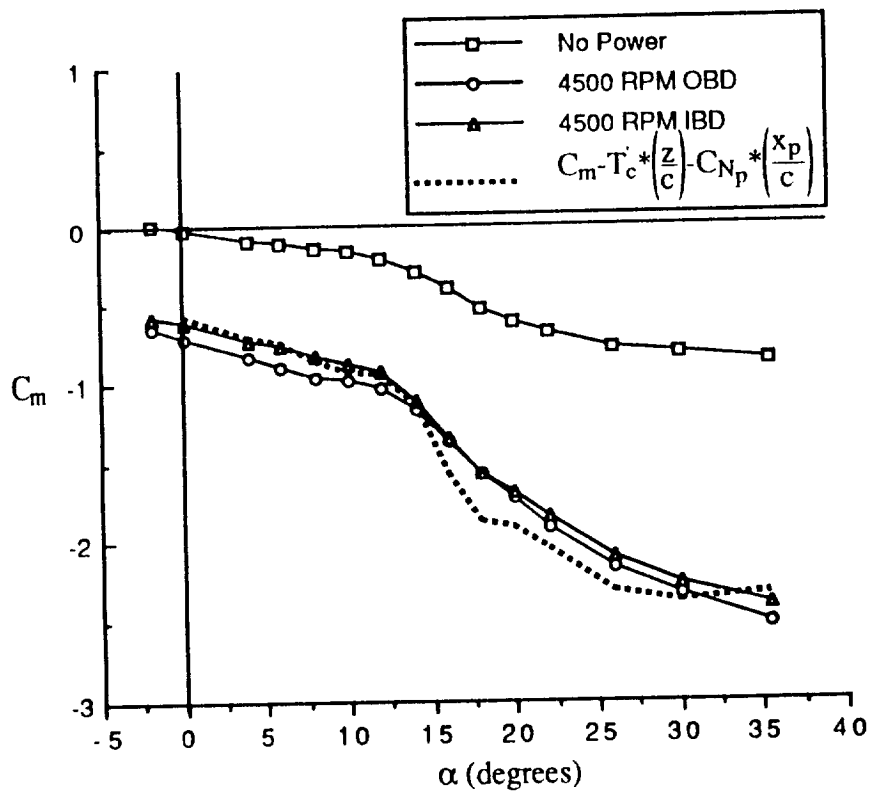


Figure 33 - Effect of Power on Configuration Pitching Moment, $\delta_f = 0^\circ$

propeller normal force in the lift direction at zero α . A look at the C_L curve at stall shows that there is no distinct configuration stall with power. In fact, the wing is stalling, but the propeller thrust and normal forces have components acting in the direction of lift. The basic power-off lift plus the component of thrust acting in the direction of lift, $T'_c \sin(\alpha)$, is also plotted on the graph. This is meant to show any post-stall lift increase which is not due to the thrust vector. In fact, more than half of the additional lift after stall with power is not due to the thrust vector, but rather due to the propeller normal force and increased stabilizer lift. This is again a characteristic of the highly loaded propeller blades. The difference between the IBD and OBD cases is not as significant for the full configuration.

A look at the pitching moment curve shows that power causes a large decrement in C_m , due to the thrust acting above the CG producing a negative moment and also to the increased lift on the horizontal tail which also produces a negative moment. With power, the stable break at stall is more pronounced, due to the improved flow and increased lift on the horizontal stabilizer and nacelles. Throughout most of the range of α 's, the OBD case shows a larger decrement in C_m . Also plotted is the basic C_m plus the decrement caused by the thrust vector, C_{N_p} , and increased stabilizer lift. The reason for plotting this curve is to show there is no significant change in C_m due to the wing or body.

Figure 34 shows the variation of drag with power. From the definition of T'_c , there is propeller thrust through most of the α range for both directions of rotation, but with the propellers rotating OBD, there is thrust through the entire range of α 's tested. This increased thrust with the propellers rotating OBD parallels the result found with the body alone. Here, because the horizontal stabilizer directs the propeller inflow, there is no difference in T'_c between the two cases at zero angle of attack. The value of T'_c is 0.34. The thrust here is lower than the body alone cases because of unfavorable interference of the wing wake with the propeller inflow.

Effect on the Lateral/Directional Characteristics of the Full Configuration. Figures 35 and 36 show the effect of power on the directional and lateral stability of the full

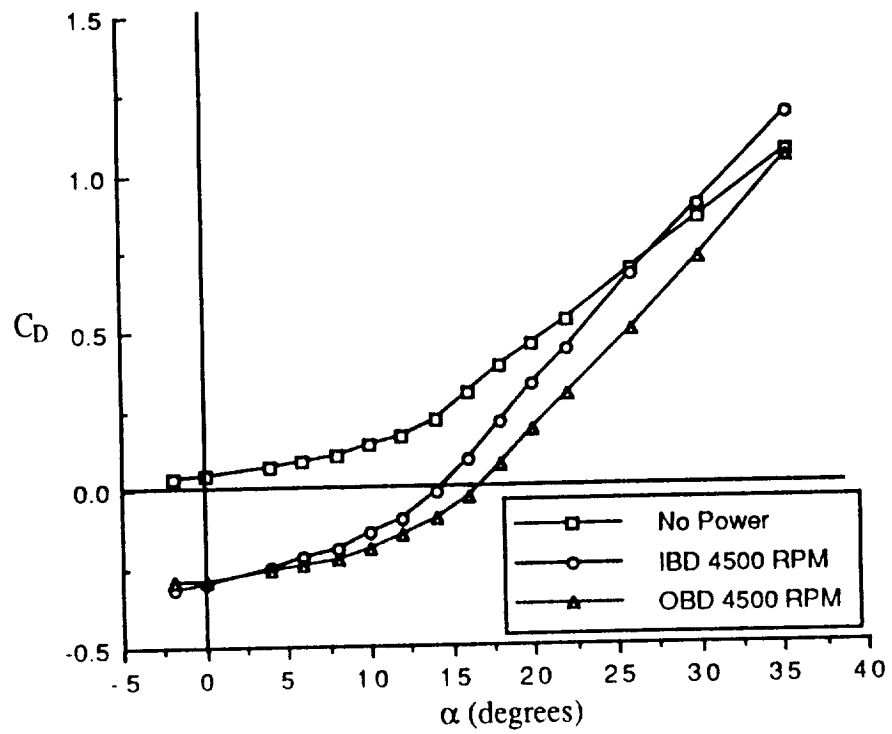


Figure 34 - Effect of Power on Configuration Drag, $\delta_f = 0^\circ$

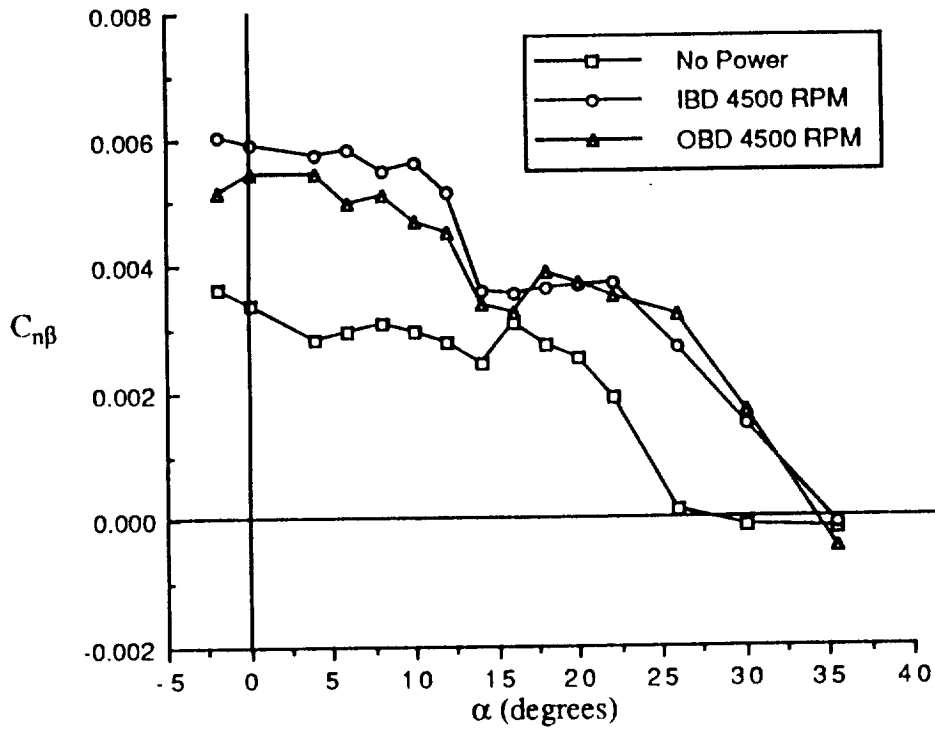


Figure 35 - Effect of Power on Directional Stability, $\delta_f = 0^\circ$

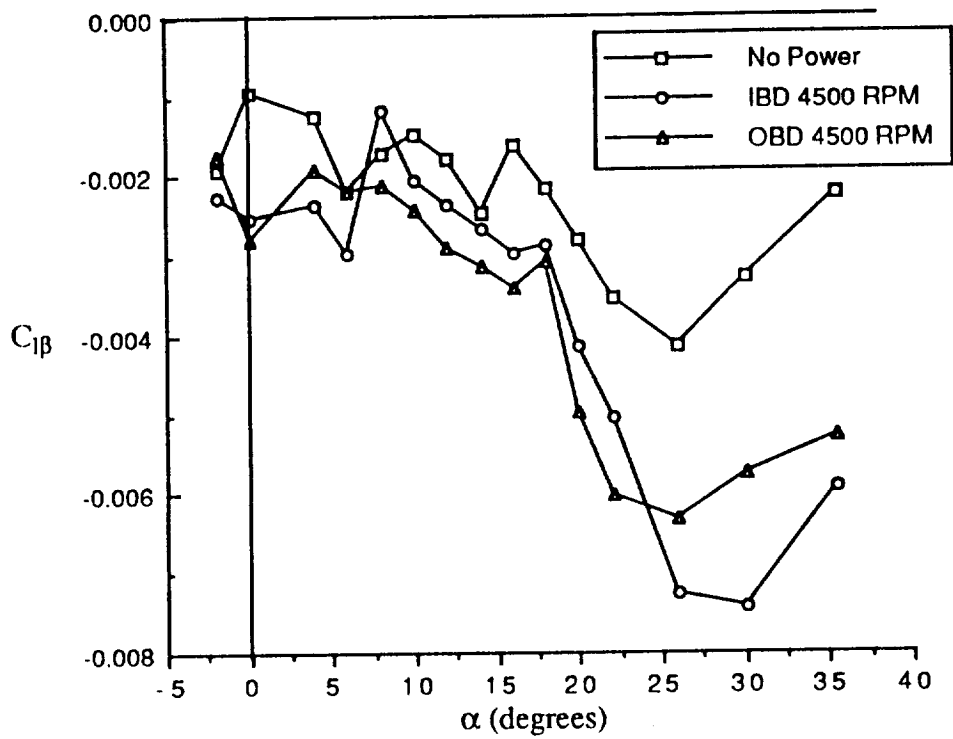


Figure 36 - Effect of Power on Lateral Stability, $\delta_f = 0^\circ$

configuration. Through the entire α range, there is an increase in directional stability, $C_{n\beta}$. When the aircraft is in sideslip the propellers produce a side force, similar to the normal force experienced with the propellers at α . This side force is behind the CG and therefore causes a restoring moment which increases $C_{n\beta}$. There is also an increase in lateral stability (negative $C_{l\beta}$) with power. This is a direct result of the thrust axis being located above the CG. Again, when the propellers are at sideslip, a side force is produced. This side force causes a restoring rolling moment which decreases $C_{l\beta}$.

Effect of Fillet Fairings on Propellers Rotating in Both Directions. Removeable fillet fairings were built which served as a duct for the flow between the propeller disk and the tail surfaces. The intention by ducting the flow was to confine the propeller slipstream to create a thrust increment from the cases without fillets. Figure 37 shows a slight thrust increment for the propellers rotating OBD with the fillets installed compared to the case without the fillets. With the propellers rotating IBD, there is actually a reduction in thrust for the case with fillets compared to the case without fillets. The fillets serve to enhance the crossflow effect described earlier. With the propellers rotating OBD, the flow converges into a smaller area yielding more thrust. With the propellers moving down inboard, the flow diverges outward further reducing the thrust. The T'_c for the IBD case is 0.32 and the T'_c for the OBD case is 0.37. The effect is similar when looking at the lateral and directional characteristics.

Characteristics of Final Configuration

The final configuration was chosen to be the case for the propellers rotating OBD with the fillets in place. This was chosen because of the greatly increased thrust at high alphas for the OBD rotation and for the enhanced crossflow effects with the fillets in place.

Effect of Fillets on full Configuration without power. Figures 38, 39 and 40 show the effect of the fillets on the longitudinal characteristics of the full configuration without power. There is no significant change in lift or drag. There is a slight negative shift in C_m through the alpha range.

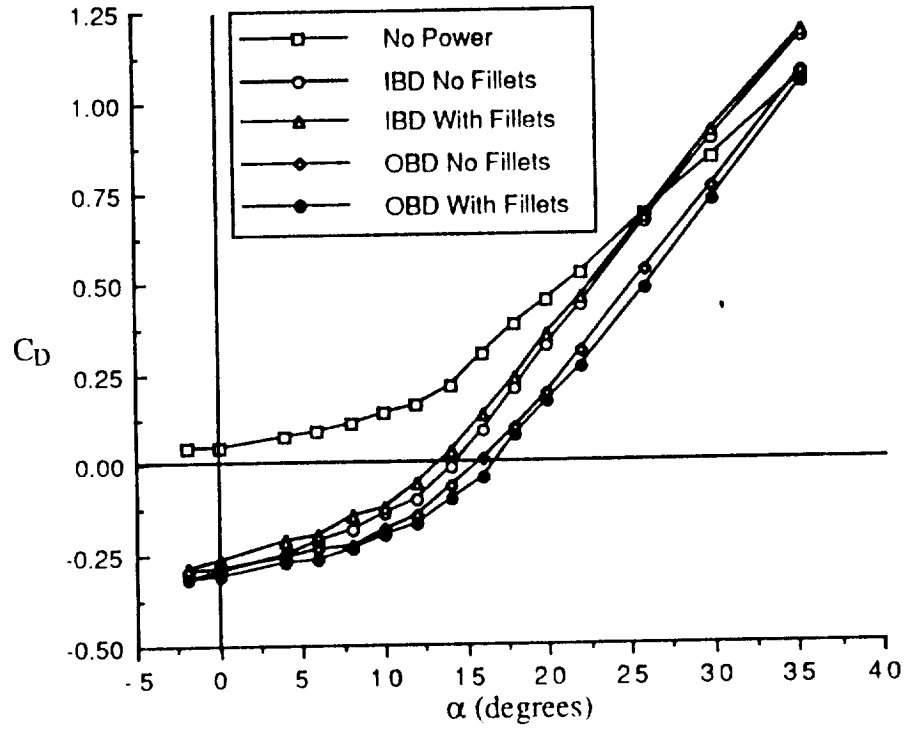


Figure 37 - Effect of Fillets on Drag and Installed Thrust, $\delta_f = 0^\circ$

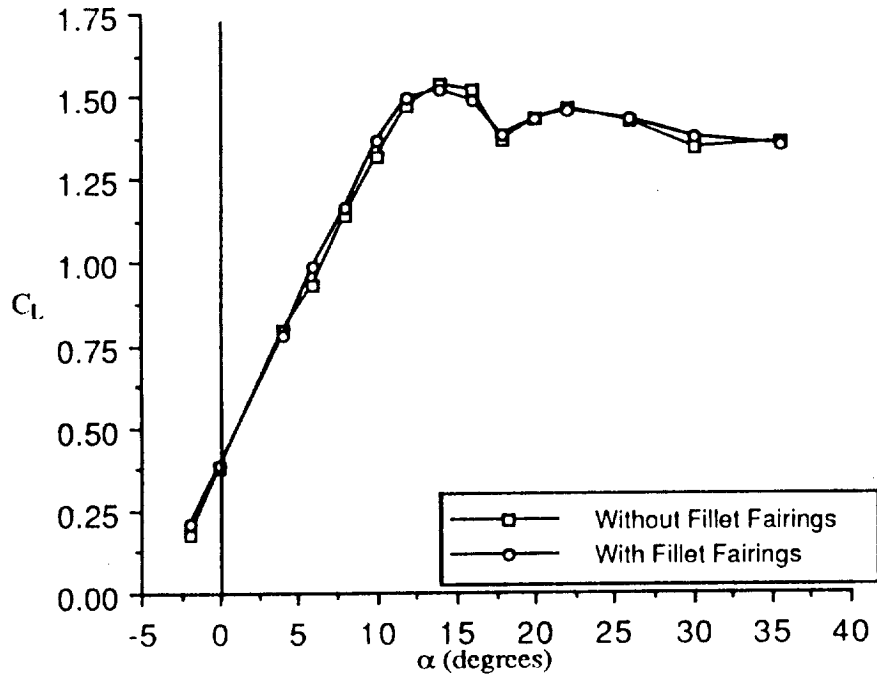


Figure 38 - Effect of Fillets on Full Configuration Lift, $\delta_f = 0^\circ$

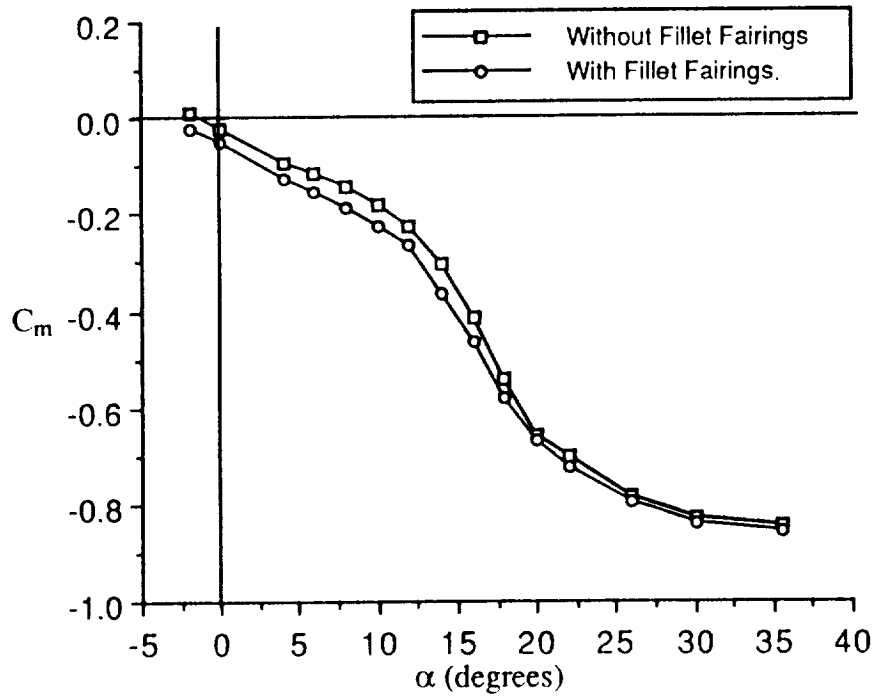


Figure 39 - Effect of Fillets on Configuration Pitching Moment, $\delta_f = 0^\circ$

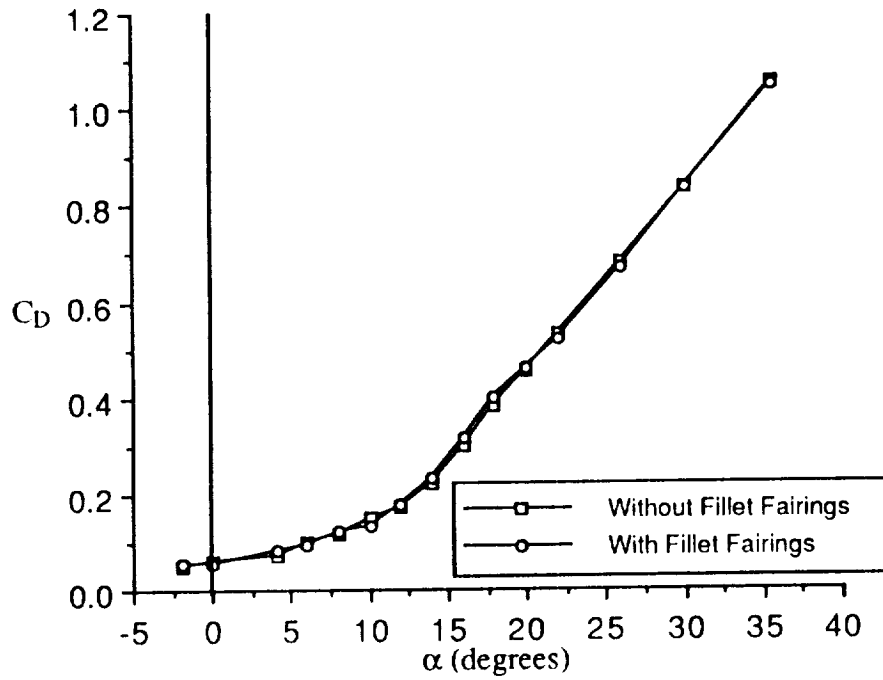


Figure 40 - Effect of Fillets on Full Configuration Drag, $\delta_f = 0^\circ$

Effect of Power on Longitudinal Characteristics. Figures 41, 42 and 43 show the effect of power on the longitudinal characteristics of the final configuration. The basic model with no power is seen to have a $C_{L\alpha}=0.098$ per degree with a $C_{Lmax}=1.52$ at a stall α of 14 degrees. The propellers rotating at 3500 RPM corresponds to a $T'_c=0.2$. There is a slight increase in $C_{L\alpha}$ to 0.103 per degree due to increased lift on the tail and propeller normal force. The zero α lift is increased from 0.385 to 0.493 due to increased lift over the horizontal tail. The propellers rotating at 4500 RPM corresponds to a $T'_c=0.37$. The value of $C_{L\alpha}$ is increased to 0.11 per degree. The zero α lift increases to 0.568 and is larger than the 3500 RPM case due of course to a larger blowing effect over the horizontal tail. For each of the power settings, the configuration exhibited a large negative shift in C_m for the entire range of α 's. This shift was due to the thrust line being located above the CG, increased lift on the horizontal stabilizer, and propeller normal force. This C_m change has a corresponding trim alpha change of approximately 25 degrees from the unpowered to the full power case. The large trim α change between the power off and power on cases may be severe enough to warrant an all-moving stabilizer if a prototype flying aircraft were built; however, a proper configuration design could minimize the trim change. There is an increase in longitudinal stability with power. The basic configuration has a $C_{m\alpha}=-0.0173$ per degree corresponding to a SM of 17.6%. With $T'_c=0.2$, $C_{m\alpha}$ decreases to -0.0263 per degree and a SM of 25.5%. With $T'_c=0.37$, $C_{m\alpha}$ decreases further to -0.0305 per degree and a SM of 27.7%. The large increase in SM with power could result in dynamic control sluggishness in flight. The static trim problem will be discussed in more detail when describing the elevator effectiveness below. The drag curve shows that the propellers produce thrust through the entire range of α 's, and induce acceleration through approximately 13 degrees for 3500 rpm and 18 degrees for 4500 rpm.

Effect of Power on Lateral/Directional Characteristics. Figures 44 and 45 show the effect of power on the lateral and directional characteristics of the final configuration. There is a positive increment in C_n for each of the power settings. The probable cause of

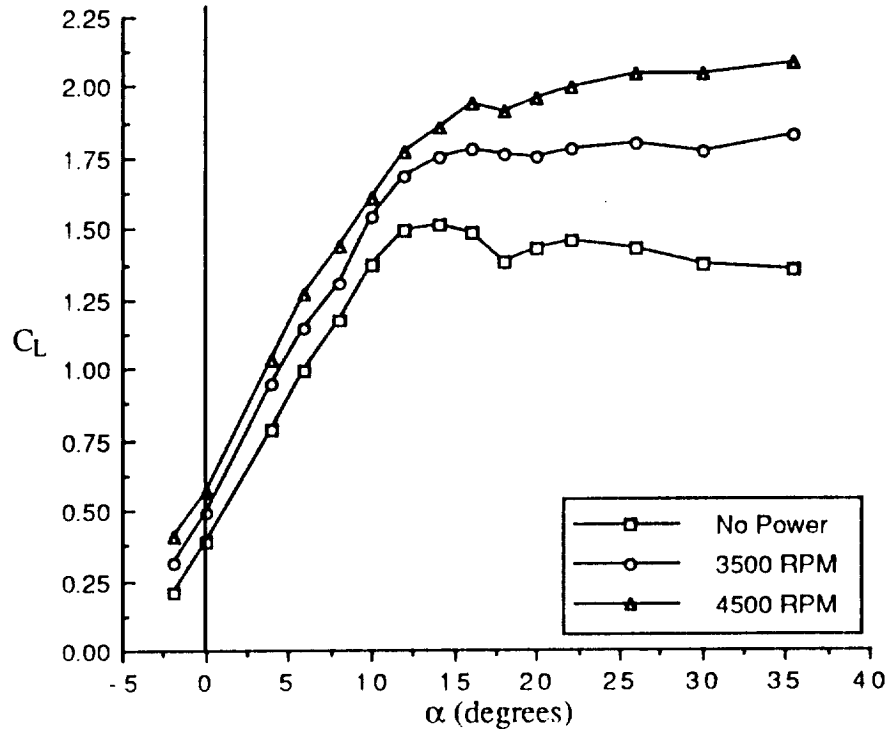


Figure 41 - Effect of Power on Final Configuration Lift, $\delta_f=0^\circ$

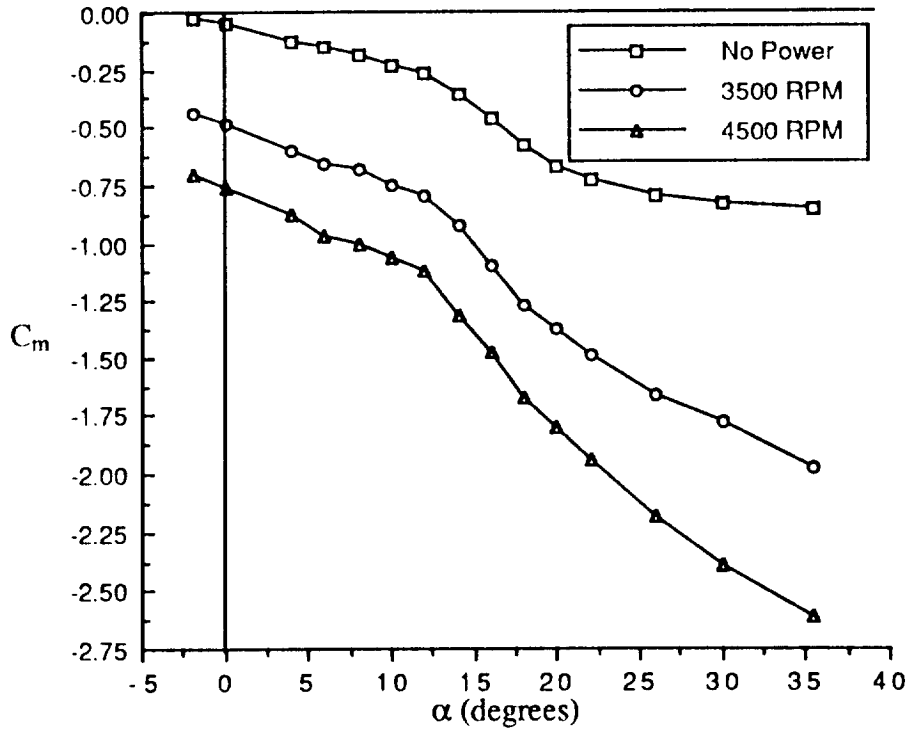


Figure 42 - Effect of Power on Final Configuration Pitching Moment, $\delta_f=0^\circ$

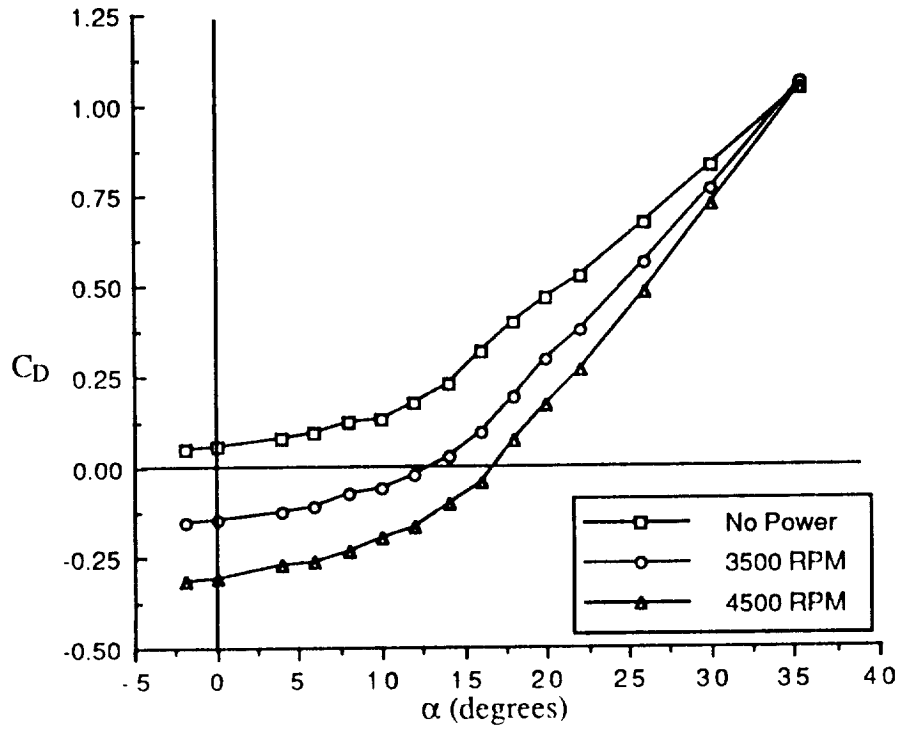


Figure 43 - Effect of Power on Final Configuration Drag, $\delta_f = 0^\circ$

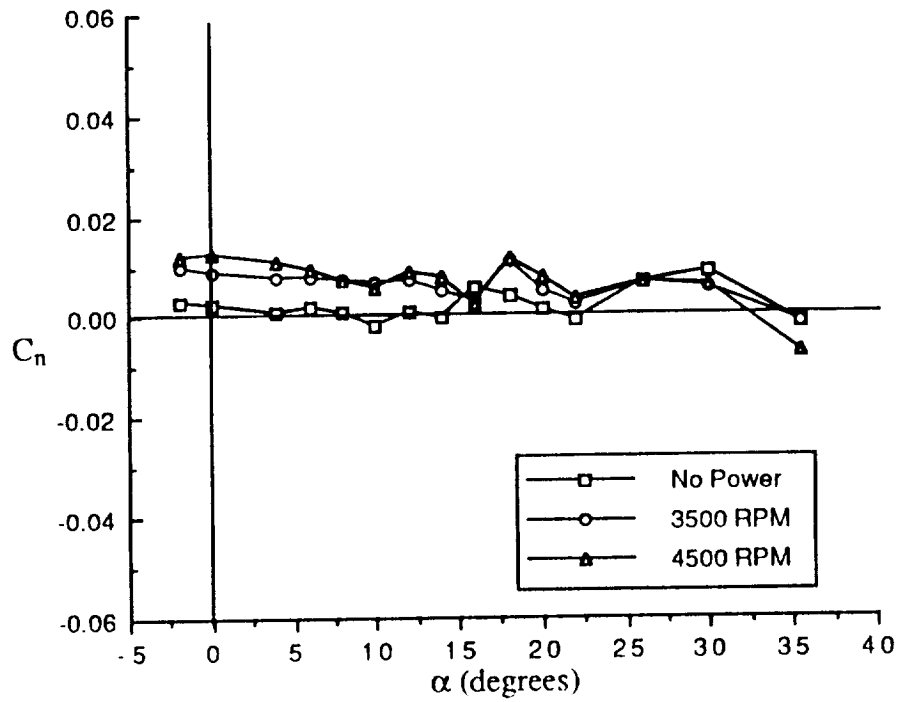


Figure 44 - Effect of Power on Yawing Moment, $\delta_f = 0^\circ$

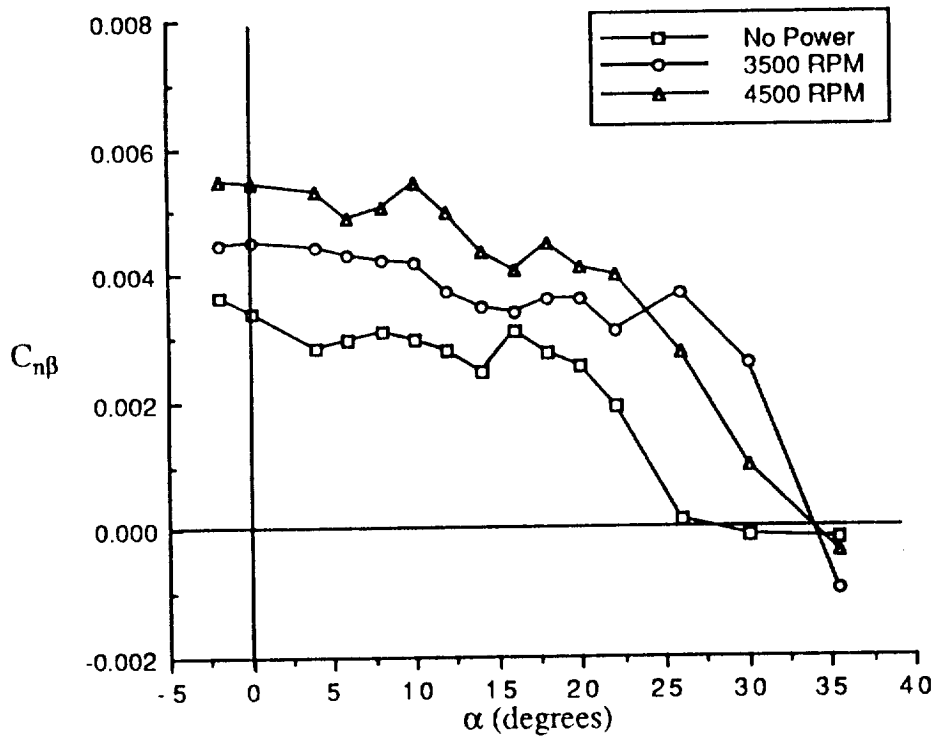


Figure 45 - Effect of Power on Directional Stability, $\delta_f = 0^\circ$

this increment comes from one of the reasons described below. The propellers each consisted of a complex hub/pitch adjustment assembly which allow the blade angle to be varied: however, the blades could only be locked down in certain positions. The construction of the blades did not allow both the left and right assemblies to be set at “exactly” the same blade angle. For this reason, there was a slight difference in the blade angle between the two hub assemblies. In addition, the propellers were driven by separate air turbines which were supplied pressure from different sources. In a situation such as this, it is impossible to regulate the propellers so that each air motor was running identically at the same speed. Thus, there was a difference in thrust from one side of the model to the other which resulted in an increment in yawing moment. A similar effect occurs for higher α 's in rolling moment. As expected, power increases the directional stability, $C_{n\beta}$, due to the propeller side force when the model was in sideslip. An increase was also seen in lateral stability .

Effect of Flaps. As seen in figure 46, the flaps decrease $C_{L\alpha}$ from 0.098 per degree to 0.086 per degree. There is a shift in C_L due to flaps of 0.41 with 35 degrees flaps. With 35 degrees of flaps, C_{Lmax} is increased to 1.64. There is only a slight change in the shape of the C_L curve at stall indicating the droop is still effective in the landing configuration. A look at the pitching moment curve in figure 47 shows the same effect as figure 22 above, an increase in pitching moment through the entire range of α 's with flaps deflected. As described earlier, this increase is due to the increased down-loading on the horizontal tail with a large V_H . There is no large change in SM with flaps.

Effect of Flaps on Lateral/Directional Stability. Figure 48 shows the flaps slightly increase the directional stability through the low and high α 's. This is because the flaps slightly increase the vertical area behind the CG providing a larger restoring C_n . Figure 49 shows the lateral stability is not affected significantly.

Effect of rudder on Directional Characteristics. Figure 50 shows the rudder authority with a full rudder deflection and the rudder effectiveness for the full rudder and

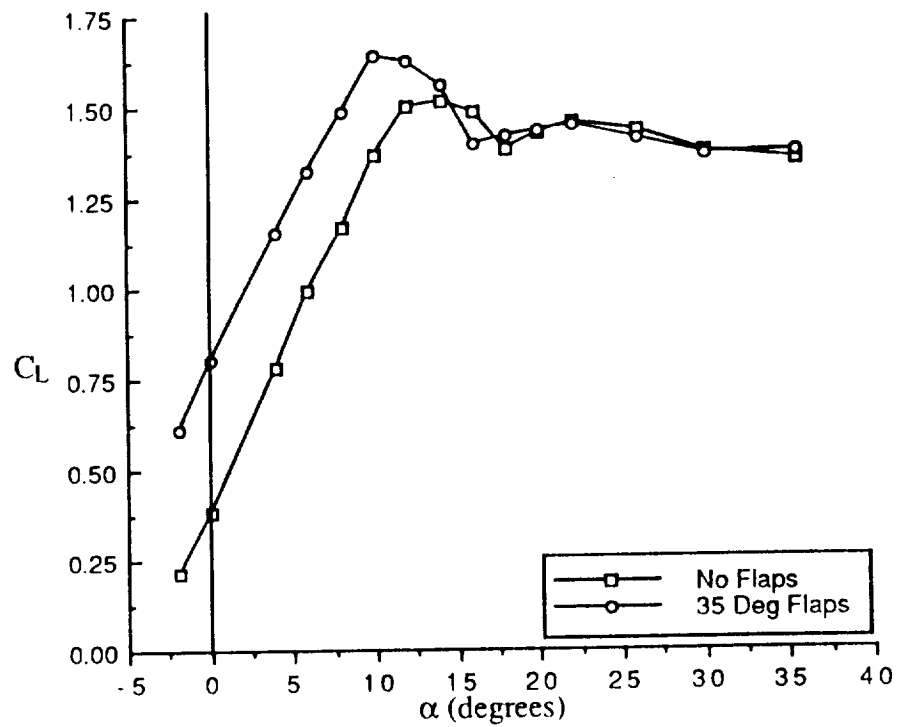


Figure 46 - Effect of Flaps on Final Configuration Lift

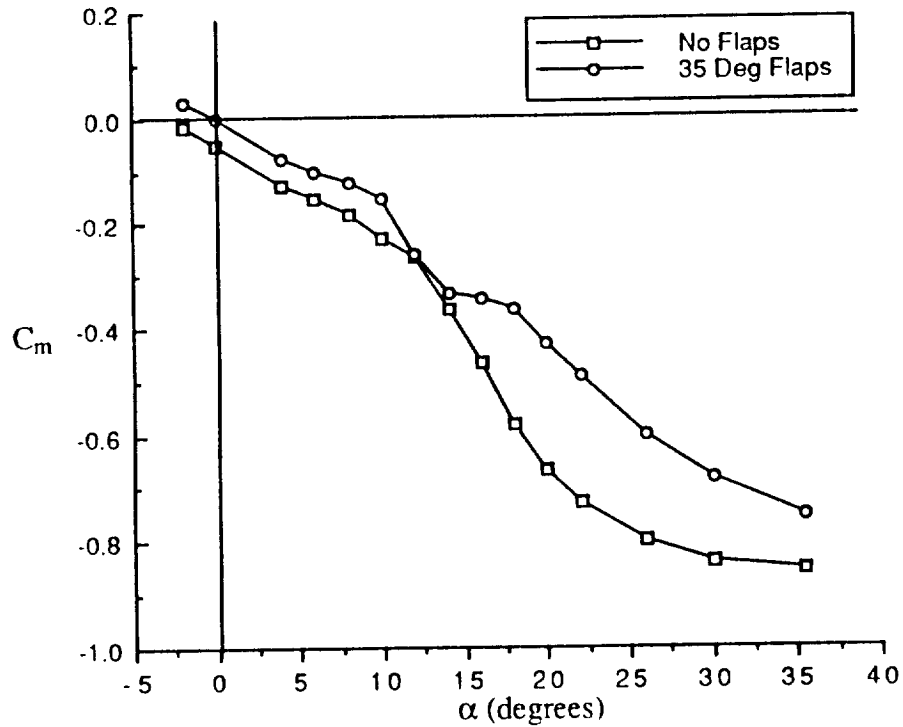


Figure 47 - Effect of Flaps on Final Configuration Pitching Moment

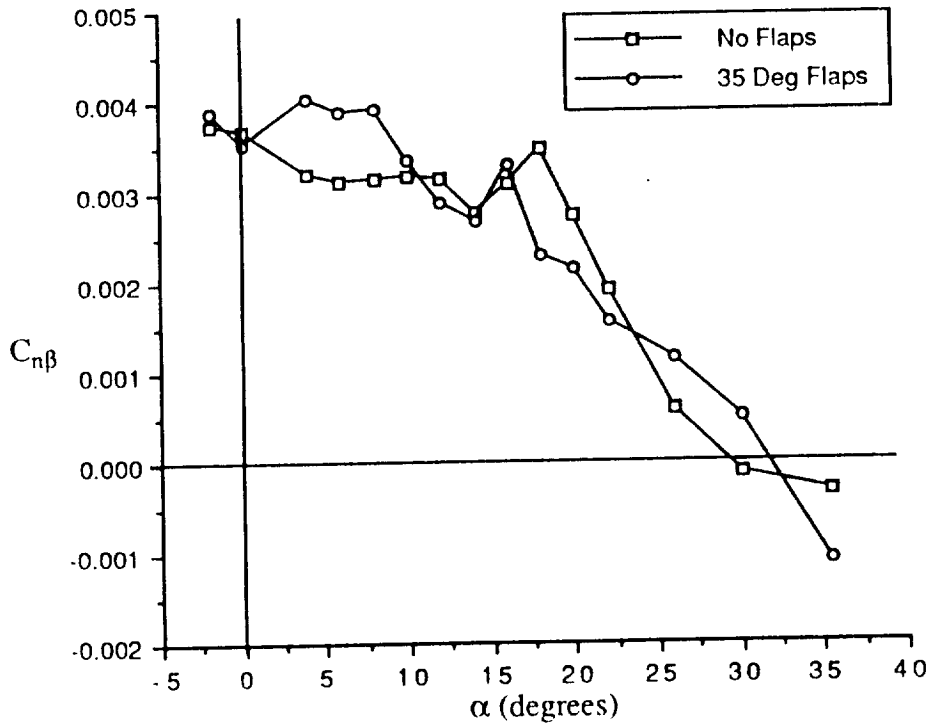


Figure 48 - Effect of Flaps on Directional Stability

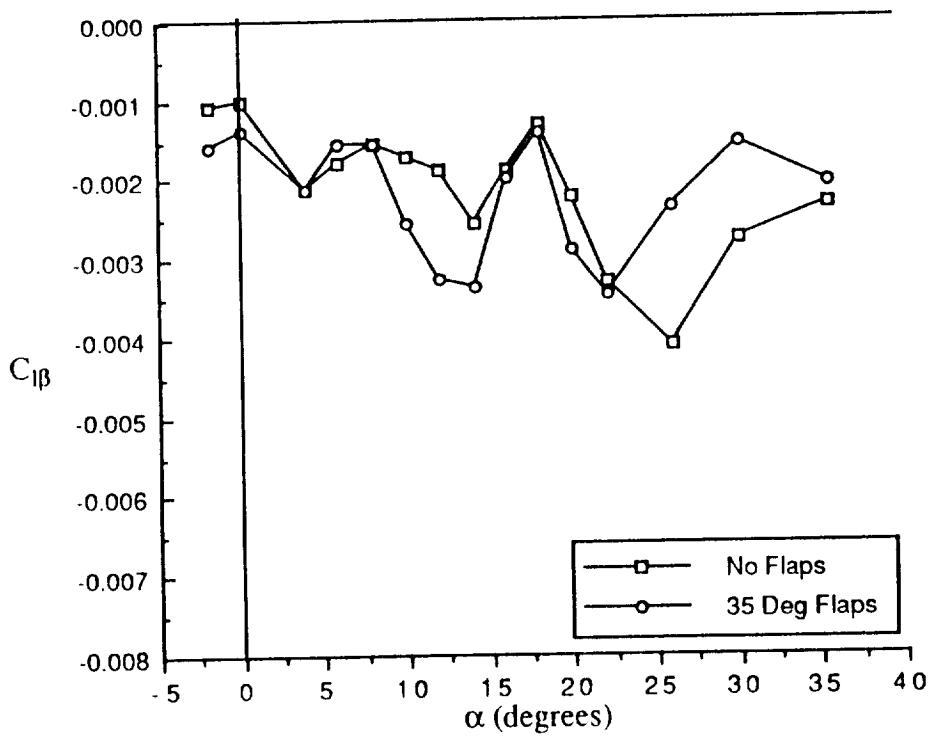


Figure 49 - Effect of Flaps on Lateral Stability

lower rudder only. The rudder maintains its full authority until just after stall and drops off through the post-stall α 's due to the vertical fin being located in the stalled wake of the wing and fuselage. The lower rudder provides an average of 61% of the effectiveness of the full rudder which corresponds approximately to the ratio of the lower rudder area to the full rudder area of 0.591. Figure 51 shows the effect of power on the rudder effectiveness. A comparison is shown for the lower and full rudders. It is shown that power increases the rudder effectiveness significantly. This is due to the propeller blowing over the vertical tail which increases the circulation for a rudder deflection. Smoke flow visualization verified that the flow in the prop-wash was blowing across the deflected rudder. It is also seen that the lower rudder with full power is more effective than the full rudder without power. From this result it is possible to speculate the lower rudder alone might be sufficient for cruise flight.

Effect of Elevator on Longitudinal Characteristics. Figure 52 shows the effect of elevator on pitching moment for several deflections of the full elevator. In addition, it shows the elevator effectiveness for the full elevator and for the inboard elevator alone. It is shown that the full elevator without thrust can trim the aircraft to approximately 22 degrees α with a corresponding C_L of 1.27. The elevator effectiveness varies through the α range but remains more or less constant for α less than 10 degrees. Above 14 degrees, the effectiveness drops off sharply due to the horizontal stabilizer beginning to stall. The inboard elevator alone has slightly more than half of the full elevator effectiveness which roughly corresponds to the ratio of the inboard elevator area to the full elevator area. Figure 53 shows the effect of power on the full and inboard elevator effectiveness. It is shown that power increases the effectiveness noticeably for α below 10 degrees. This is due to the improved flow over the horizontal stabilizer with power because of propeller blowing. At 10 degrees α , the effectiveness drops off sharply, approaching the power-off elevator effectiveness. In fact, the full elevator effectiveness is lower than the power-off effectiveness from an α of 12 to 26 degrees. This result is likely due to the combined

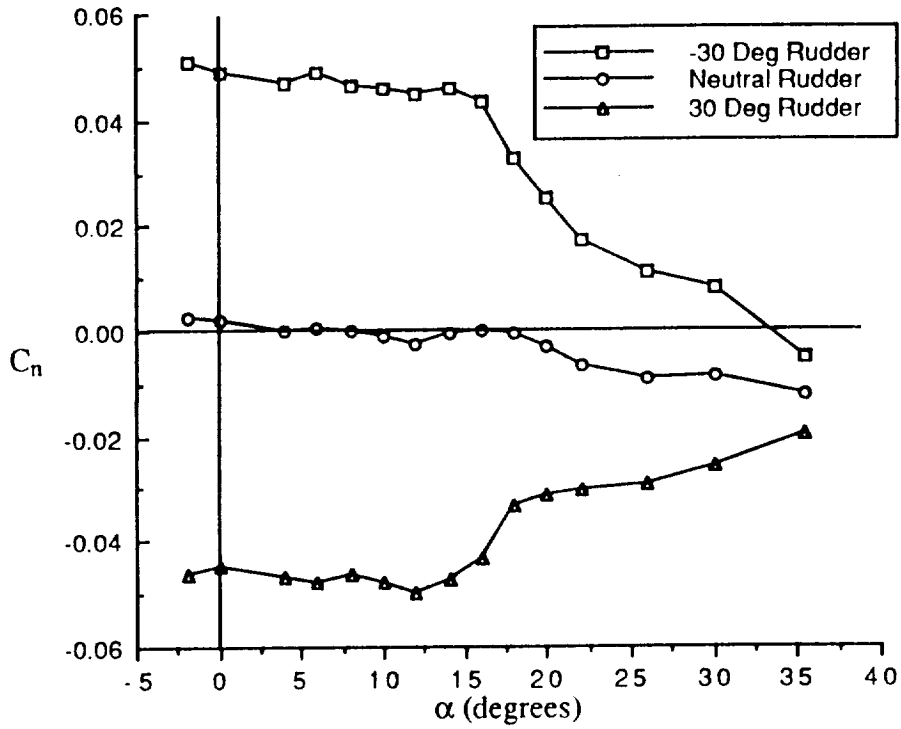


Figure 50 - Final Configuration Full Rudder Authority, $\delta_r=35^\circ$

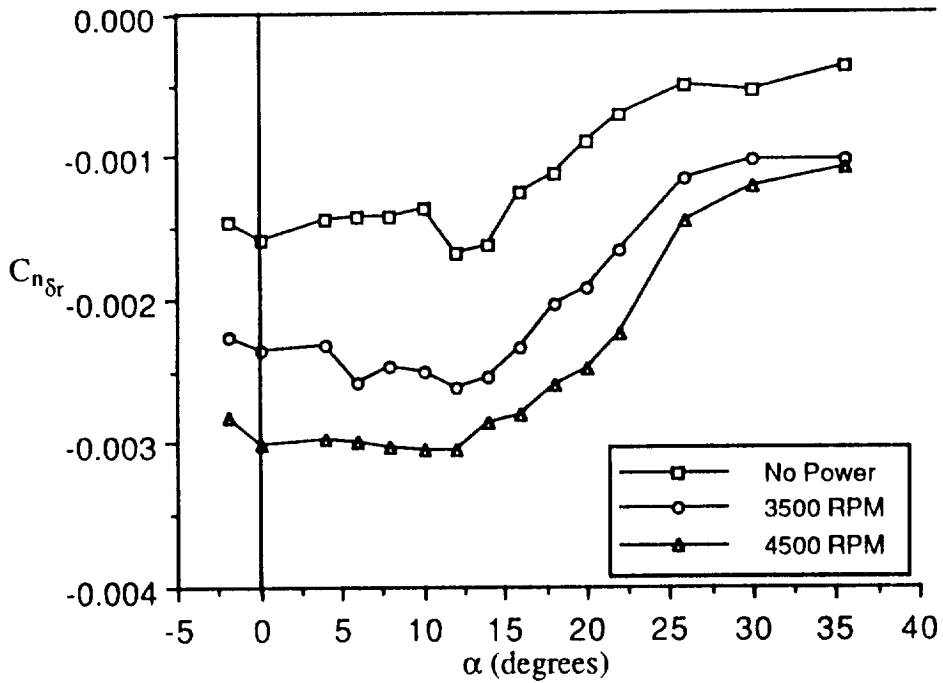


Figure 51 - Effect of Power on Rudder Effectiveness, $\delta_r=35^\circ$

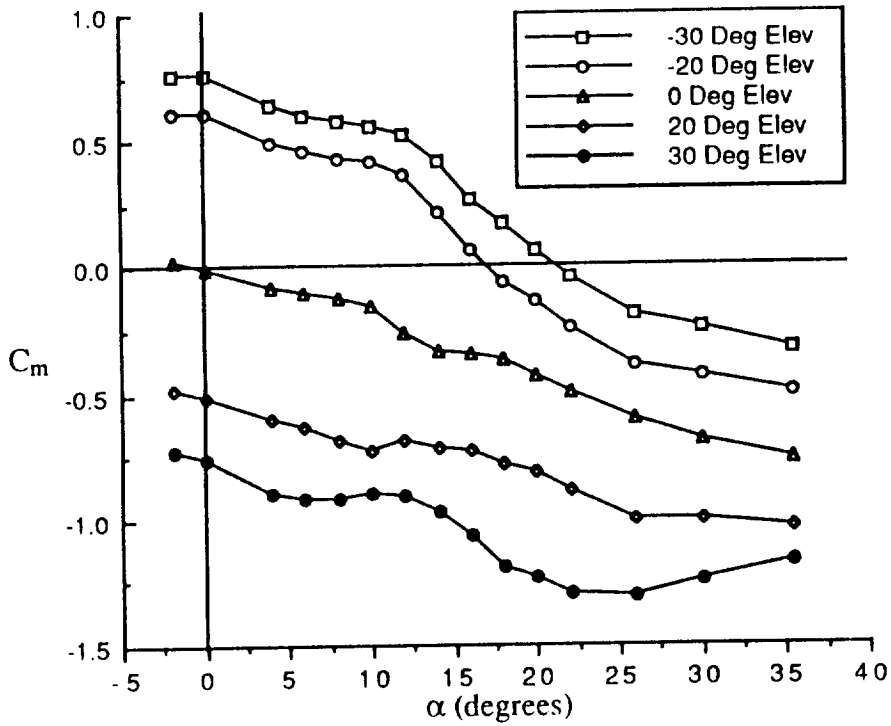


Figure 52 - Effect of Elevator on Pitching Moment, $\delta_f = 35^\circ$

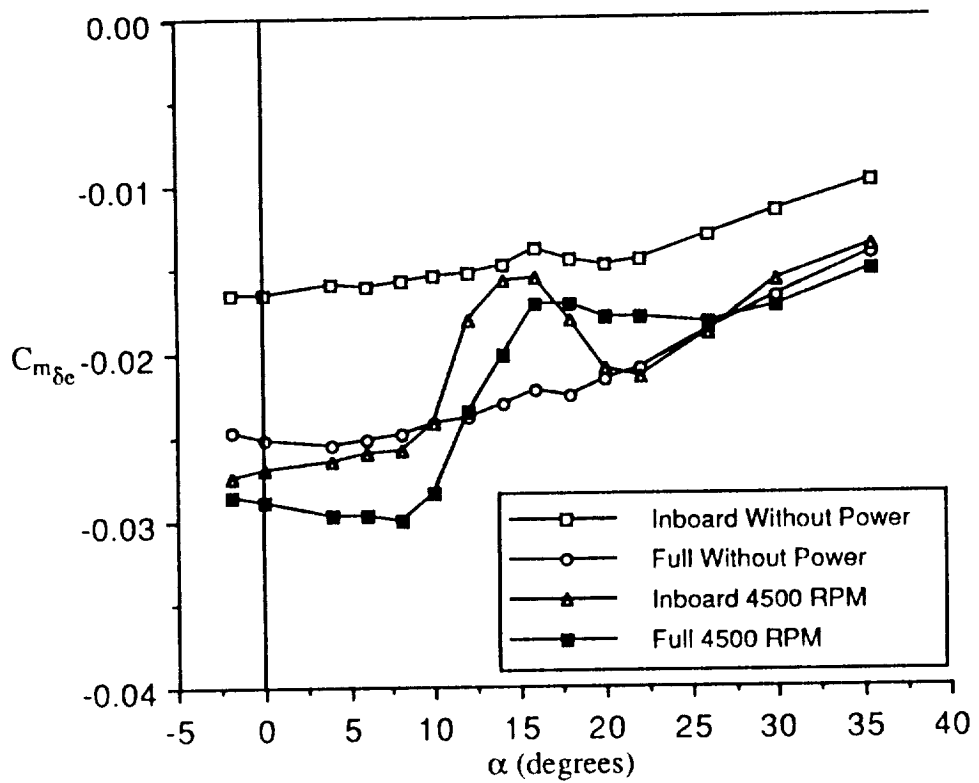


Figure 53 - Effect of Power on Elevator Effectiveness, $\delta_f = 35^\circ$

influence of the increasing wing downwash and propeller propwash moving away from the stabilizer and interfering with the local flow over the elevator, eliminating the blowing effect and distorting the local flow over the elevator. At α 's above 26 degrees, the propwash is close enough to the stabilizer to affect the inboard elevator while the stabilizer is below the wing wake such that the effectiveness is again increased from the power-off case. Another interesting result is that the increase of effectiveness of the inboard elevator is substantially more than the increase of effectiveness of the full elevator. In fact, most of the full elevator effectiveness with power is provided by the inboard elevator. This is because the propeller is blowing across the inboard portion of the horizontal stabilizer, so the inboard elevator is seeing a large effect of the blowing while the outboard elevator sees little. For the full power case, the inboard elevator is more effective than the full elevator with no power through most of the α range.

Effect of Power on Trim Capability. Figure 54 shows a series of full elevator deflections for the full power climb, missed approach condition of full power with a δ_f of 35 degrees. The neutral elevator case shows a large negative trim α due, of course, to power effects on the pitching moment. It is shown that the configuration can trim at approximately zero degrees α with -20 degrees of elevator and at approximately 8 degrees α with -30 degrees of elevator. A reasonable upper limit on allowable elevator deflection is 30 degrees. With a larger deflection, there would be no appreciable gain in elevator authority. With a minimum of 20 degrees deflection required purely to trim, there remains only 10 degrees of deflection for pitch control. However, it was shown that power increases the elevator effectiveness significantly. Because of this, the elevator is probably effective to a deflection higher than 30 degrees. With a reasonable climb angle of 3 degrees, this missed approach condition was accepted as being reasonable considering the potential to trim up to 10 degrees α for the flaps down full power climb case. It is expected that the flaps up cruise condition would not have a trim problem because the cruise thrust setting would be lower than the full power climb, resulting in a lower pitching moment due

to power. Thus, the power effects on elevator effectiveness are significant enough to overcome the unfavorable pitching moment change with power.

Effect of Ailerons on Lateral Characteristics. Figure 55 shows the variation in aileron effectiveness with α in addition to the aileron authority for a full deflection of + and - 20 degrees. The effectiveness varies approximately linearly with angle-of-attack through the entire range of α 's. This reduction in effectiveness is caused by trailing edge separation which is shown the the wing stall pattern (figure 8). Had the wing droop proved to be more effective, the aileron effectiveness would have been expected to remain constant to higher α 's.

Figure 56 shows the yawing moment with neutral ailerons and with a 20 degree positive aileron deflection. A slight amount of positive yawing moment with the 20 degree deflection indicates adverse yaw through most of the angle-of-attack range.

Figure 57 shows the effect of power on the aileron effectiveness. There appears to be an increase in effectiveness until around 25 degrees α due to some effects induced by the airflow into the propeller disks.

Engine Out Characteristics. A major concern with multiple engine transport aircraft is the ability to trim and continue flying with one or more engines out. Results presented above show the capability to trim with full power and with no power. Figure 58 shows the yawing moment curve. The symmetric full power case produces negligible yawing moment until near stall where the wing wake begins to interfere with the propeller disks. With the left engine windmilling and the right engine at full power, the aircraft experiences a sharp negative yawing moment. However, with full corrective rudder deflection in addition to the engine out condition, the yawing moment is shifted positive. The rudder provides enough yawing moment to nearly double the engine-out yawing moment. the aircraft can trim with one engine out until approximately 22 degrees. When one propeller is inoperative, a rolling moment is produced due to the increased lift on the side of the operative propeller. This is shown in figure 59. The curve with full corrective ailerons

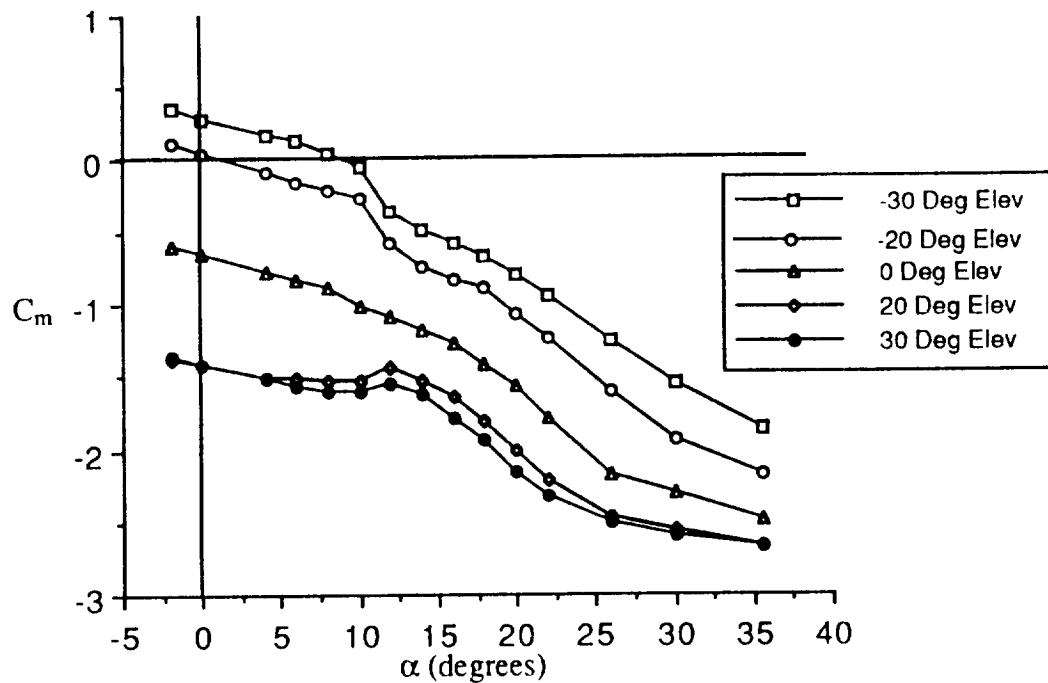


Figure 54 - Effect of Power on Trim Capability, $\delta_f = 35^\circ$

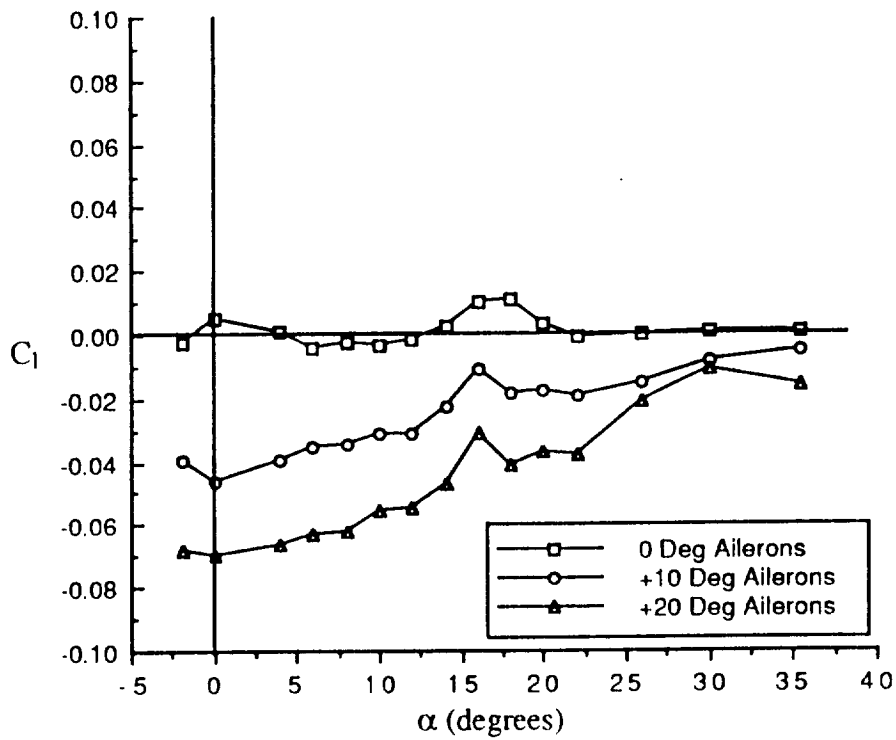


Figure 55 - Effect of Ailerons on Rolling Moment, $\delta_f = 35^\circ$

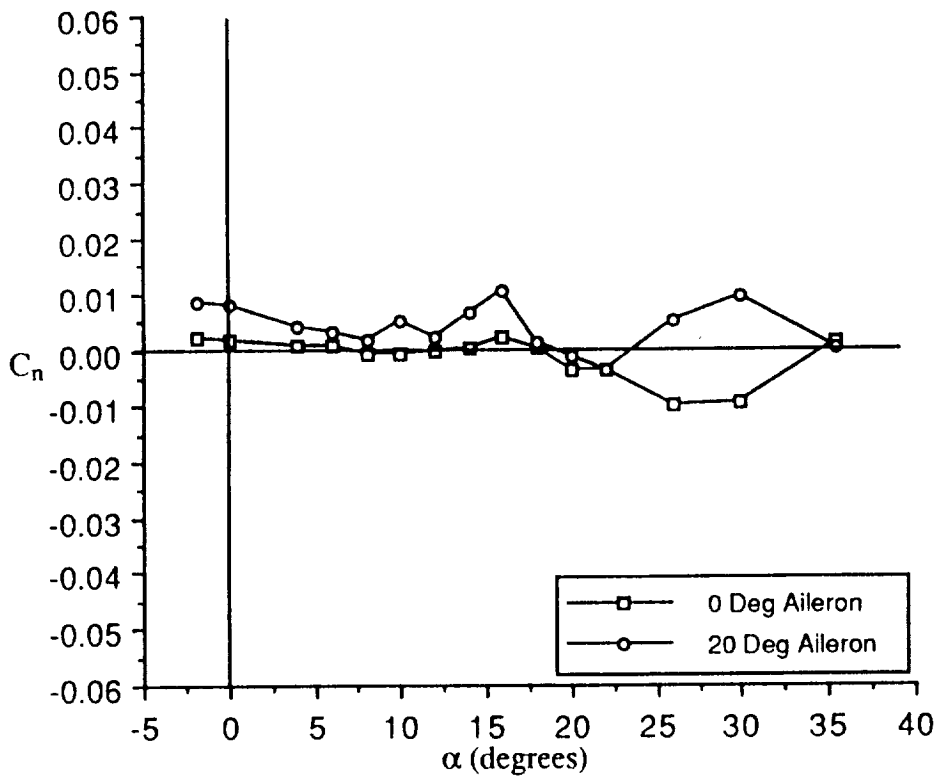


Figure 56 - Effect of Ailerons on Yawing Moment, $\delta_f = 35^\circ$

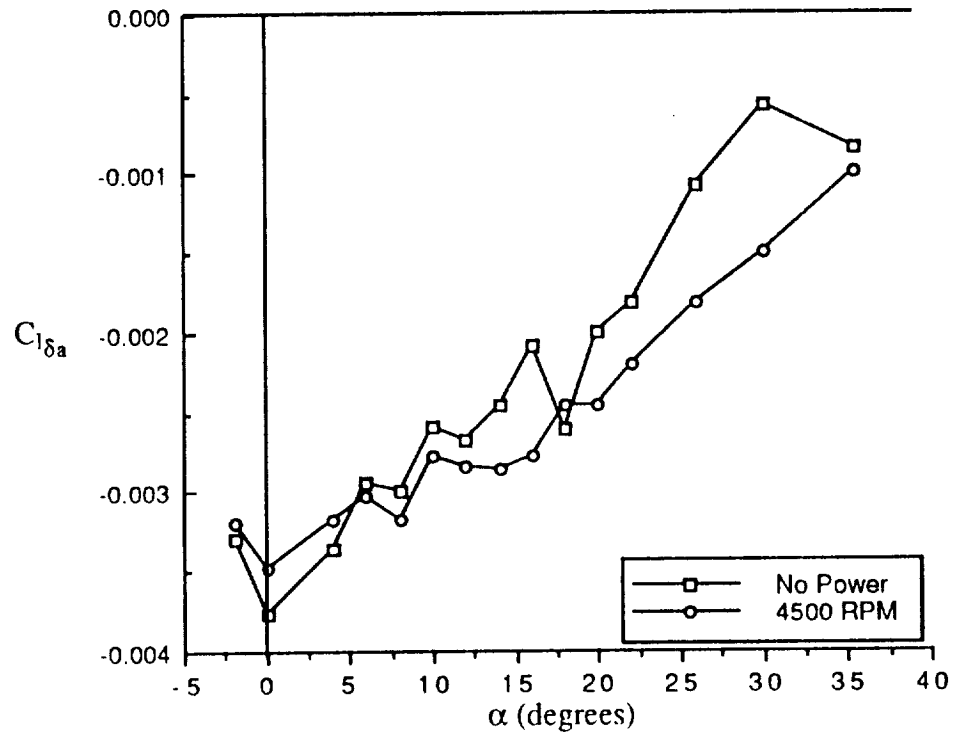


Figure 57 - Effect of Power on Aileron Effectiveness, $\delta_f = 35^\circ$

shows the ailerons have enough authority to overcome the engine-out rolling moment through the entire α range.

Comparison To Theoretical Results

In order to provide a good overall set of data for the aircraft, the configuration was analyzed with a first-order potential flow "doublet" panel method to parallel the wind tunnel data. Such methods have proven to be excellent sources of basic aerodynamic characteristics of full configurations. The panelling method, QUADPAN (ref 18), was used since it provides a full surface analysis with relatively simple geometry input. In addition, QUADPAN includes the capability to approximate propeller effects on the configuration using a simple slipstream model. An orthographic view of the completed panel model is shown in figure 60. The model contains 2070 quadrilateral panel elements. QUADPAN calculates the potential flow over the model by the use of doublet and source elements on the surface of the model. In order to assure proper alignment and positioning of the elements, which would assure the satisfaction of all boundary conditions, some minor adjustments were made from the true geometry to the panel model geometry; however, no dimension was changed more than approximately 1/4 inch which is much smaller than any major dimension on the model. Thus, the model represented the full wind tunnel model.

Comparing the Results. Figures 61 and 62 show a comparison between the wind tunnel results and the QUADPAN results for the longitudinal characteristics of the cruise configuration without power ($\delta_T=0$). There is a good comparison in the lift curve. Since QUADPAN is a linear potential code, no stall is shown for the theoretical results. The slope and zero α lift are extremely close to the wind tunnel results. The pitching moment comparison is quite good as well. The SM from QUADPAN is approximately 16.1% compared to 14.9% from the wind tunnel. The trim α is slightly low from QUADPAN, but the difference shown in the wind tunnel data could be due to viscous effects, model support effects, etc.

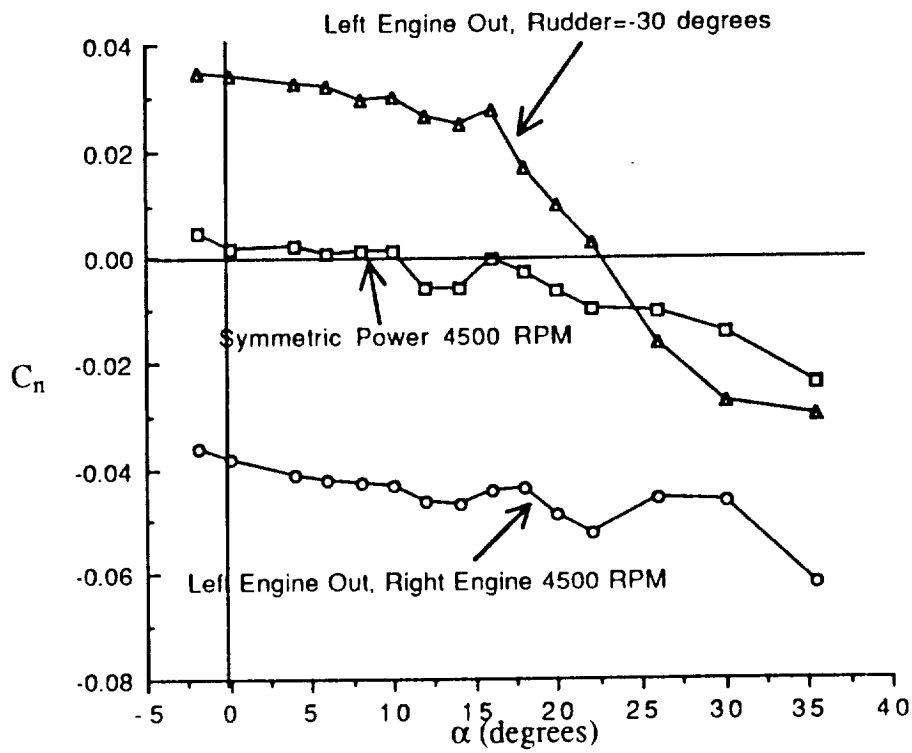


Figure 58 - Engine-out Yawing Moment, $\delta_f = 35^\circ$

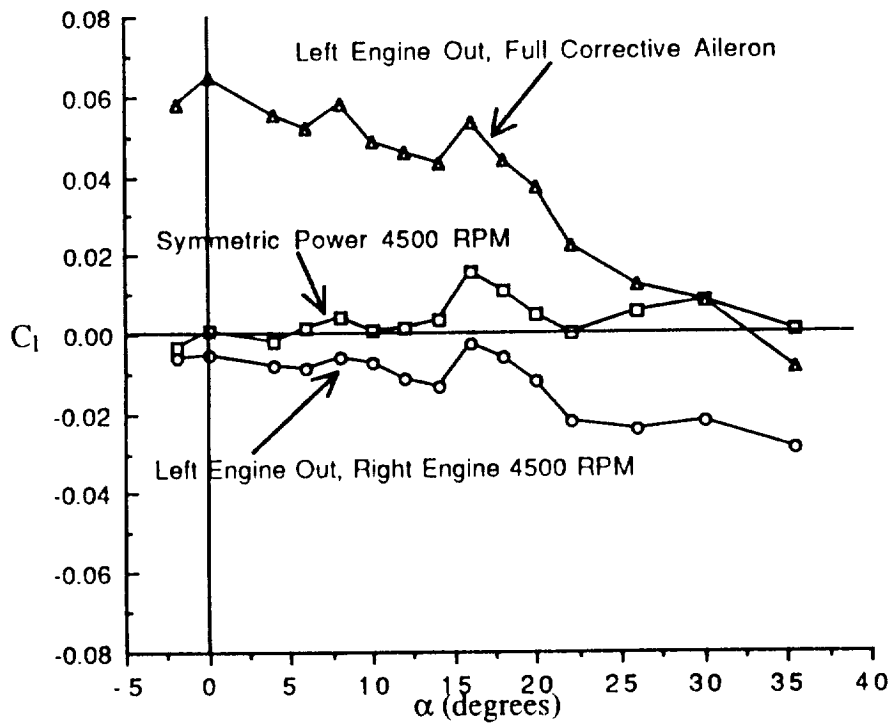


Figure 59 - Engine-out Rolling Moment, $\delta_f = 35^\circ$

NASA-LANGLEY ATP-OTT FULL CONFIGURATION

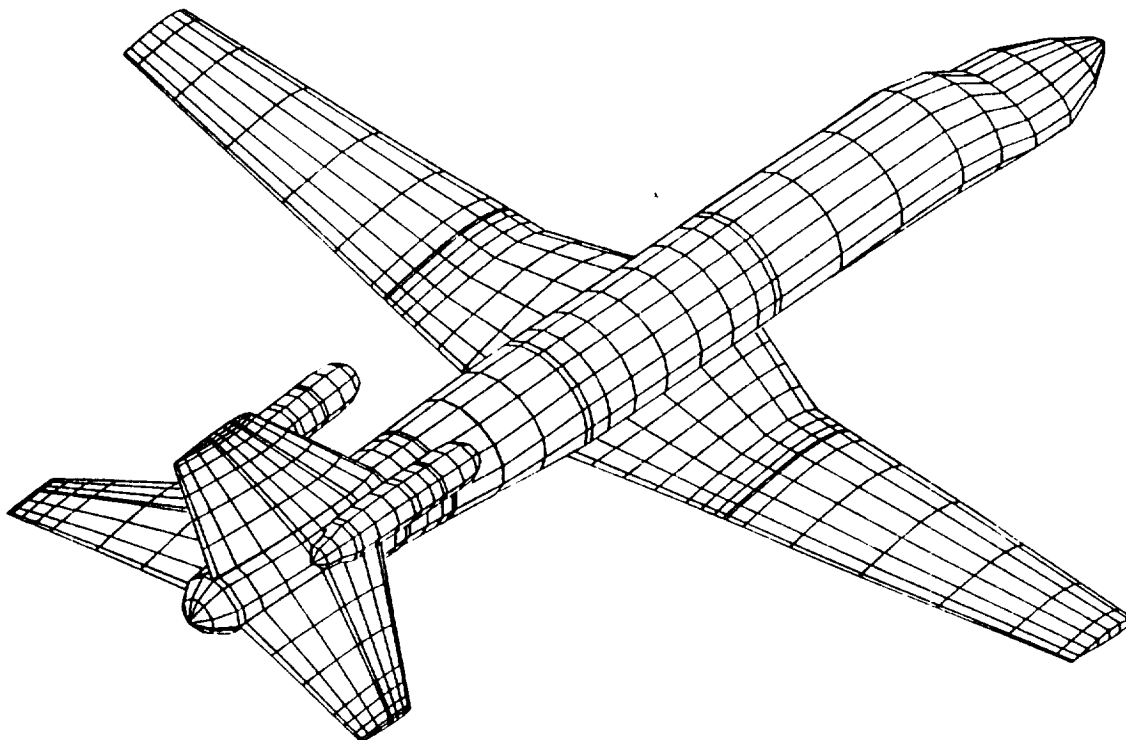
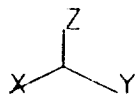


Figure 60 - Orthographic View of QUADPAN Panel Model

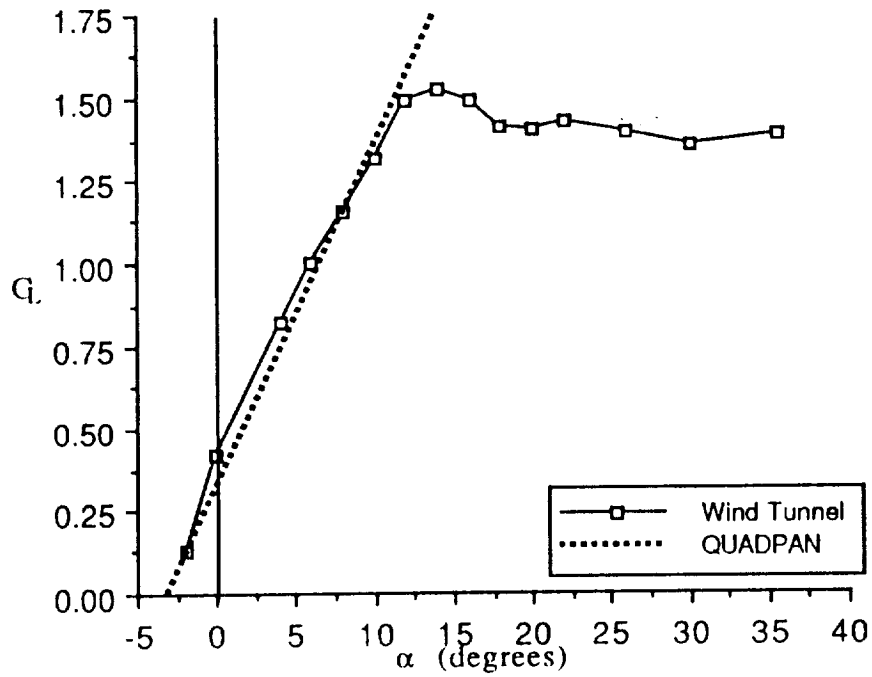


Figure 61 - Comparison to Potential Lift, $\delta_f = 0^\circ$

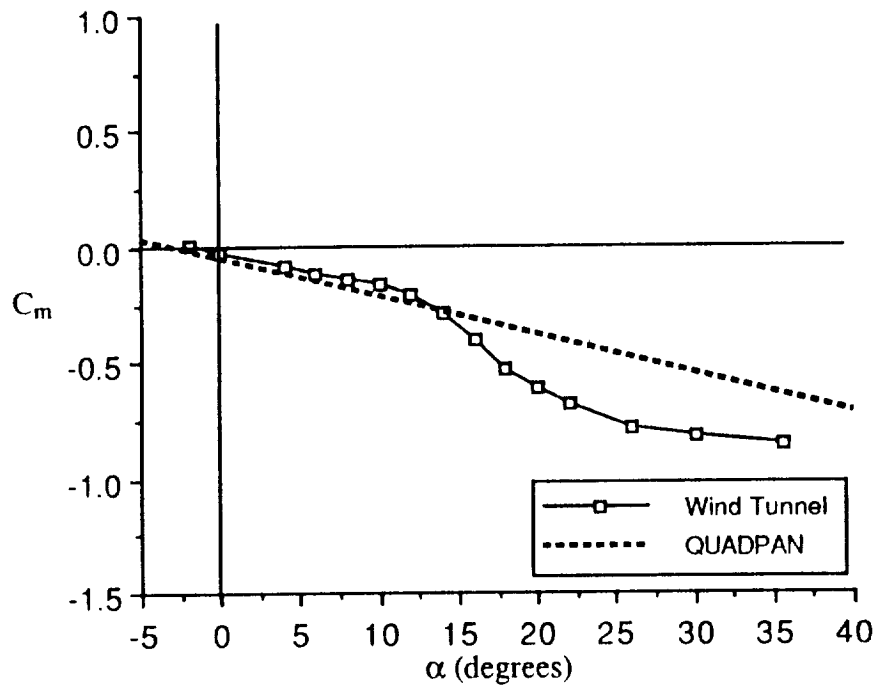


Figure 62 - Comparison to Potential Pitching Moment, $\delta_f = 0^\circ$

Figures 63 and 64 show a comparison for the lateral and directional characteristics of the same configuration. The directional stability is slightly low from QUADPAN. A variety of element arrangements were checked to see if this underestimate in $C_{n\beta}$ was due to an underestimate in side force on the vertical tail with sideslip; however, the value of the side force on the vertical tail, and consequently $C_{n\beta}$, never changed much. From this it is possible to conclude that the yawing moment due to the body, pylons and nacelles was underestimated. If an average $C_{l\beta}$ is taken in the linear range from the lift curve, the QUADPAN value of $C_{l\beta}$ corresponds nearly exactly.

Figures 65 and 66 show QUADPAN's estimate to lift and pitching moment due to the propeller slipstream effects. These results are for a total T'_c (left + right) of 0.36. For the plot, the vector component of thrust was added to both the lift and pitching moment. For C_L , there was negligible change due to power. This did not compare well to the wind tunnel results which showed a large change in lift due to blowing over the horizontal tail which was not well represented by QUADPAN. The pitching moment shift with power was low as well. From the plot, the theoretical shift in C_m was approximately half of the wind tunnel shift. In addition, the majority of this shift was due to the thrust line being above the CG. Because QUADPAN did not predict the increased lift on the horizontal tail, it also did not show the pitching moment change due to the additional lift on the tail. Figures 67 and 68 shows similar under-predictions of the effect of power on $C_{n\beta}$ and $C_{l\beta}$. Thus, QUADPAN does not well predict the aerodynamic effects due to propeller slipstream blowing over the tail surfaces for this configuration.

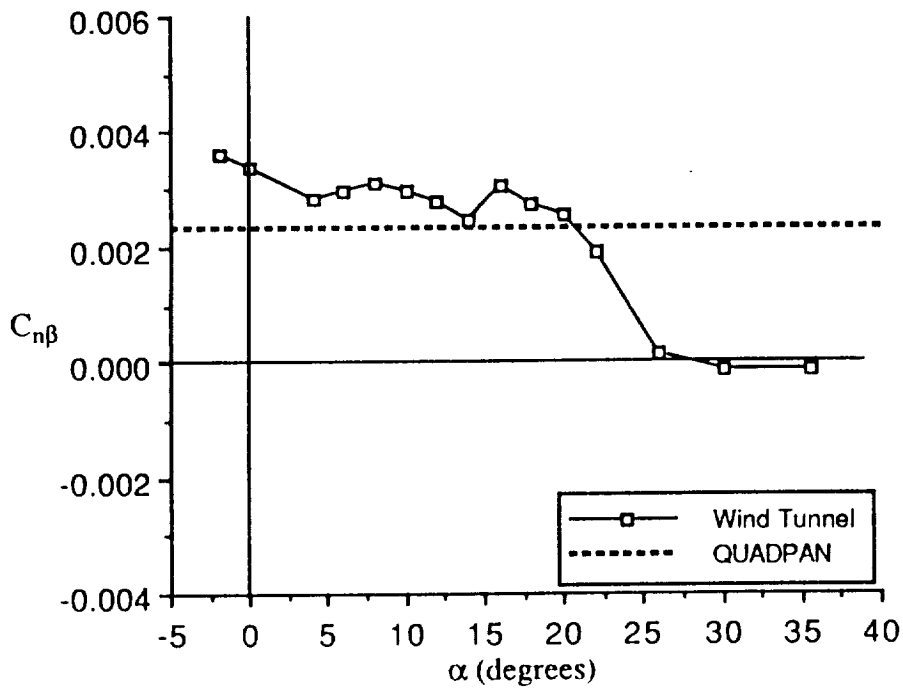


Figure 63 - Comparison to Potential Directional Stability, $\delta_f = 0^\circ$

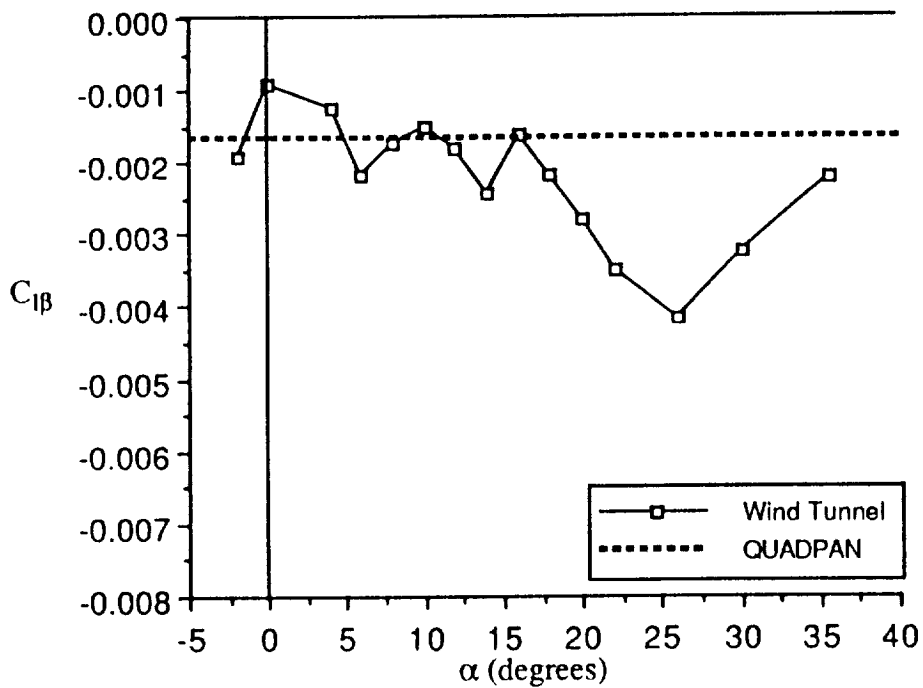


Figure 64 - Comparison to Potential Lateral Stability, $\delta_f = 0^\circ$

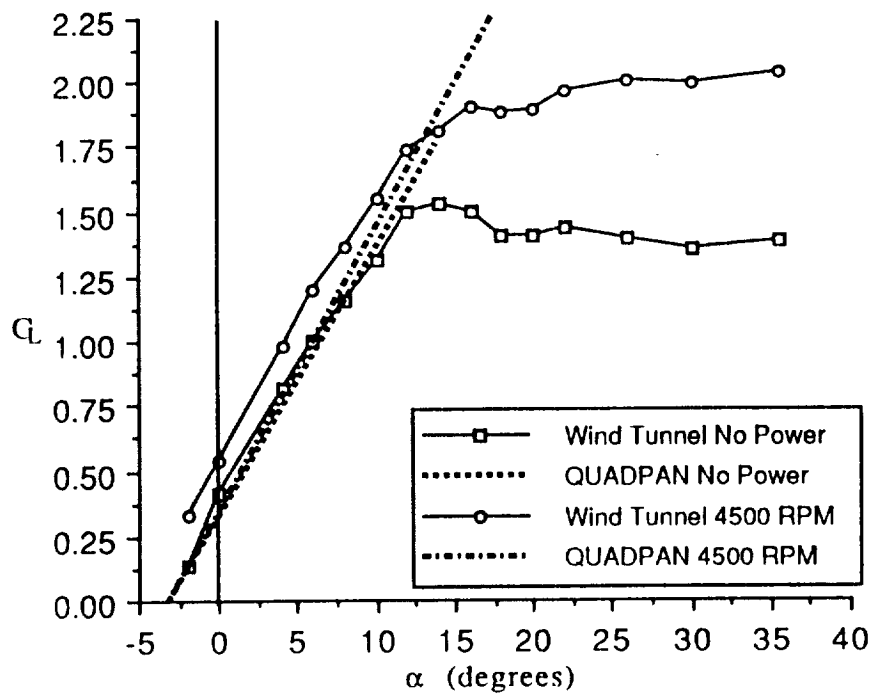


Figure 65 - Predicted Power Effects on Lift, $\delta_f = 0^\circ$

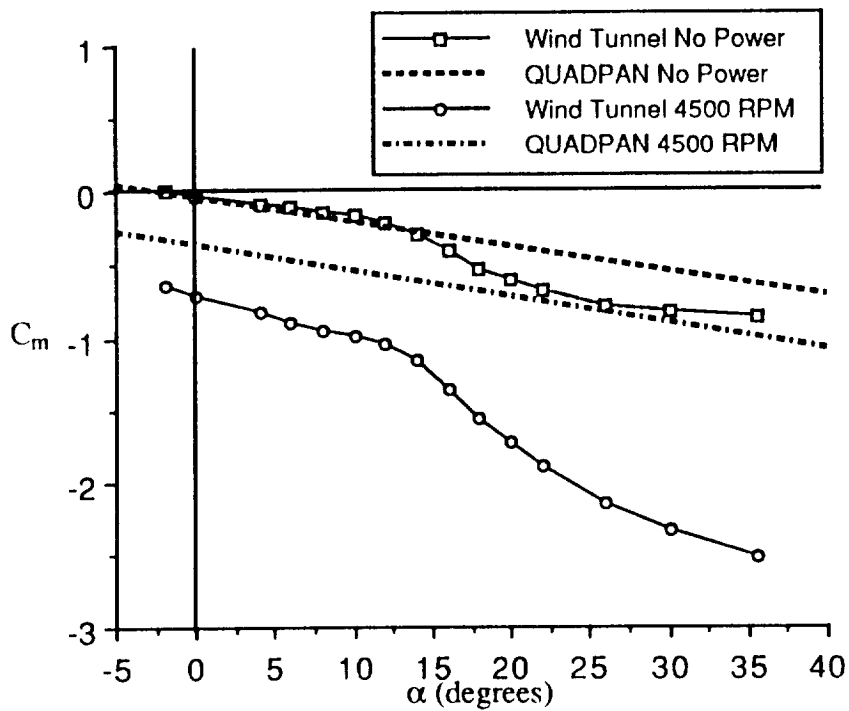


Figure 66 - Predicted Power Effects on Pitching Moment, $\delta_f = 0^\circ$

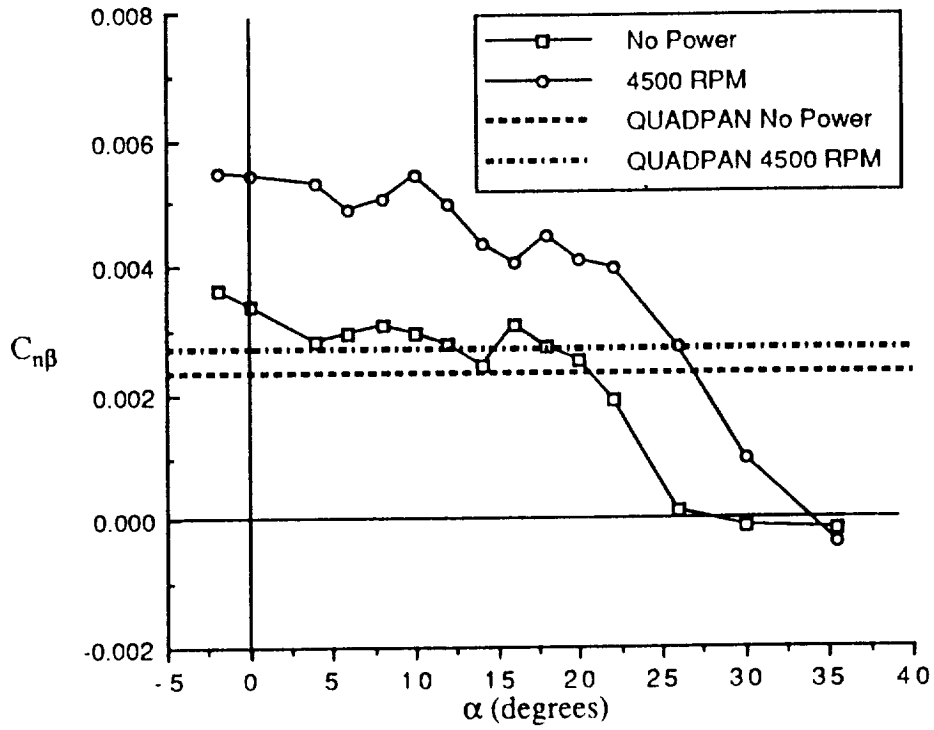


Figure 67 - Predicted Power Effects on Directional Stability, $\delta_f = 0^\circ$

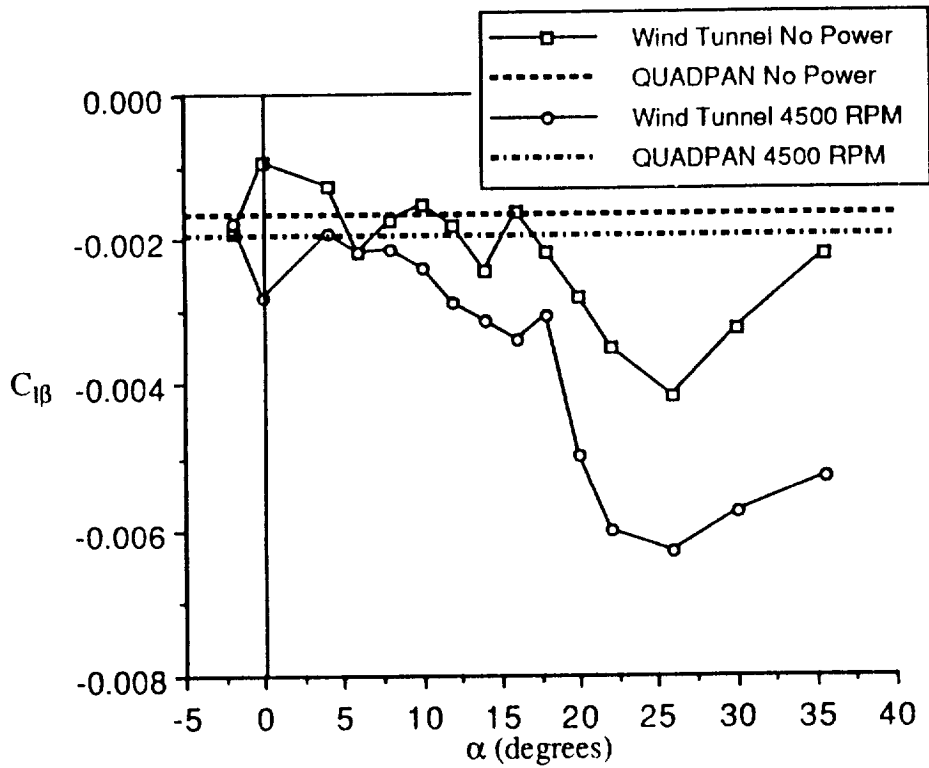


Figure 68 - Predicted Power Effects on Lateral Stability, $\delta_f = 0^\circ$

Concluding Remarks

As part of a cooperative effort between NASA Langley Research Center and North Carolina State University, an exploratory wind tunnel investigation was performed in the 30x60 Foot Wind Tunnel to determine the static stability and control characteristics into deep stall of an advanced turboprop configuration with the propellers placed above the horizontal tail. A list of the major discoveries is presented below.

1) The model had fair longitudinal stall characteristics. A leading edge droop modification on the wing somewhat reduced a tendency to autorotate at stall.

2) A large horizontal and vertical tail provided both longitudinal and directional stability for the unpowered configuration.

3) Power improved the static longitudinal and directional stability through the entire angle of attack range and improved the lateral stability in the post-stall angle of attack range. In addition, power greatly increased the elevator and rudder control effectiveness through the entire angle of attack range tested.

4) The case for the propellers rotating with the outboard blades moving down was shown to have more installed thrust than the case for the propellers rotating with the inboard blades moving down. This result was due to a "crossflow" behind the propeller disk which varied depending on the direction of propeller rotation.

5) A set of fillet fairings which ducted the flow behind the propeller disks was shown to enhance the crossflow effect and enhance the difference in installed thrust between the two directions of propeller rotation.

6) Power was shown to drastically change the longitudinal trim angle of attack, primarily due to the thrust line being located above the center of gravity. It is believed that a proper configuration design could minimize this trim change.

7) The model was shown to have sufficient rudder and aileron authority to trim with one engine inoperative and the other engine at full power.

8) A potential flow doublet panelling code, QUADPAN, accurately predicted the lift and pitching moment of the full configuration. In addition, directional and lateral stability were predicted with a fair degree of accuracy. The code was insufficient in predicting propeller induced effects

References

1. Hager, Roy D., and Vrabel, Deborah. *Advanced Turboprop Project*. NASA SP-495. 1988.
2. Ziemianski, Joseph A., and Whitlow, John B., Jr. *NASA/Industry Advanced Turboprop Technology Program*. NASA TM-100929. August 1988.
3. Aljabri, A.S. *Wind Tunnel Tests On A One-Foot Diameter SR-7L Propfan Model*. AIAA Paper 87-1892. June 1987.
4. Dittmar, James H. *Feasibility of Wing Shielding of the Airplane Interior From The Shock Noise Generated by Supersonic Tip Speed Propellers*. NASA TM-79042. December 1978.
5. Dittmar, James H. *An Experimental Investigation of Reducing Advanced Turboprop Cabin Noise by Wing Shielding*. NASA TM-87112. July 1986.
6. Willis, Conrad M., Mayes, William H., and Daniels, Edward F. *Effects of Propeller Rotation Direction on Airplane Interior Noise Levels*. NASA TP-2444. July 1985.
7. Coe, Paul L., Jr., Turner, Steven G., and Owens, D. Bruce. *Low-Speed Wind-Tunnel Investigation of the Flight Dynamic Characteristics of an Advanced Turboprop Business/Commuter Aircraft Configuration*. NASA TP-2982. April 1990.
8. Dunham, Dana Morris., et al. *Low-Speed Aerodynamic Characteristics of a Twin Engine General Aviation Configuration With Aft-Fuselage-Mounted Pusher Propellers*. NASA TP-2763. October 1987.
9. Applin, Zachary T., and Coe, Paul L., Jr. *Low-Speed Stability and Control Characteristics of a Transport Model With Aft-Fuselage-Mounted Advanced Turboprops*. NASA TP-2535. April 1986.
10. Coe, Paul L., McLemore, H. Clyde, and Shivers, James P. *Effects of Upper-Surface Blowing and Thrust Vectoring on Low-Speed Aerodynamic Characteristics of a Large-Scale Supersonic Transport Model*. NASA TN D-8296. November 1976.
11. Hale, Francis J. *Introduction to Aircraft Performance, Selection, and Design*. John Wiley and Sons, Inc. Copyright 1984.
12. Johnson, J.L., Jr., and White, E.R. *Exploratory Low-Speed Wind-Tunnel Investigation of Advanced Commuter Configurations Including an Over-The-Wing Propeller Design*. AIAA Paper 83-2531. October 1983.
13. Johnson, Joseph L., Jr., Yip, Long P., and Jordon, Frank L., Jr. *Preliminary Aerodynamic Design Considerations For Advanced Laminar Flow Aircraft Configurations*. Presented at SAE/AIAA/NASA/FAA Laminar Flow Aircraft Certification Workshop. April 1985.
14. Williams, L.J., Johnson, J.L., Jr., and Yip, L.P. *Some Aerodynamic Considerations For Advanced Aircraft Configurations*. AIAA Paper 84-0562. January 1984.

15. Baals, Donald D., and Corliss, William R. *Wind Tunnels of NASA*. NASA SP-440 1981.
16. Coe, Paul L., Jr., Gentry, Garl L., Jr., and Dunham, Dana Morris. *Low-Speed Wind-Tunnel Tests of an Advanced Eight-Bladed Propeller*. NASA TM-86364. July 1985.
17. Rae, William H., and Pope, Alan. *Low-Speed Wind Tunnel Testing*, second edition. John Wiley and Sons, Inc. Copyright 1984.
18. Youngren, Harold H., Bouchard, Eugene E., and Coopersmith, Robert M. *Quadrilateral Element Panel Method (QUADPAN) User's Manual Version 3.2*. Lockheed-California Company LR-30563. Copyright 1984.
19. Bertin, John J., and Smith, Michael L. *Aerodynamics For Engineers*. Prentice-Hall, Inc. 1979.
20. Margason, Richard J., et al. *Subsonic Panel Methods - A Comparison of Several Production Codes*. AIAA Paper 85-0280. 1985.
21. Staff of Langley Research Center: *Exploratory Study of the Effects of Wing-Leading Edge Modifications on the Stall/Spin Behavior of a Light General Aviation Airplane*. NASA TP-1589. December 1979.
22. Stinton, Darrol. *The Design of the Aeroplane*. BSP Professional Books, Great Britain
23. Samuelsson, Ingemar. *Low Speed Wind Tunnel Investigation of Propeller Slipstream Aerodynamic Effects on Different Nacelle/Wing Combinations: Part 1: Total Forces and Moments and Pressure Distributions on Nacelle/Wing at Different Angles of Attack and Yaw and at Different Thrust Coefficients*. The Aeronautical Research Institute of Sweden FFA TN 1987-22. 1987.
24. Johnston, R.T., Witkowski, D., and Sullivan, J.P. *Propeller Wakes and Their Interaction With Wings*. in proceedings for 9th International Symposium on Air Breathing Engines. September 1989.